

Investigation of the biological function of arginine methyltransferase PRMT5 in human cancers

Li Jin

Department of Oncology

Linacre College

University of Oxford

Hilary 2020

A thesis submitted for the degree of Doctor of Philosophy at the University of Oxford

Investigation of the biological function of arginine methyltransferase PRMT5 in human cancers

Li Jin Department of Oncology

Linacre College University of Oxford

A thesis submitted for the degree of Doctor of Philosophy

Abstract

PRMT5 is a major type II arginine methyltransferase and plays a crucial role in tumorigenesis. PRMT5 is overexpressed in multiple tumour cell lines, and a high level of PRMT5 was identified as an independent factor for poor clinical outcomes in patients with cancer. PRMT5 has been identified as a potential clinical target for antitumour therapy to enable the treatment of cancers efficiently and selectively. However, studies on the role of PRMT5 are limited and there is a need to understand the mechanisms underlying the biological function of PRMT5 and its therapeutic potential. In this study, we have uncovered a functional role for the PRMT5-E2F1 axis on different aspects of cancer cell biology, including cancer cell viability, apoptosis, migration, invasion, and adhesion. Additionally, we performed a genome-wide expression analysis and identified a group of E2F1 targets that modulate cell adhesion and cellular migratory pattern, resulting in metastasis and invasion, via a PRMT5-dependent mechanism. Furthermore, the expression of *PRMT5* and *E2F1* was correlated, with high levels of *PRMT5* and *E2F1* indicating poor clinical outcomes. This study is the first time to show that the PRMT5-E2F1 axis influences cancer cell growth and division, and also augments the migration and invasive properties of tumour cells. As a positive regulator of the E2F1 axis, this strengthens the case for the use of inhibitors for PRMT5 as a viable therapeutic target, and further suggests the clinical utility of drugs targeting PRMT5.

Acknowledgment

I would first like to sincerely thank my supervisor Professor Nick La Thangue for providing me an opportunity to finish my DPhil study in his group and guiding me with patience.

I would also like to thank my mentors Dr Heidi Olzscha, Dr Simon Carr, Dr Wojciech Barczak, Dr Shonagh Munro and Dr Geng Liu for their valuable scientific insights and their passionate participation and input.

Finally, I must express my gratitude to my parents for their support and kindness.

This accomplishment would not have been possible without them. Thank you.

Table of Contents

Chapter 1: Introduction 1
1.1 Cancer incidence and mortality worldwide 1
1.2 The hallmarks of cancer 3
1.3 Proto-oncogenes and tumour suppressor genes 10
1.4 The cell cycle 13
1.5 Cyclin-dependent kinases (CDKs) 16
1.6 Invasion and metastasis 19
1.7 An overview of cortactin 21
1.8 An overview of E2F family members 26
1.9 Protein arginine methyltransferases (PRMTs) 37
1.10 PRMT5 inhibitors in clinical trials 48
1.11 Research objectives 54

Chapter 2: Materials and Methods 57
2.1 Cell culture 57
2.2 PRMT5 inhibitors 57
2.3 Western blotting and antibodies 58
2.4 Bradford assay 58
2.5 MTT assay 59
2.6 Determination of the IC50 of PRMT5 inhibitors 59
2.7 Enzyme assay of PRMT5 inhibitors 60
2.8 Cell proliferation assay 60
2.9 Colony formation assay 61
2.10 Apoptosis and necrosis assay 61
2.11 Flow cytometry assay 62
2.12 Generation of stable CRISPR-Cas9 knockout cell lines 62
2.13 Small interfering RNA (siRNA) 67
2.14 RNA isolation and quantitative Polymerase Chain Reaction (qPCR) 68
2.15 Transwell cell migration and invasion assay 69
2.16 Cell adhesion, migration and invasion assays via xCELLigence real-time quantitative cell analysis (RTCA) instrument 70
2.17 Chromatin immunoprecipitation (ChIP) 71
2.18 RNA sequencing (RNA-Seq) analysis 75
2.19 Parametric gene set enrichment analysis (PGSEA) 76
2.20 Xena browser functional genomics analysis 77
2.21 Kaplan-Meier survival analysis 77
2.22 ENCODE ChIP sequencing (ChIP-Seq) data analysis 78
2.23 Statistical analysis 78

Chapter 3: J579-44 is an effective small-molecule inhibitor of PRMT5 in cell-based and enzyme assays 79
3.1 Introduction.....79
3.2 The IC50 values of PRMT5 inhibitors identified by MTT assays 80
3.3 Measurement of the EC50 of PRMT5 inhibitors via enzyme assays 87
3.4 Chapter summary.....90

Chapter 4: PRMT5 inhibition induces cellular responses through E2F1 92
4.1 Introduction.....92
4.2 PRMT5 inhibition triggers cell apoptosis and induces cell accumulation in the sub-G1 phase 93
4.3 PRMT5 inhibition impairs cell proliferation and viability.....101
4.4 PRMT5 inhibition decreases cell migration and invasion.....106
4.5 Generation of stable E2F1 CRISPR cells using CRISPR-Cas9 genome editing 109
4.6 PRMT5 inhibition regulates cell apoptosis through E2F1 118
4.7 Targeting PRMT5 activity inhibits cell migration and invasion in association with E2F1.....123
4.8 Chapter summary.....127

Chapter 5: RNA-Seq profiling reveals a cluster of E2F1 target genes involved in PRMT5 modulated cellular processes 128
5.1 Introduction.....128
5.2 RNA-Seq experimental design 129
5.3 Summary of results for RNA-Seq 133
5.4 RNA-Seq profiling reveals a cluster of adhesion related genes dependent on E2F1 and PRMT5 activity.....143
5.5 Chapter summary.....146

Chapter 6: PRMT5 regulates cell adhesion and migration in an E2F1-dependent manner.....149
6.1 Introduction.....149
6.2 ChIP analysis indicates the presence of E2F1-binding site for *CTTN* near the transcription start site.....150
6.3 PRMT5 regulates cellular adhesion and migration by modulating the expression of *CTTN* 154
6.4 Gene expression profiling and survival analysis of *PRMT5*, *E2F1* and *CTTN* ...158
6.5 Chapter summary.....167

Chapter 7: Discussion.....169
7.1 Summary of findings 169

7.2 J579-44 is an effective inhibitor of arginine methyltransferase 5 in cell-based and enzyme assays.....171
7.3 The PRMT5 inhibitor induces cellular responses via E2F1.....175
7.4 PRMT5 regulates cellular adhesion and migration by modulating the expression of E2F1 target *CTTN* and its co-expressed genes.....177
7.5 Clinical use for *PRMT5*, *E2F1*, and *CTTN*.....182
7.6 Conclusions.....184

References

List of Figures

Figure 1.1 The hallmarks of cancer 9
Figure 1.2 A summary of the cell cycle.....15
Figure 1.3 Schematic diagram of cortactin's primary structure 25
Figure 1.4 The domain structures of the E2F family members 34
Figure 1.5 Pathways for E2F1-induced apoptosis 35
Figure 1.6 The pRB-E2F1 complexes 36
Figure 1.7 Arginine methylation reactions catalysed by PRMTs.....44
Table 1 PRMTs dysregulation in cancer.....45
Figure 1.8 Structure of the human PRMT5:MEP50 hetero-octameric complex 46
Table 2 Major PRMT5 protein substrates and their function 47
Figure 1.9 Comparison of two typical PRMT5 inhibitors.....53

Figure 3.1 Characterisation of candidate PRMT5 inhibitors.....83
Figure 3.2 The selection of the PRMT5 inhibitor via the MTT assay.....84
Figure 3.3 Enzymatic assays using J579-44 and the analogue J578-68 89
Figure 3.4 Characterisation of the PRMT5 inhibitor J579-44 and its analogue J578-68 91

Figure 4.1 PRMT5 inhibition triggers cellular apoptosis 96
Figure 4.2 PRMT5 inhibition induces cell accumulation in the sub-G1 phase 99
Figure 4.3 PRMT5 inhibition impairs cell proliferation and viability.....103
Figure 4.4 PRMT5 inhibition decreases cell migration and invasion.....108
Figure 4.5 An outline of CRISPR CRISPR-Cas9 genome editing.....112
Figure 4.6 Validation of *E2F1* CRISPR-edited cells using western blotting and Sanger sequencing 113
Figure 4.7 Growth curves for the two *E2F1* CRISPR cell types.....117
Figure 4.8 E2F1 plays a crucial role in regulating PRMT5 inhibition-induced apoptosis 120
Figure 4.9 J579-44 inhibits cell migration and invasion in association with E2F1..125

Figure 5.1 Experiment design of RNA-Seq preparation.....131
Figure 5.2 Flowchart of RNA-Seq analysis.....137
Figure 5.3 Venn diagrams and heatmap of DEGs 138
Figure 5.4 Functional analysis of DEGs.....140
Figure 5.5 List of adhesion related genes regulated by E2F1 and PRMT5 activity.142
Figure 5.6 Verification of *CTTN* and co-expressed genes.....144

Figure 6.1 Motif scan and ENCODE search suggest that *CTTN* is E2F1 target gene 152

Figure 6.2 PRMT5 regulates cell adhesion and migration by modulating the expression of *CTTN* 156
Figure 6.3 Gene expression profiling and survival analysis using expression data for *PRMT5*, *E2F1* and *CTTN* from the TCGA database 162

Figure 7.1 The PRMT5-E2F1 model illustrates the interplay between PRMT5, E2F1, and E2F1target gene *CTTN* in regulating cellular adhesion and migratory phenotypes 181

Abbreviations

53BP1	p53 binding protein 1
ADMA	asymmetric ω-NG, ω-NG- dimethylarginine
Apaf-1	apoptosis protease-activating factor 1
Arp	actin-related protein
ATM	ataxia-telangiectasia mutated
ATR	ataxia-telangiectasia and Rad3-related kinases
BID	twice-daily
CAK	CDK-activating kinase
CDKN2A	cyclin-dependent kinase inhibitor 2A
CDKs	Cycline-dependent kinases
ChIP	Chromatin immunoprecipitation
ChIP-Seq	ChIP sequencing
Chk1	Checkpoint kinase 1
Chk2	Checkpoint kinase 2
CKIs	CDK inhibitory subunits
CTLs	cytotoxic T cells
DEGs	differentially expressed genes
DMEM	Dulbecco's Modified Eagle Medium
DMSO	dimethyl sulfoxide
EC50	half maximal effective concentration
ECM	extracellular matrix
EGFR	epidermal growth factor receptor
ELAM	EC-leukocyte adhesion molecule
EMT	epithelial-mesenchymal transition
EMT-TFs	EMT-activating transcription factors
ENCODE	The Encyclopedia of DNA Elements
ERα	estrogen receptor α
F-actin	filamentous actin
FAK	focal adhesion kinase
FBS	Fetal bovine serum
FGFs	fibroblast growth factors
FOXO1	forkhead box protein 1
GO	Gene Ontology
GS	growth signals
GTEx	Genotype-Tissue Expression
H3R8	histone H3 arginine 8
H4R3	histone H4 arginine 3
HDAC6	histone deacetylase 6
HOXA9	homeobox A9
IC50	half-maximal inhibitory concentration
MCL	mantle cell lymphoma

MDS	myelodysplastic syndromes
MDSCs	myeloid-derived suppressor cells
MMA	ω-NG-mono-methylarginine
MTA	methylthioadenosine
MTAP	5-methylthioadenosine phosphorylase
MTD	maximum tolerated dose
MTT	3-(4,5-dimethylthiazol-2-yl)-2,5-diphenyltetrazolium bromide
N-WASP	neural WASP
NES	nuclear export signal
NGS	next generation sequencing
NHEJ	non-homologous end joining
NHL	non-Hodgkin lymphoma
NK cells	natural killer cells
NLS	nuclear localisation signal
OS	overall survival
p300/CAF	p300/CREB-binding protein-associated factor
p300/CBP	300/CREB-binding protein
PAM	protospacer-adjacent motif
PARP	poly (ADP-ribose) polymerase
PBS	phosphate-buffered saline
PcG	Polycomb group
PD	pharmacodynamics
PDCD4	programmed cell death protein 4
Pen-Strep	Penicillin-Streptomycin
PFS	progression-free survival
PGSEA	parametric gene set enrichment analyses
PK	pharmacokinetics
pRB	retinoblastoma protein
PRMTs	protein arginine methyltransferases
PTM	post-translational modification
R30	arginine 30
RNA-Seq	RNA sequencing
RP2Ds	recommended Phase 2 dose(s)
RTCA	Real Time Cell Analysis
RT-PCR	Reverse transcription polymerase chain reaction
SAM	S-adenosylmethionine
SDMA	ω-NG, N'G-symmetric dimethylarginine
sgRNA	single guide RNA
SH2	Src homology 2
SH3	Src homology 3
siRNA	small interfering RNA
TCGA	The Cancer Genome Atlas
TGF-ß	transforming growth factor beta
TGI	tumour growth inhibition

TIM	triosephosphate isomerase
Tregs	regulatory T cells
VCAM-1	vascular cell adhesion molecule 1
VEGF	vascular endothelial growth factor
VEGF-A	vascular endothelial growth factor A
WHO	World Health Organization
WIP	WASP-interacting protein
WT	wild-type

Chapter 1: Introduction

1.1 Cancer incidence and mortality worldwide

The World Health Organization (WHO) describes cancer as the second leading cause of death worldwide, and was responsible for an estimated 9.6 million deaths in 2018. Globally, ~1 in 6 deaths result due to cancer. The three most frequent cancers are lung (2.09 million cases), breast (2.09 million cases), and colorectal cancers (1.80 million cases). The most common cancers resulting in death are attributed to lung (1.76 million deaths), colorectal (862,000 deaths), and stomach cancers (783,000 deaths)[1].

The incidence of cancer and the resulting mortality is growing rapidly worldwide. The last release of the GLOBOCAN database (September 2018) included estimates of the incidence of, mortality due to cancer, and includes data for the prevalence of 36 types of cancer, as well as all cancer types combined across 185 countries. The report states the prediction that if recent trends for the incidence of major cancer types and population growth continue, there will be 27.5 million new cases of cancer worldwide each year by 2040[2].

The economic impact of cancer is significant and is increasing. Global spending on cancer medicines is rising continually, with the costs for therapeutic and supportive

care at $133 billion globally in 2017, up from $96 billion in 2013[1]. Thus, cancer is a huge economic and social burden and challenge.

1.2 The hallmarks of cancer

There are more than 100 different types of cancer, and subtypes of tumours can be found within specific organs[3]. Hannahan and Weinberg have shown that the manifestation of ten essential alterations collectively dictates malignant growth from among the vast catalogue of cancer cell genotypes. These ten capabilities are shared in common by most and perhaps all types of tumours in humans. The ten capabilities were described as self-sufficiency in growth signals, insensitivity to growth-inhibitory (anti-growth) signals, evasion of programmed cell death (apoptosis), limitless replicative potential, sustained angiogenesis, tissue invasion and metastasis, genome instability and mutation, tumour-promoting inflammation, reprogramming of energy metabolism, and evasion of immune destruction (Figure 1.1) [3,4].

Self-Sufficiency in Growth Signals: Normal cells require mitogenic growth signals (GS) to transition from a quiescent to an active proliferative state. In cancer, some oncogenes may mimic normal growth signalling. There are three common strategies for achieving GS autonomy, and these involve the alteration of extracellular growth signals, the transcellular transducers of the signals, and intracellular circuits that translate these signals into action. Self-sufficiency enables cancer cells to synthesise growth factors to which they are responsive, thus creating a positive feedback signalling loop resulting in autocrine stimulation. Additionally, growth signal receptors normally harbour tyrosine kinase activities in their cytoplasmic domains, and

these receptors are overexpressed in many cancers, enabling the hyper-responsiveness of cancer cells and promoting cell proliferation[3].

Insensitivity to anti-growth signals: Normal tissues have multiple anti-proliferative signalling activities, including soluble growth inhibitors and immobilised inhibitors embedded in the extracellular matrix to maintain cellular quiescence and homoeostasis. Blocking of cell proliferation activates two distinct anti-growth signal phenotypes. First, cells may be forced out of the active proliferative cycle into the quiescent (G0) state. Second, cells can permanently turn over their proliferative potential by being induced to enter post-mitotic states, that are usually related to the acquisition of specific differentiation-associated traits. However, cancer cells are not sensitive to anti-growth signals and evade these anti-proliferative activities. An example is the disruption of the retinoblastoma protein (pRB) pathway, which liberates E2Fs and allows cell proliferation to occur. At the molecular level, many anti-proliferative signals are funnelled via pRB and its two relatives p107 and p130. In its hypophosphorylated state, pRB blocks proliferation by sequestering and altering the function of E2F transcription factors that control the expression of genes associated with the cell cycle clock[3].

Evading Apoptosis: The expansion of tumour cell populations depends on the rates of cell proliferation and cell attrition. Programmed cell death via apoptosis is a major mechanism that contributes to cellular attrition. The cellular apoptotic machinery

can be grouped into two distinct classes of components, i.e., sensors and effectors. Sensors monitor the signals from the extracellular and intracellular environment for the prevalence of normal or abnormal conditions and decide whether a cell lives or dies. These signals are responsible for the second class of components, i.e. the apoptotic death-related effectors. As apoptosis is a major barrier to cancer cells, they acquire the ability to resist apoptosis using several strategies, the most common being the loss of a proapoptotic regulator through mutations involving *TP53*. The functional inactivation of p53 removes key components of the DNA damage sensor that may induce the apoptotic effector cascade in cancer cells[3].

Limitless Replicative Potential: Cells in culture have finite replicative potential and stop proliferating after a certain number of doublings. On average, human cell types have the capacity for ~70 doublings. Over the past decade, components for counting for cell generation have been identified and include the ends of chromosomes and telomeres. The loss of telomeric DNA from the ends of chromosomes is associated with cellular replication, and telomere maintenance is present in virtually all types of cancer cells, as these upregulate the expression of the telomerase enzyme to permit unlimited cellular replication[3].

Sustained angiogenesis: Oxygen and nutrients supplied by the vasculature are crucial for cellular function and survival. The process of angiogenesis is transitory and carefully regulated after tissue formation. In many human cancers, the induction of

angiogenesis occurs at an early to mid-stage during tumorigenesis. Neovascularization is a prerequisite for the rapid cellular clonal expansion associated with the formation of macroscopic tumours. By controlling the balance of angiogenesis inducers and the countervailing inhibitors, tumours can self-activate the angiogenic switch by commonly occurring strategies such as the alteration of gene transcription. The expression of the vascular endothelial growth factor (VEGF) and the acidic and basic fibroblast growth factors (FGFs) is upregulated in multiple cancer types[3].

Tissue invasion and metastasis: Metastases can result in chemotherapy failure and death. They are characterized by the migration of pioneer primary tumour cells, the invasion of adjacent tissues, travel to distant sites, and the seeding of new colonies. The capability for invasion and metastasis enables cancer cells to colonise other tissues and organs causing extensive tumour growth. Tumour invasion and metastasis are complex processes, and a variety of related proteins such as E-cadherin are involved. E-cadherin is a homotypic cell-to-cell interaction molecule that is ubiquitously expressed on epithelial cells and functions as a suppressor of invasion and metastasis in epithelial cancers. Additionally, E-cadherin is associated with the 'epithelial-mesenchymal transition' (EMT) regulatory program. During the EMT, transformed epithelial cells acquire the ability to invade tissues, resist apoptosis, and disseminate. Various transcription factors induced by EMT orchestrate most steps in the invasion-metastasis cascade, thus regulating invasion and metastasis[4].

Genome instability and mutation: The genome maintenance systems detect and resolve DNA defects and ensure that the rates of spontaneous mutation are low during cell generation in normal cells. The DNA-maintenance machinery performs several processes such as the detection of DNA damage and activation of the DNA repair machinery, repairing of damaged DNA, and the inactivation of mutagenic molecules. During tumorigenesis, genome maintenance systems are impaired[4].

Tumour-Promoting Inflammation: In many cancer types, tumour-associated inflammatory responses have the unanticipated and paradoxical effect of enhancing tumorigenesis and cancer progression, permitting incipient neoplasia to acquire various capabilities that are a hallmark of cancer. By supplying bioactive molecules to the tumour microenvironment, the inflammation response processes contribute to multiple capabilities, and include growth factors that sustain proliferative signalling, survival factors that limit cell death, proangiogenic factors, extracellular matrix-modifying enzymes that facilitate angiogenesis, invasion, and metastasis, and inductive signals that lead to the activation of EMT and other cancer hallmark-facilitating programs[4].

Reprogramming energy metabolism: In aerobic conditions, glucose metabolism in normal cells includes the formation of pyruvate via glycolysis in the cytosol, and the formation of carbon dioxide in the mitochondria. Glycolysis is favoured, and relatively little pyruvate is despatched to the oxygen-consuming mitochondria. Interestingly, cancer cells can reprogram glucose metabolism even in the presence of oxygen, and

cellular energy production leads to a state of 'aerobic glycolysis' by predominantly limiting energy metabolism to glycolysis. Two energy-generating pathways have been identified that contribute to cancer glucose metabolism: lactate production and import by glucose-dependent cells and its utilisation as their main energy source, with the process involving a part of the citric acid cycle. The redirection of energy metabolism pathways in cancer cells results due to the instability and chaotic organisation of the tumour-associated neovasculature[4].

Evading Immune Destruction: In normal cells, the immune system monitors cells and immune surveillance contributes to the recognition and elimination of the vast majority of incipient cancer cells and nascent tumours. Tumours have been shown to avoid immune system detection or acquire the ability to limit the extent of immune-system dependent killing and subsequently evade eradication. Cancer cells evade immune destruction by disabling components of the immune system such as paralysis of infiltrating cytotoxic T cells (CTLs) and natural killer (NK) cells through the secretion of transforming growth factor-beta (TGF-ß) or other immunosuppressive factors. Cancer cells can also avoid immune destruction through the recruitment of immunosuppressive cells. Regulatory T cells (Tregs) and myeloid-derived suppressor cells (MDSCs) are the main immunosuppressive cells during the immune destruction-mediated escape of cancer[4].

Figure 1.1 The hallmarks of cancer

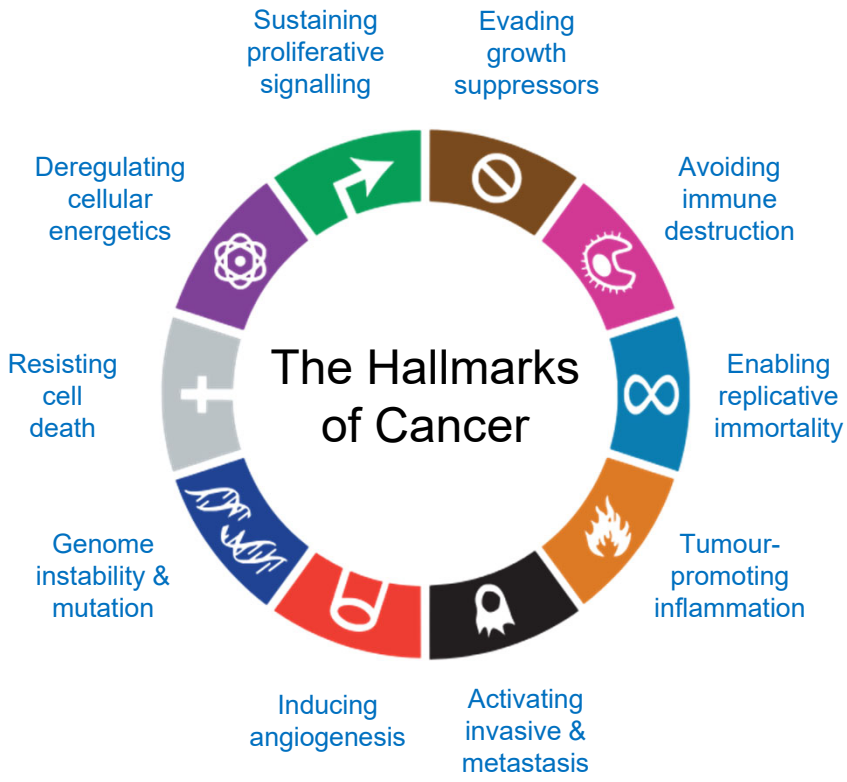


Figure 1.1 The hallmarks of cancer. The figure summarizes the ten capabilities shared by most cancers, including self-sufficiency in growth signals, insensitivity to growth-inhibitory (anti-growth) signals, evasion of programmed cell death (apoptosis), limitless replicative potential, sustained angiogenesis, tissue invasion and metastasis, genome instability and mutation, tumour-promoting inflammation, reprogramming energy metabolism, and evasion of immune destruction[3,4].

1.3 Proto-oncogenes and tumour suppressor genes

Proto-oncogenes operate as growth regulators in normal cells, causing these to become cancerous when the genes are activated[5]. Dysregulation of proto-oncogenes can lead to uncontrolled cell growth and dysfunctional signal transduction, resulting in the occurrence of cancer[6]. Examples of proto-oncogenes includes *RAS*[7], *MYC*[8], and *ERK*[9]. Oncogenes are activated proto-oncogenes, dysregulated, or mis-expressed genes that contribute to cancer. An oncogene encodes oncoproteins, which play an important role in tumorigenic cell growth[6].

Proto-oncogenes can be activated to become oncogenes via three basic modes. First, a mutation in a proto-oncogene or within a regulatory region may change the structure of the encoded protein, which may cause a change in the protein activity and result in a loss of regulation. Second, the accumulation of the encoded protein in cells breaks down its stability and deregulates its activity. Third, it may lead to a chromosomal translocation in cells, creating a fusion between a proto-oncogene and another gene, leading to an increase in oncogenic activity[6,10].

Unlike the cellular proliferation-stimulating function of proto-oncogenes and oncogenes, tumour-suppressor genes protect cells from carcinogenesis by encoding proteins with the opposite function[10]. Mutation of a tumour suppressor gene causes a loss or reduction in its function, disrupts cellular homoeostasis, and causes cells to

progress to cancer. The functions of tumour suppressor genes can be classified into several categories i.e., affecting the cell cycle and inhibiting cell division, driving the cell cycle to DNA damage response, initiating cellular apoptosis, inhibiting metastasis of tumour cells, and encoding DNA repair proteins[10,11]. For example, *the TP53* gene encodes p53, which activates DNA repair and arrests cellular growth at the G1/S regulatory checkpoint for DNA damage recognition, and plays an important role in the regulation of cell cycle progression, apoptosis, and the maintenance of genomic stability[12].

Oncogene overexpression drives cancer initiation and regulates the maintenance of the cancer phenotype[13]. Therefore, oncogenes are ideal targets for anti-tumour therapies. Successful examples include the targeting of *BCR-ABL* by imatinib*, EGFR* by gefitinib, and *HER2* by trastuzumab[14,15]. In contrast to the clinical success with small molecules targeting oncogenes, the pharmacological exploitation of tumour-suppressor mutations is more difficult. It is difficult to use a small molecule to restore or mimic the function of a protein that is either mutated or absent due to the lack of a target positive signalling pathway[16]. It may be possible to find clinically relevant compounds that target oncogenes by directly comparing target tumour-suppressor mutations. An example is the cyclin-dependent kinase (CDK) inhibitor. The loss of Rb, p16, p21, or p27 leads to the upregulation of CDK activity which controls the cell cycle.

Tumours with the loss of these suppressors may be controlled by the use of CDK inhibitors[17].

1.4 The cell cycle

The cell cycle or cell-division cycle involves a series of events that causes cells to divide into two daughter cells after DNA replication and division of the cytoplasm. Each daughter cell continues the interphase of a new cycle after cell division. The cell cycle consists of four distinct and sequential phases: the G1 (growth) phase, S phase (synthesis), and G2 (growth) phase together constituting the interphase, and the M phase (mitosis), followed by cytokinesis (division of the cell into two identical daughter cells) for the nuclear and cytoplasmic division of the cells, respectively[18]. Several signals impinge on cells to commit them to a round of growth and division, or to become temporarily quiescent. The activation of each phase is dependent on the proper progression of the cell cycle and the completion of the previous phase. After a cell divides, the daughter cells accumulate nutrients and undergo DNA replication in preparation for the next round of mitosis (Figure 1.2) [18].

G0 phase (quiescence): Cells in the G0 phase have stopped dividing (are quiescent), and have temporarily exited the cell cycle. Fully differentiated cells normally enter the G0 phase from G1 where they stay for long periods. Some cells enter the G0 phase semi-permanently, for example, certain liver and kidney cells, and others do not enter the G0 phase and continue the cell cycle, such as epithelial cells[19].

G1 phase: The G1 period is the first part of the interphase, and includes the gap

phase between the end of mitosis and the beginning of DNA synthesis. Cells in the G1 phase synthesise mRNA and proteins in preparation for mitosis. The duration of G1 is highly variable and differs between species and the cell types in the same species. Cells in the G1 phase may continue to the S phase, re-enter the G0 phase, or become arrested in the G1 phase. The deciding or restriction mechanism that decides whether the cell remains in the G1 phase is called the checkpoint. Additional checkpoints are present for transition to other phases[19].

S phase: The S phase commences from the beginning of its DNA duplication and the chromosomes are replicated in this phase[19].

G2 phase: The G2 phase comes after DNA duplication and is used for the synthesis of proteins for mitosis. Microtubules start to reorganise and form spindles during this phase. Cells in this phase must cross the G2 checkpoint to enter mitosis[19]. If DNA damage occurs, the G2 checkpoint activates the DNA damage response, triggering cellular apoptosis or the DNA damage repair machinery. The p53 regulatory protein, encoded by *TP5*3, is mainly responsible for the regulation of the G2 checkpoint. Mutations in *TP53* may cause p53 to be dysfunctional, and the G2 checkpoint may be unable to trigger the DNA damage response or the apoptosis pathway[20]. Cells with damaged DNA continue through the cell cycle and drive the process of cancer.

Figure 1.2 A summary of the cell cycle

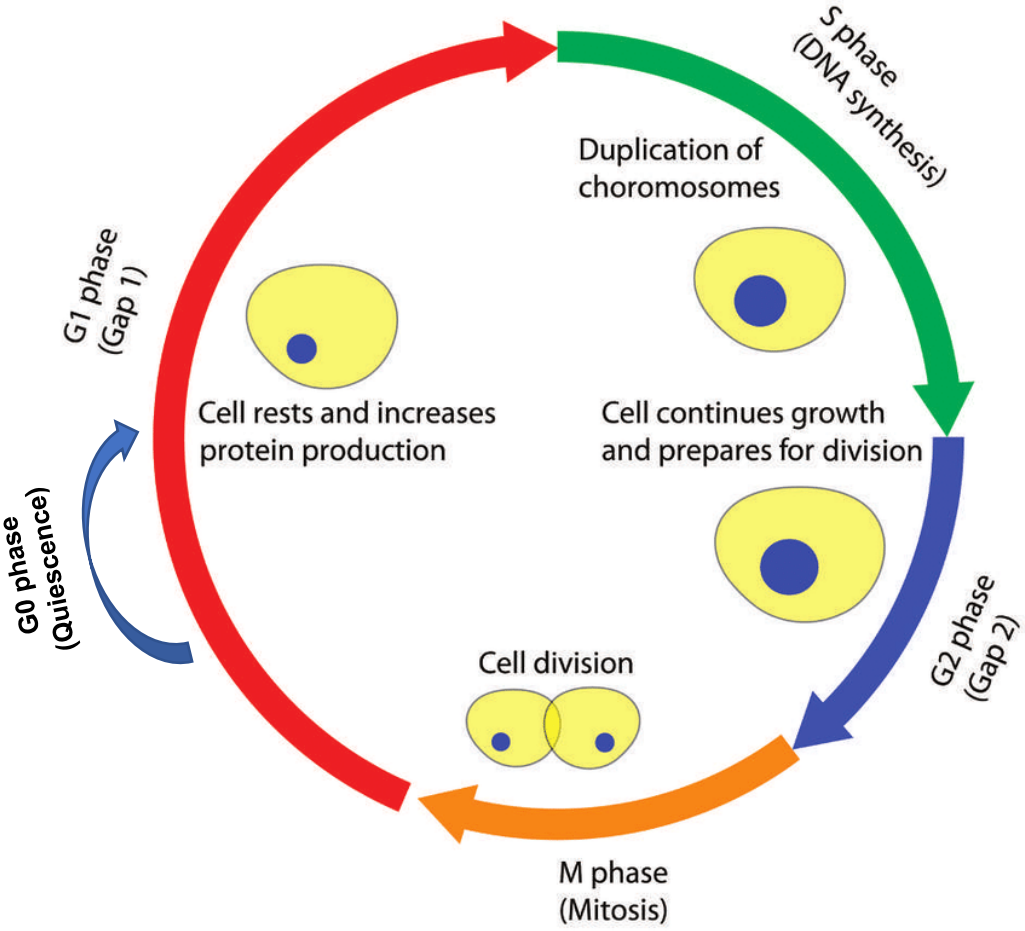


Figure 1.2 A summary of the cell cycle. The cell cycle consists of four distinct and sequential phases: the G1, S, G2, and M phases, followed by cytokinesis. Cells are activated by multiple signals before committing to a round of growth and division, or to become temporarily quiescent and enter the G0 phase[18,19].

1.5 Cyclin-dependent kinases (CDKs)

The regulatory restriction points of the cell cycle are associated with CDKs and their partner cyclins. There are 21 serine/threonine protein kinases classified as CDKs[21]. Several aspects of cell growth, proliferation, and transcriptional regulation in response to extracellular and intracellular signals are regulated by CDKs that play specific or redundant roles in these processes[22-24].

The kinase activity of CDKs depends on their binding with a regulatory protein cyclin. CDKs have low kinase activity without activation by cyclins[24,25]. Therefore, the cyclin-CDK complex alone forms an active kinase. The four major mechanisms involved in regulation by CDKs are cyclin binding, CDK-activating kinase (CAK) phosphorylation, regulatory inhibitory phosphorylation, and binding of CDK inhibitory subunits[25].

CDKs have a modified ATP-binding site with a cleft between a small amino-terminal lobe and a larger carboxy-terminal lobe. Without cyclin, a flexible loop blocks the ATP-binding site. Additionally, the position of key amino acid residues does not permit ATP binding. With the binding of cyclin, two α-helices change the position of key amino acid residues and rearrange the flexible loop, enabling access to the active site[23,25]. In addition to cyclin binding, the cyclin-CDK complex requires activation by phosphorylation to optimise its kinase activity[26,27]. Another regulatory mechanism is

the modulation of CDKs via inhibitory phosphorylation of their catalytic subunit[23,25-27]. For example, the Wee1 and Cdc25 kinases can inhibit entry into mitosis by the addition of an inhibitory phosphate on various proteins, and the Cdc25 phosphatase can alleviate this inhibition and promote entry into mitosis, thereby coordinating cellular growth and division at the G2/M transition[28-30]. CDK inhibitors (CKIs) also regulate the cyclin-CDK complex[31]. CKIs block kinase activity during G1, in response to signals from the environment, or damaged DNA through interaction with the cyclin-CDK complex[32,33]. Two major CKI gene families have been identified: the INK4 family and the CIP/KIP family[34,35]. The INK4 gene family encodes the $p16^{INK4a}$, $p15^{INK4b}$, $p18^{INK4c}$, and $p19^{INK4d}$ regulators, all of which bind to CDK4 and CDK6 and inhibit their kinase activities by interfering with their association with D-type cyclins[36-39]. The CIP/KIP family members $p21^{Cip1/Waf1}$ (p21, encoded by *CDKN1A*), $p27^{Kip1}$ (p27, *CDKN1B*), and $p57^{Kip2}$ (p57, *CDKN1C*) share a conserved N-terminal domain that mediates binding to cyclins and CDKs but diverge in the remainder of their sequence, suggesting that each of these proteins could have distinct functions and cell cycle regulation. CKIs of the CIP/KIP family bind to both cyclin and CDK subunits and can modulate the activities of cyclin D-, E-, A-, and B-CDK complexes[40,41].

CDKs play an important role in the initiation and progression of cancer. The deregulation of cell cycle control results in sustained proliferation, which is a key hallmark of cancer[4]. For example, CDK4 and CDK6 have a specific preference for the

phosphorylation of the tumour suppressor retinoblastoma protein (pRB). The phosphorylation of pRB by CDK4/6 initiates an intricate process of phosphorylation-mediated disruption of pRB function that releases E2F. E2F proteins control the expression of a multitude of positive-acting factors that are critical for progression through the S phase and the G2-M transition[25,42]. CDK4/6 also phosphorylates the transcription factor FOXM1 which is required for the expression of key genes such as *CCNE1*, *CCNE2*, and *E2F2* that regulate G1/S phase progression[25,43].

CDKs are considered a potential target for anti-cancer therapy due to their role in the cell cycle[44-47]. CDK inhibitors such as seliciclib have been shown to induce cellular apoptosis and mediate inflammation[48]. Palbociclib, a selective inhibitor of CDK4/6, has been approved for the management of oestrogen receptor-expressing metastatic breast cancer in combination with endocrine therapy[49,50]. Overall, abnormal CDK function drives cancer cell proliferation, resistance to therapy, and carcinogenesis.

1.6 Invasion and metastasis

Metastasis was first defined by Dorland as the transfer of disease from one organ or part to another not directly connected with it[51]. Invasion and metastasis are identified as distinguishing characteristics of cancer in Hanahan and Weinberg's classic review[3]. Therapeutic failures in metastasis result due to multiple secondary tumour growths and not necessarily because of primary tumours. Metastasis is the major cause of treatment failure in cancer patients and of cancer-related deaths[52].

The migration of cancer cells from a primary tumour to its colony sites involves a series of complex biological steps. After primary tumour formation, cancer cells localise invasiveness and enable carcinoma cells present *in situ* to invade the basement membrane, and subsequently, cells may intravasate into the lymphatic or blood microvessels. Cancer cells are transported through the general circulation to distant anatomical sites and tissues, where they become trapped. The trapped cancer cells subsequently extravasate and form dormant micrometastases, and the newly formed micrometastases can eventually acquire the ability to colonise the tissue, thereby forming macroscopic metastasis and causing the colonization of tissues[52].

EMT plays a crucial role in tumour metastasis, and enables polarised epithelial cells to assume a mesenchymal cell phenotype through a series of biochemical changes that include enhanced migratory capacity, invasiveness, elevated resistance to

apoptosis, and greatly increased production of extracellular matrix (ECM) components[53,54]. EMT is executed by EMT-activating transcription factors (EMT-TFs) mainly from the SNAIL[55], TWIST[56], and ZEB families[57], enabling carcinoma cells to become invasive and causing an increase in cancer cell motility, leading to their dissemination[58]. EMT-TFs can be activated in the vast majority of tumour types, including non-epithelial tumours[59]. Two extreme variants of progression towards metastasis are driven by EMT-TFs: a route with phenotypic plasticity and a genetic route. Almost all tumour cells use an EMT-TFs induced programme to different extents[60].

The aberrant regulation of cancer cell migration drives invasion and metastasis, which is required for many biological processes, such as embryonic morphogenesis, immune surveillance, tissue repair, and regeneration[61-63]. Cell motility involves the continuous restructuring of the actin cytoskeleton in different parts of a cell as well as the construction and disconnection of the attachments between migrating cells and ECM[63]. A group of Ras-related proteins controls the detailed management of cellular shape and motility. Rho proteins, such as Ras, operate as binary switches, being functionally active while binding GTP and becoming inactive once they hydrolyse their bound GTP to GDP[64,65].

1.7 An overview of cortactin

Cortactin is encoded by the *CTTN* gene and maps to chromosome 11q13[66]. It is known to be a prominent substrate for several non-receptor protein tyrosine kinases, including Src, Fer, and Syk[66,67]. Cortactin has a unique structure that consists of four major domains: the N-terminal acidic, 6.5 tandems repeat, proline-rich domain, and C-terminal Src homology 3 (SH3) domains[67] (Figure 1.3). The N-terminal acidic domain plays a role in binding and activating the actin-related protein (Arp) 2/3 complex. The Arp2/3 complex is a seven-subunit complex and plays a central role in the formation of filamentous actin (F-actin)[68]. The subsequent 6.5 tandems repeat structure contains a series of six complete 37-amino-acid tandemly repeating segments and one incomplete segment 20 residues in length, mediating cortactin binding to F-actin. Between the repeat and SH3 domain lie an α-helical region, a proline-rich domain that is enriched in sites of tyrosine, serine/threonine phosphorylation residues[66]. Cortactin also contains a SH3 domain at the distal C-terminus that mediates the interaction with proteins involved in multiple cellular processes, including endocytosis, lamellipodial protrusion and cell migration[69,70].

The principal function of cortactin is to activate the actin cytoskeleton assembly via promoting and stabilising the branched chained F-actin networks induced by the Arp2/3 complex[67]. As a prominent factor in the formation of branched F-actin, the Arp2/3 complex links cortactin to the polymerisation of actin during cell motility

through its direct interaction with cortactin[66]. Cortactin also binds to several cytoskeletal proteins through its SH3 domain and is directly involved in lamellipodial protrusion and cellular migration[67]. Several SH3 domain-binding partners have been identified, including Neural WASP (N-WASP), WASP-interacting protein (WIP), and dynamin 2. These proteins bind to the SH3 domain and promote the ability of cortactin to activate the Arp2/3 complex[71].

Recent studies have focused on the post-translational modifications (PTMs) of cortactin, including phosphorylation and acetylation. PTMs of cortactin activate the Arp2/3 complex and recruit cortactin-binding partners through interactions with Src homology 2 (SH2) domains, which positively modulates its capability to lead to cell migration[72]. Src kinase phosphorylates cortactin at three tyrosine residues, including Y421, Y466, and Y482[73]. Tyrosine phosphorylation triggers the recruitment of SH2 domain proteins and the cytoplasmic protein Nck adaptor protein 1, which links cortactin with N-WASP and WIP, enhancing the activation of the Arp2/3 complex[74]. In addition to phosphorylation, cortactin activity can also be modulated by acetylation by histone acetyltransferase p300 and deacetylation by histone deacetylase 6 (HDAC6). Acetylation neutralises charged lysine residues within the binding domain of F-actin, thereby abrogating the capability of cortactin to bind to F-actin and decreasing cellular motility. HDAC6 enhances the binding capacity of cortactin to actin filaments via modifying a charge patch in the repeat domain[75].

Cortactin also stimulates the endurance of invadopodia and induces the formation of the protrusions[76]. As important actin-based membrane protrusions, invadopodia are involved in the assembly of branched actin, cell adhesion and protease secretion that spatially converge to promote ECM remodelling. Podosomes are similar to invadopodia, which play a role in crossing tissue barriers or ECM remodelling. Evidence has shown that cortactin improves the capability of the cells to produce dominant invadopodia in response to stimulation of growth factors. Moreover, cortactin phosphorylation via Src kinase is required for the formation of podosomes mediated by cortactin. Cortactin is also crucial for the formation of podosomes as an intact SH3 domain is necessary for cortactin transposition to early podosomes[67,76].

The overexpression of cortactin has been observed in multiple cancers, including head and neck squamous cell carcinoma[77], oral squamous cell carcinoma[78], lung squamous cell carcinoma[79], gliosarcoma[80], breast cancer[81], colorectal cancer[82] and melanoma[83]. Cortactin is crucial for cancer cell invasion and metastasis as it promotes membrane trafficking and recruits ECM-degrading proteinases to invadopodia sites; thereby, cortactin plays an essential role in the process of ECM degradation associated with invadopodia[67,72,84]. Tyrosine phosphorylation of cortactin correlates strongly with the aggressiveness of cancer cells and has been demonstrated to promote metastasis in a mouse model, whereas inhibition of phosphorylation decreases cancer cell metastasis[84].

In summary, the actin-nucleation-promoting factor cortactin has emerged not only as a crucial regulator of actin cytoskeletal dynamics, but also as a key player in cancer cell invasion and metastasis[72]. However, more insight is required to clarify the functions of cortactin. For example, the exact functions of cortactin phosphorylation in tumour progression and numerous binding partners of cortactin during cell metastasis remain unclear. The context of these protein-protein interactions and PTMs requires further studies.

Figure 1.3 Schematic diagram of cortactin's primary structure

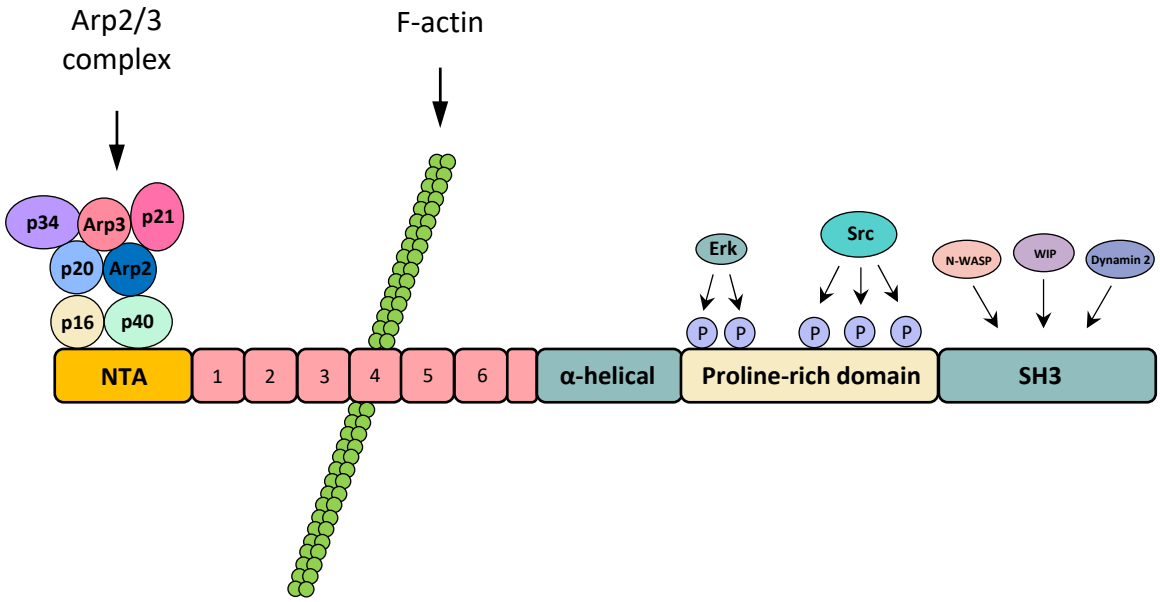


Figure 1.3 Schematic diagram of cortactin's primary structure. The amino terminus of cortactin harbors a domain rich in acidic amino acids (N-terminal acidic domain; NTA) that interacts with the seven subunit Arp2/3 complex. Cortactin has a central domain with 6.5 repeats of a 37-residue long sequence that binds F-actin. This domain is followed by a α-helical region and a proline-rich region, containing phosphorylation sites for the tyrosine and serine/threonine kinases Erk and Src. The carboxy-terminal SH3 domain of cortactin mediates binding to cytoskeletal, membrane trafficking, and signaling proteins[66-70].

1.8 An overview of E2F family members

E2F transcription factors were first identified as proteins that bind to the promoter of the adenoviral gene E2[85]. The E2F family has eight members from E2F1 to E2F8[86]. Additionally, DP-1 and DP-2 share conserved DNA-binding and dimerisation domains with E2F1-6, and form functional transcription factors that bind to downstream gene promoters via their consensus binding sites. As the DP proteins activate transcriptional activity indirectly by potentiating the activity of E2Fs, the function of the E2F-DP heterodimer is determined primarily by E2Fs[86,87].

Both sets of E2Fs have similar domains (Figure 1.4). E2F1-6 contains a conserved DNA-binding domain and a dimerisation domain, and E2F1-5 has a C-terminal transactivation domain, which provides an interface for interaction with RB and the two pocket-protein family members p107 and p130[88]. E2F1-3 shares a nuclear localisation signal (NLS) at its N-terminus, and the NLS is absent in E2F4 and E2F5, which contain a nuclear export signal (NES) instead. E2F7 and E2F8 do not contain pocket and DP protein binding domains and appear to associate with DNA using two separate DNA-binding domains[89].

The E2F family members can be classified as transcription activators and repressors depending on the effects on the cell cycle. E2F1, E2F2, and E2F3a promote the cell cycle and are transcriptional activators. In contrast, transcriptional repressors

such as E2F3b and E2F4-8 inhibit the cell cycle[88,89]. Cell cycle progression is regulated by the balance between the two components[89]. E2F1 has a pRB binding domain at its carboxy-terminal region through which the RB family of proteins bind to E2F and negatively regulate their transcriptional activity[88]. Activator E2Fs predominantly interact with pRB, E2F4 binds to all pRB members, and E2F5 preferentially associates with p107 and p130. E2F4-5 functions mainly to facilitate cell cycle exit and terminal differentiation by recruiting pocket proteins to E2F-regulated promoters. Besides, E2F4 forms part of the p130-E2F4 complex, which participates in the G2/M checkpoint in the DNA damage response[89]. E2F6 represses transcription through its association with the Polycomb group (PcG) of proteins[89,90]. The repressors E2F7 and E2F8 are atypical E2F family members with unique structural characteristics such as a duplicated conserved E2F-like DNA-binding domain instead of a DP1, 2-dimerization domain[88,89]. Depletion of E2F7 or E2F8 drives abnormal trophoblastic proliferation accompanied by advanced cellular apoptosis in animal models. Phenotypically, this causes the placenta to show disruptions in cellular architecture and large clusters of undifferentiated trophoblastic cells, which have lost the capability to invade the maternal decidua. The E2F7 and E2F8 proteins act as repressors independently of interaction with DP[91-96]. Although studies for E2F7-8 are limited, their major functions appear to be associated with repression.

E2F activates transcription via several mechanisms. Through direct interaction

with the basal transcription factors TBP and TFIIH, E2F can enhance the initiation and elongation phase of transcription[97,98]. Further, E2F can activate transcription by its ability to bend DNA, and regulate transcription through its ability to bind other transcriptionally active factors, which augments the level of regulation by E2F[99,100].

E2F family members control the cell cycle by regulating the transcription of a variety of cell cycle-related genes. During the S phase, *CDKN2C* (encoding p18), *CDKN2D* (p19), *CDKN1C* (p57), *E2F7*, *RB1* (pRB), and *RBL1* (p107) are upregulated by the E2F family members[101,102]. Interestingly, the expression of the E2F family members differs during different cell cycle phases. E2F1-3 mRNA and protein levels are undetectable in quiescent cells but are induced in the G1/S phases[103-106]. The E2F4-5 mRNA and proteins are expressed in quiescent cells and remain at constant levels throughout the cell cycle[107,108]. Further, during the cell cycle, the expression levels of DP1 and DP2 do not vary significantly[109,110].

E2F family members play a critical role in regulating cell growth and apoptosis[92]. Researchers have found that induction of apoptosis is a unique property of E2F1, as overexpression of other E2Fs is unable to induce apoptosis[112], while others have shown that E2F2 and E2F3 possess the ability to cause cellular apoptosis as the overexpression of E2F1, E2F2, and E2F3 drives quiescent cells into the S phase[113,114]. In animal models and tissue culture studies, E2F can induce apoptosis in both p53-dependent and p53-independent manner, and can stabilise p53 via the transcriptional induction of the

p14/Arf complex. P14/Arf binds directly to MDM2 and inhibits its ability to degrade p53, thereby maintaining the cellular level of p53[115]. In addition, E2F1 directly up-regulates the expression of p53 apoptotic cofactors, including ASPP1, ASPP2, JMY, and TP53INP1[116]. E2F1 can also activate many apoptotic genes that are not directly related to p53 pathways in a p53-independent manner. In cells lacking p53, *p73* has been shown to play a crucial role in E2F-induced cellular apoptosis[117]. Another mechanism involves the inhibition of antiapoptotic signalling, specifically the tumour-necrosis factor receptor-associated survival response[118]. Further, E2F1 also directly activates the expression of the apoptosis protease-activating factor 1 (*Apaf-1*) gene[119]. In addition to *p73* and *Apaf-1*, E2F1 also transcriptionally induces other genes implicated in apoptosis, such as the BH3-only proteins PUMA, BIM, NOXA, Hrk/DP-5, and several caspase family members such as CASP-3, CASP-7, CASP-8, and CASP-9[86,120,121]. Moreover, E2F1 induces apoptosis via survival signalling pathways, such as the cell survival regulator NF-κB and the anti-apoptotic Bcl-2 family members, including Bok, Bad, Bak, and Bid1[122,123]. Figure 1.5 shows a summary of E2F1 induced apoptotic pathways.

E2F mediates the DNA damage response in various cancer cell lines, and the deregulation of E2F1 sensitises tumour cells to apoptosis induced by DNA damaging agents[114,120,121]. In addition, E2F1 protein levels are increased in response to DNA damage due to the activation of the ATM- Checkpoint kinase 2 (Chk2) pathway.

Consequently, Chk2 phosphorylates and activates E2F1, inducing apoptosis[124]. DNA damage itself induces the p300/CREB-binding protein associated factor(P/CAF)-dependent acety- lation of E2F1, and forms a stable protein complex with P/CAF leading to E2F1 accumulation[125]. Furthermore, the increased level of E2F activates DNA damage through the corresponding upregulation of checkpoint kinase 1 (Chk1), which encodes an essential component of the DNA damage signalling pathway, and ensures that DNA replication is completed before entry into the M phase[126,127]. Another mechanism by which E2F1 regulates DNA damage relates to the function of KAP1, which is a nuclear corepressor that interacts with chromatin modification factors such as HDAC1, SETDB1, and HP1. In response to DNA damage, phosphorylated KAP1 stimulates the formation of the E2F1-HDAC1 complex and inhibits E2F1 acetylation, blocking the apoptotic function of E2F1[128].

E2F1 plays an important role in angiogenesis and endothelial cell proliferation via the regulation of VEGF[129,130]. Knocking down the expression of E2F1 in mice leads to an increased level of angiogenesis, endothelial cell proliferation, and reperfusion in a model for hind limb ischaemia that resulted due to elevated vascular endothelial growth factor A (VEGFA) expression. The deficiency of E2F1 is a result of the overproduction of VEGF, which could be prevented by blocking VEGF. In cells, E2F1 downregulates the promoter activity of VEGF via p53[129]. This suggests that there is a promoter structure context-dependent regulatory mechanism that regulates the expression of

VEGF. A recent study showed that the repression of VEGFA transcription occurs through the E2F1-mediated pathway in a p53-independent manner. This effect occurs through the activation of the serine/arginine-rich splicing protein SC35, a splicing factor of VEGFA. E2F1 induces the expression of SC35 and mediates the ratio of proangiogenic versus antiangiogenic isoforms of VEGFA. These results have been verified in an *in vitro* model and nude mice. Further, E2F1 may affect the expression of VEGF through the involvement of additional transcription factors and splicing factors[130].

E2F1 plays an important role in tumorigenesis owing to its oncogenic properties, and as a transcription factor, it activates a variety of genes required for S phase entry, DNA replication, and synthesis. Consistent with this, in certain situations the activating E2Fs override various growth-arrest signals, including from TGF-β and the CKIs p16, p21, and p27[89]. Another important pathway is the pRB-E2F1 axis (Figure 1.6). The pRB-E2F1 complex plays an important role in tumorigenesis, as pRB is absent or mutated in at least one-third of all human tumours[131,132]. pRB interacts with E2F1 and blocks the transcriptional activity of E2F1 before the G1/S transition. The ability of pRB to bind to E2F is regulated by its cell-cycle-dependent phosphorylation in untransformed cells[133-135]. In this model, unphosphorylated pRB binds to E2F1 in G0/G1, leading to the dysregulation of E2F1 in G0 and early G1, resulting in the repression of E2F1 downstream target genes. In contrast, as the pocket proteins are

phosphorylated by cyclin D-CDK4/6 and cyclin E-CDK2 in mid-to-late G1, free E2F1 is released, driving the cell into S phase[42,133-135]. The accumulation of free E2F1 triggers the apoptotic response in cells. This model of the pRB-E2F1 complex contributes to essential steps in tumorigenesis[133-135].

E2F1-mediated apoptosis makes E2F1 a therapeutic target for anti-cancer treatment. It has a wide spectrum of therapeutic activity, as E2F1-induced apoptosis is independent of the endogenous status of p16, pRB, and p53[86]. Several compounds can induce E2F1-dependent apoptosis, for example, the HDAC inhibitor TSA or SAHA[136]. Pharmacological inhibition of HDAC selectively activates the proapoptotic Bcl-2 family members, which is related to E2F1-dependent apoptosis[136]. Furthermore, E2F1 contains a cyclin A/CDK2 binding domain, and the pharmacological inhibition of cyclin A/CDK2 enhances E2F1 activity and activates E2F1-related apoptotic pathways[136-138]. Thus, therapeutic approaches aimed at promoting the ability of E2F1 to induce apoptosis provide insight into new potential anti-neoplastic treatments[86].

Although E2F1 may provide a therapeutic option for anti-tumour therapy, several questions remain unanswered. E2F1 is a protein with paradoxical behaviour, as it acts as an oncogene or a tumour suppressor depending on the context. In colon cancer, E2F1 may function as a tumour suppressor. Unlike mutations in most cancer types, pRB in colorectal cancer is rarely mutated. The constant activity of pRB allows E2F1 activity to be maintained at a low level, as it is associated with aggressive phenotypes and poor

disease outcomes[139,140]. Overall, E2F1-dependent apoptosis may be useful in anti-cancer therapy, and its relation to other cancer pathways needs to be demonstrated.

Figure 1.4 The domain structures of the E2F family members

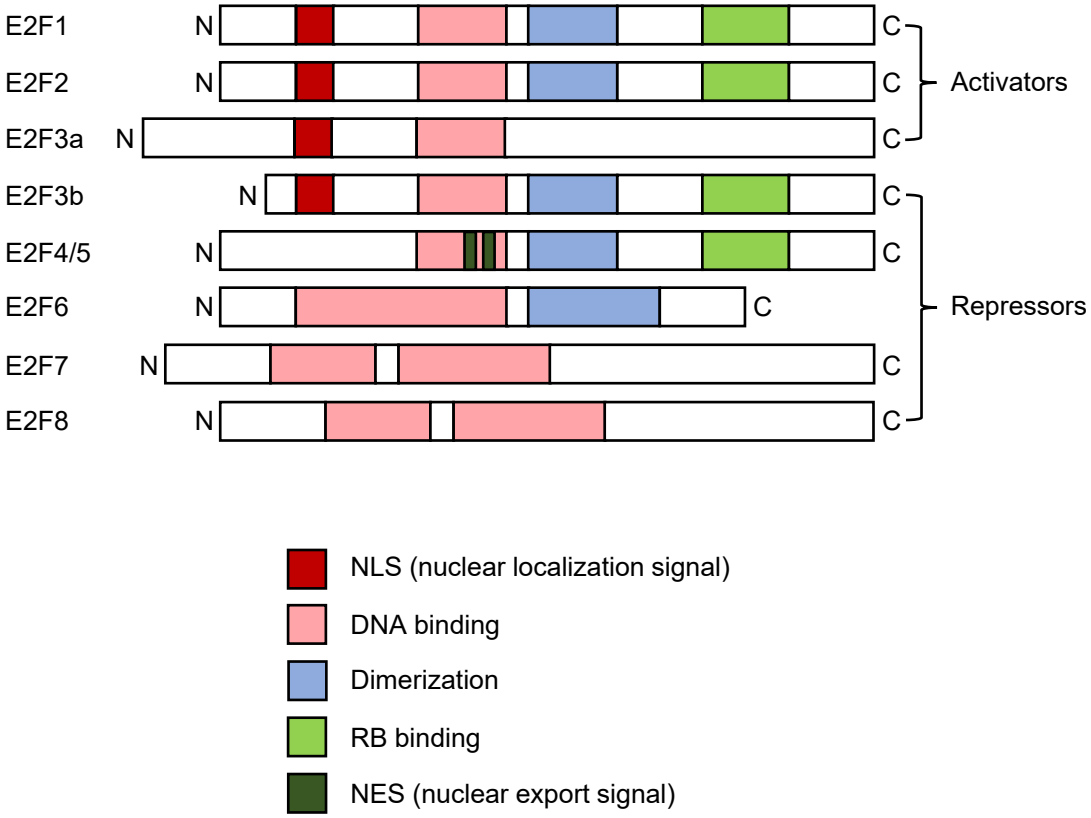


Figure 1.4 The domain structures of the E2F family members. E2F1-6 contains a conserved DNA-binding domain and a dimerization domain. The pocket protein binding domains are present in the C-terminus of E2F1–E2F5 alone. E2F1–E2F3 share a nuclear localization signal (NLS) at their N-terminus, which is absent in E2F4 and E2F5 that harbour a nuclear export signal (NES) instead. E2F7 and E2F8 have two DNA-binding domains and lack transactivation and pocket protein binding domains. The E2F family contains various transcriptional activators and repressors. Activators such as E2F1, E2F2, and E2F3a promote and implement the cell cycle, and repressors such as E2F3b and E2F4-8 inhibit the cell cycle[86-89].

Figure 1.5 Pathways for E2F1-induced apoptosis

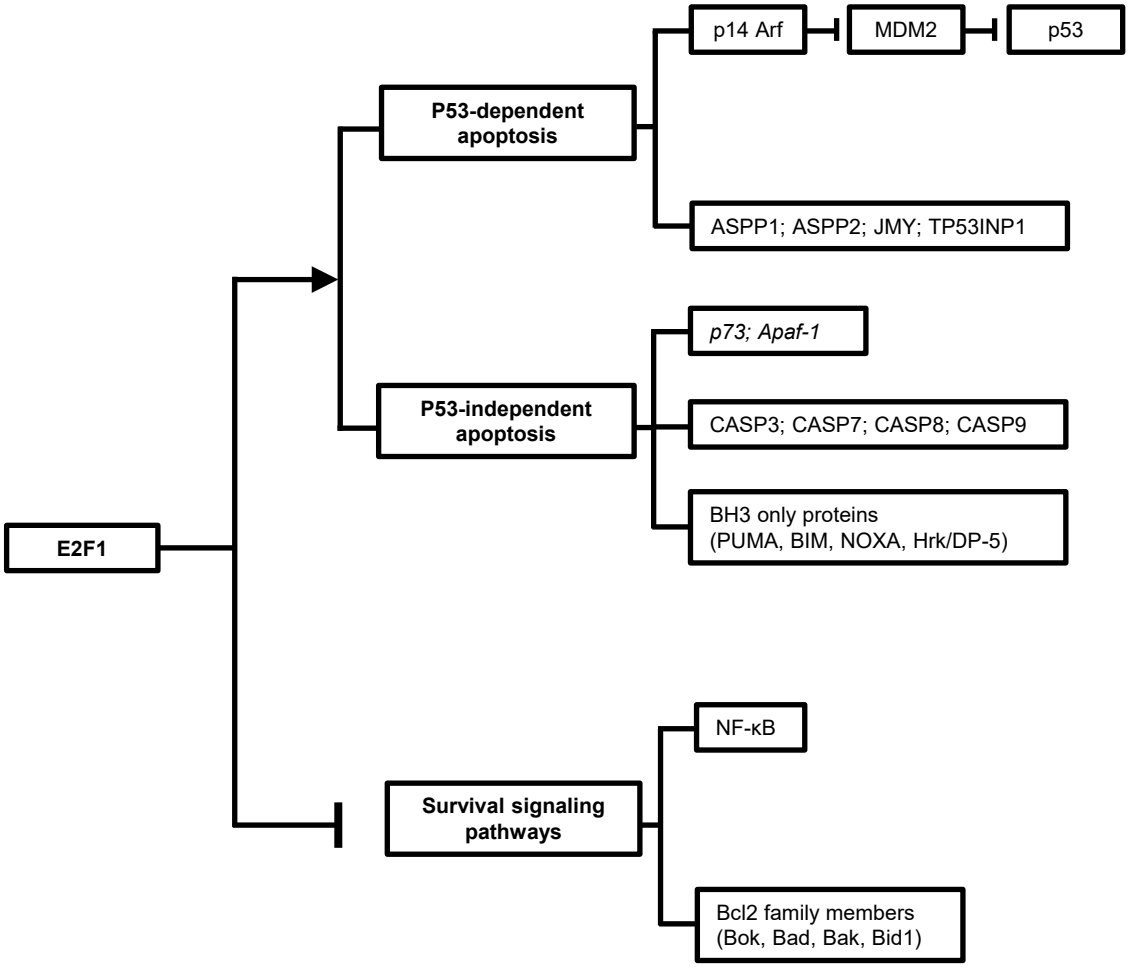


Figure 1.5 Pathways for E2F1-induced apoptosis. E2F1 can induce cellular apoptosis through a p53-dependent pathway, p53-independent pathway, and the inhibition of survival signals to induce apoptosis[111-123].

Figure 1.6 The pRB-E2F1 complexes

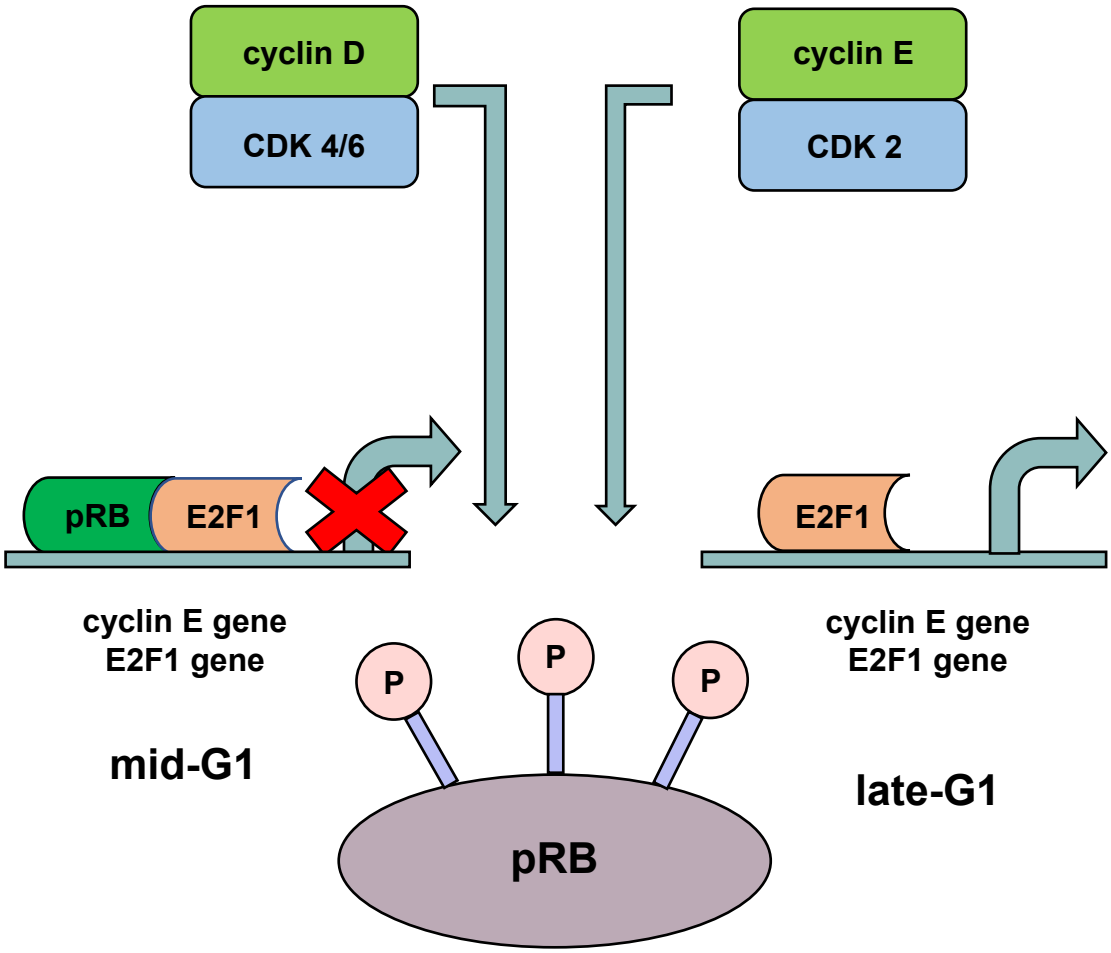


Figure 1.6 The pRB-E2F1 complexes. pRB interacts with E2F1 and blocks its transcriptional activity before the G1/S transition. In untransformed cells, the ability of pRB to bind to E2F is regulated by its phosphorylation in a cell-cycle-dependent manner. In this model, unphosphorylated pRB binds to E2F1 in G0/G1, leading to the dysfunction of E2F1 in G0 and early G1, causing the repression of E2F1 downstream target genes. However, as the pocket proteins are phosphorylated by cyclin D-CDK4/6 and cyclin E-CDK2 in mid-to-late G1, free E2F1 is released, driving the cell into the S phase. The model of the pRB-E2F1 complex shows its contribution to essential steps in tumorigenesis[42,131-135].

1.9 Protein arginine methyltransferases (PRMTs)

Arginine methylation is a common PTM, with ~2% of arginine residues showing methylation in rat liver nuclei[141]. The modification is implemented by a family of PRMTs, which contain nine PRMTs and are classified into three types. The classification depends on the ability to transfer one or two methyl groups to the nitrogen atoms of the guanidinium side chains of arginine residues using S-adenosylmethionine (SAM) as the methyl donor, resulting in three types of methyl arginine species: ω-NG-mono-methylarginine (MMA), asymmetric ω-NG, ω-NG-dimethylarginine (ADMA), and ω-NG,N'G-symmetric dimethylarginine (SDMA) (Figure 1.7)[141-145].

PRMT1 and PRMT5 are the primary enzymes responsible for asymmetric and symmetric demethylation[141,146,147]. Knockout mice lacking *PRMT1* and *PRMT5* die very early, whereas *PRMT2*, *PRMT3*, and *PRMT6* knockout mice are viable, suggesting that the *PRMT1* and *PRMT5* genes have housekeeping functions[145,147].

Arginine methylation acts as a driving force for the development and aggressiveness of several cancer types, and promotes the progression of tumorigenesis. Dysregulated PRMT expression has been observed in a variety of human malignancies, including lung cancer, breast cancer, prostate cancer, colorectal cancer, bladder cancer, leukaemia, and lymphoma[148-167]. The roles and cancer types related to each PRMT are highlighted in Table 1. Although the dysregulated expression of PRMTs and their

abnormal enzymatic activity are associated with many types of cancers, there are limited functional studies on PRMTs. PRMT1 and PRMT5 are thought to be potentially useful therapeutic targets for anti-cancer therapy, and their selective inhibition has anti-proliferative effects *in vivo* and *in vitro*[144,145,147]. In this study, we have focused on PRMT1 and PRMT5 and their link with cancer.

PRMT1: PRMT1 is a type I arginine methyltransferase that is responsible for generating more than 85% of the asymmetrically dimethylated proteins within cells[146]. Many identified PRMT1 substrates are key regulators of cancer cell growth, survival, and invasion signalling. PRMT1 directly methylates the estrogen receptor α (ERα) at arginine (R) 260. The methylated ERα promotes cancer cell survival and invasiveness through its interaction with Src, focal adhesion kinase (FAK), and the regulatory subunit of PI-3 kinase (p85)[168,169]. PRMT1 drives the DNA damage response and activates DNA repair pathways through its methylation of MRE11 and p53 binding protein 1 (53BP1), which is linked to p53-related pathways[170,171]. In addition, PRMT1 can increase oxidative stress-induced cell death by methylating the forkhead box protein 1 (FOXO1)[172]. PRMT1 is related to Wnt signalling through its methylation of the Axin protein, which increases its stability and decreases β-catenin protein levels, negatively regulates Wnt signalling, and impacts actin cytoskeletal dynamics[173,174]. The tumour suppressor gene *BRCA1* is a substrate of PRMT1. Methylation alters the recruitment of *BRCA1* to specific promoters, thereby affecting cell cycle transcription,

DNA damage response, and chromatin remodeling[174]. PRMT1 was involved in EMT through its substrate histone H4 arginine 3 (H4R3). The methylation of H4R3 at the ZEB1 promoter activates its transcription, thus altering the EMT process by repressing the transcription of E-cadherin[173,175].

Thus, the results from studies indicate that PRMT1 may be a potentially valuable therapeutic target because it has a significant impact on the vital processes involved in the development, progression, and aggressiveness of several cancer types. However, our knowledge of this target is limited, and the biological function of PRMT1 and its link with tumorigenesis requires further study and analysis.

PRMT5: PRMT5 is the major type II arginine methyltransferase. As indicated in Table 1, the overexpression of PRMT5 is associated with multiple cancer types[157-163]. The majority of vertebrate PRMT5 complexes contain MEP50, a 7-blade containing WD40 repeat β-propeller protein which can directly bind PRMT5 and greatly enhance its histone methyltransferase ability, primarily through increased affinity for the protein substrate[176]. The crystal structure of the PRMT5-MEP50 complex has been elucidated (Figure 1.8). The PRMT5 molecules form a tetramer at the centre of the complex, with MEP50 molecules decorating the outer surface and interacting solely with the triosephosphate isomerase (TIM) barrel domains of PRMT5 to form the PRMT54:MEP504 hetero-octameric complex. PRMT5 contains a TIM barrel on the N-terminus, a middle Rossmann-fold, and a C-terminal β-barrel containing a

dimerisation domain. The PRMT5 tetramer forms the core of the complex and MEP50 interacts with PRMT5 through the N-terminal TIM barrel domains. A monomer of human PRMT5 is illustrated in Figure 1.8B, showing the domain structures as well as the locations of the SAM and histone peptide substrates within the crystal[177]. Compared with isolated PRMT5, the extensive and tight PRMT5-MEP50 complex shows increased stability and methyltransferase activity, which constitutes the main functional biological module of PRMT5[176,178,179].

PRMT5 has multiple biological functions and methylates a myriad of substrates, including the histone H3 and H4[163], Sm proteins[180], nucleolin[181], and RAF proteins[182]. Histone arginine symmetric demethylation has been implicated as a repressor during transcriptional regulation[183,184]. As a repressor, the symmetric dimethylation of histone H4 on the R3 residue (H4R3me2s) and the R8 residue of histone H3 (H3R8me2s) represses the tumour suppressor gene *ST7*, cyclin E1, and the cell cycle regulator cyclin-dependent kinase inhibitor 2A (CDKN2A)[184-186].

A growing list of non-histone proteins have been identified as PRMT5 substrates[187]. Examples include NF-κB[188], p53[189], E2F-1[190], homeobox A9 (HOXA9)[191], and RAD9[192,193]. Their functions vary from cell signalling to differentiation, mRNA splicing, among others. PRMT5 is linked to NF-κB signalling through its methylation of NF-κB at arginine 30 (R30)[194]. In the human osteosarcoma cell line U2OS, a complex of PRMT5, Strap, and p53 is formed in response to DNA

damage[189]. *PRMT5* knockdown leads to an increase in DNA damage-induced apoptosis, indicating that arginine methylation is a part of the p53 response. p53 undergoes methylation by PRMT5 at R333, R335, and R337, resulting in cancer cells being unable to induce G1 phase arrest and triggering the p53-dependent DNA damage response[189,195]. PRMT5 induces symmetric arginine methylation at R111 and R113 on the transcription factor E2F, and reduces its ability to suppress cell growth and promote apoptosis[190]. The study also identified a reader causing symmetric methylation. The Tudor domain of the methyl binding protein TSN was identified as specifically binding symmetrically methylated R111 and R113, indicating the manner in which these methylation marks influence E2F1[196]. PRMT5 catalyses the symmetric dimethylation of Arg140 on HOXA9, and mediates cytokine induction through the EC-leukocyte adhesion molecule (ELAM) E-selectin and the vascular cell adhesion molecule 1 (VCAM-1)[191]. PRMT5 also regulates the cell cycle checkpoint through its substrate Rad9, which is methylated on arginines within the RGRR amino acid sequence by PRMT5. The methylation of Rad9 is critical for cellular resistance to hydroxyurea and the activation of the S/M and G2/M cell cycle checkpoints[192,193].

PRMT5 is involved in regulating cellular growth, proliferation, and EMT[197-203]. Knockdown of *PRMT5* is associated with a slowing of cell growth, whereas overexpression leads to cellular hyperproliferation[200,203]. PRMT5 regulates the epidermal growth factor receptor (EGFR)-RAS-ERK signalling axis, and EGFR is

methylated by PRMT5 at its R1175 residue, which enhances phosphorylation of the Y1173 residue, attenuating EGFR-mediated ERK activation. EGFR signalling is augmented by preventing R1175 methylation[197]. The R110 residue of the tumour suppressor protein PDCD4 (programmed cell death protein 4) is another substrate for PRMT5. Co-expression of *PDCD4* and *PRMT5* accelerates tumour growth in an orthotopic breast cancer model[198]. Additionally, PRMT5 promotes EMT through its interaction with the transcription factor SNAIL. PRMT5 interacts with SNAIL through a bridging molecule, AJUBA. The transcription factor SNAIL downregulates the expression of E-cadherin, which is a hallmark of EMT[147,199-202]. Further, PRMT5 may regulate EMT via the EGFR/AKT/β-catenin pathway. In the PaTu8988 and SW1990 cell models, the silencing of *PRMT5* upregulates the expression of E-cadherin and downregulates the expression of mesenchymal markers including vimentin, collagen I, and β-catenin, and the ectopic re-expression of PRMT5 partially reverses these changes[203].

PRMT5 has been shown to regulate splicing events. In one study, multiplexed quantitative proteomics was performed to globally profile PRMT5 substrates, and the new PRMT5 substrate SRSF1 was identified. The biological function of the splicing regulator SRSF1 depends on its methylation status which is dependent on PRMT5[158]. Further, the loss of PRMT5 leads to several changes in alternative splicing events driven by multiple essential genes[193].

Although multiple substrates of PRMT5 have been identified, further studies are required to uncover potentially new substrates to understand the multiple biological roles of PRMT5 in tumorigenesis (Table 2). Moreover, PRMT5 has recently emerged as a promising therapeutic target, and several PRMT5 inhibitors are currently in clinical trials for a range of solid and blood cancers. Thus, large-scale studies and a clearer understanding of the biological roles of PRMT5 are needed for future research.

Figure 1.7 Arginine methylation reactions catalysed by PRMTs

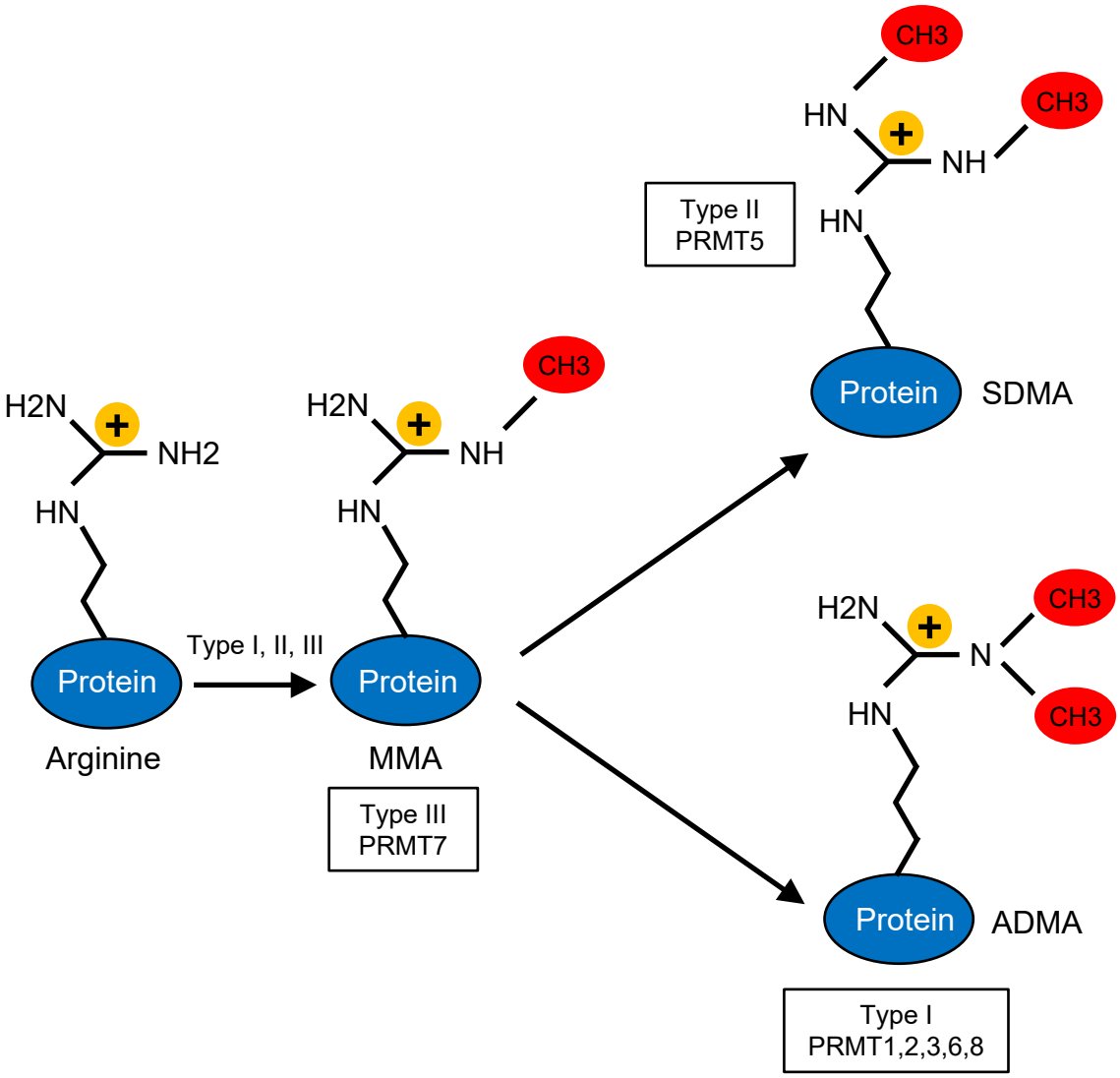


Figure 1.7 Arginine methylation reactions catalysed by PRMTs. Type I, II, and III PRMTs generate monomethylarginine as a first step, followed by asymmetrical dimethylation (Type I) and symmetrical dimethylation (Type II) on the nitrogen atoms of the guanidino group[141-145].

Table 1 PRMTs dysregulation in cancer

PRMT	Cancer type	Role(s) in cancer	Reference
PRMT1	Breast cancer, Lung cancer, Colon cancer, Bladder cancer, Acute myeloid leukemia, Mixed lineage leukemia	Cell proliferation and survival, Transformation, Resistance to DNA damaging agents, Invasion	148,149,150,151
PRMT2	Breast cancer	Cell proliferation and invasion	152,153
PRMT3	Breast cancer	Cell survival	154
PRMT4	Breast cancer, Prostate cancer	Cell proliferation	155,156
PRMT5	Lung cancer, Leukemia, Lymphoma, Breast cancer Melanoma, Gastric cancer, Colorectal cancer	Cell proliferation, Transformation, apoptosis Invasion, Resistance to DNA damaging agents	157,158,159,160, 161,162,163
PRMT6	Lung cancer, Bladder cancer	Cell proliferation	151,164
PRMT7	Breast cancer	Resistance to DNA damaging agents	165
PRMT8	Breast cancer,Ovarian cancer, Gastric cancer	Not determined	166
PRMT9	Liver cancer	Invasion	167

Figure 1.8 Structure of the human PRMT5:MEP50 hetero-octameric complex

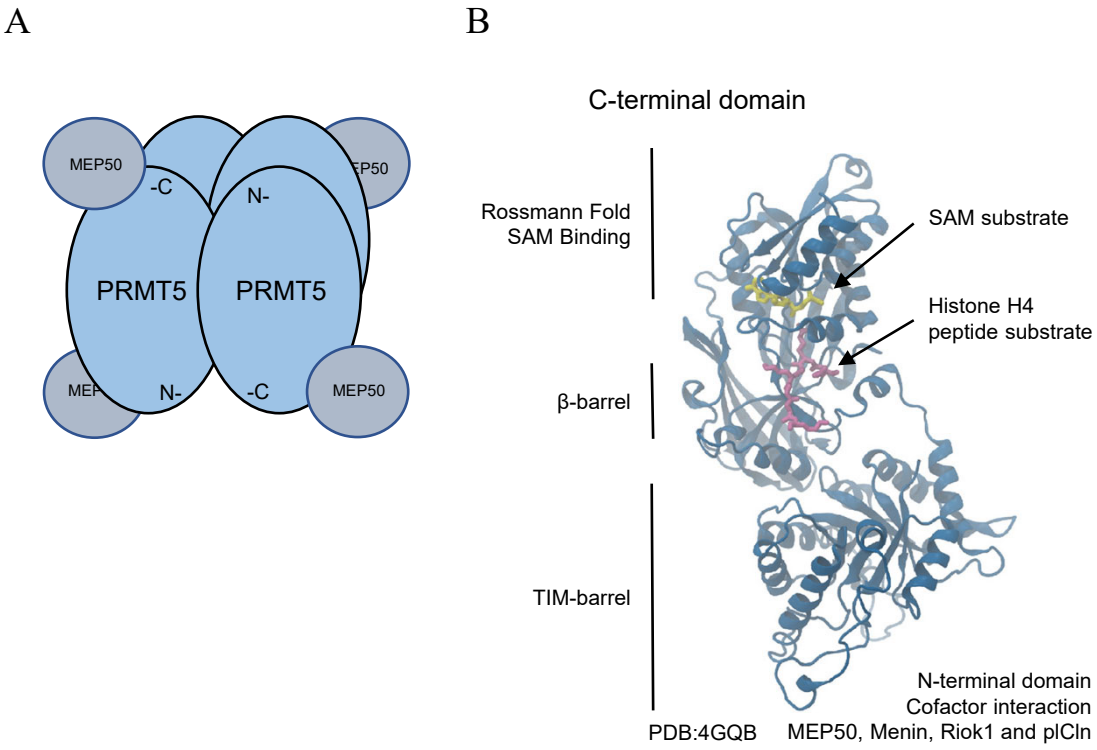


Figure 1.8 Structure of the human PRMT5:MEP50 hetero-octameric complex. (A) The subunit arrangement of the heterooctameric PRMT5–MEP50 structure shown in cartoon form, with the head-to-tail N-terminal and C-terminal PRMT5 arrangement shown by "N-" and "-C", respectively[177]. (B) Ribbon diagram of a monomer of human PRMT5 (PDB:4GQB) with the domains and substrate-binding sites as indicated. PRMT5 contains a triosephosphate isomerase (TIM) barrel on the N-terminus, a middle Rossmann-fold, and a C-terminal b-barrel containing a dimerization domain. The PRMT5 tetramer forms the core of the complex and MEP50 interacts with PRMT5 through the N-terminal TIM barrel domains[177].

Table 2 Major PRMT5 protein substrates and their function

Substrates	Effects of arginine methylation	References
H3R8, H4R3	Repress expression of tumor suppressor genes (ST7, NM23)	163
H3R2, H3R8	Transcriptional repression	163
E2F1	Controls growth regulation	190
p53	Control mechanism of p53 response	189
PDCD4	Accelerates tumor growth	198
EGFR	Contributes to attenuate EGFR-mediated ERK activation	197
CRAF	Limits the ERK1/2 signal	182
FEN1	Facilitates PCNA binding and DNA replication and repair	204
HOXA9	Immune response regulation	191
RAD9	Required for cellular resistance to DNA damaging stresses	192,193
p65	Activates NF-κB gene expression	194
RPS10	Regulates ribosome biogenesis	205
SREBP1	Metabolic regulation	206
SRSF1	Splicing	158

PDCD4: Programmed cell death-4, CRAF: Proto-oncogene C-RAF, FEN1: Flap structure-specific endonuclease 1, PCNA: Proliferating cell nuclear antigen, HOXA9: Homeobox A9, RPS10: Ribosomal Protein S10, SREBP1: Sterol regulatory element-binding protein1, SRSF1: Serine/arginine rich splicing factor 1

1.10 PRMT5 inhibitors in clinical trials

As PRMT5 may be a clinically relevant target, it may prove to be useful as an anti-cancer therapeutic agent. In the last few years, several groups have reported the identification of PRMT5 inhibitors and described the biochemical activity of PRMT5[207,208]. These inhibitors could be classified into two groups: the SAM uncompetitive inhibitors and SAM competitive inhibitors (Figure 1.9)[208].

SAM uncompetitive inhibitors: Several SAM uncompetitive inhibitors have been reported. However, most of them either have high half-maximal inhibitory concentration (IC50) values (in the mM range), or their use does not result in a phenotypic response that correlates with enzyme-specific methyl marks[208]. EPZ015666 was the first potent and selective PRMT5 inhibitor with anti-proliferative effects in both *in vitro* and *in vivo* models for mantle cell lymphoma (MCL). The IC50 value for EPZ015666 is in the nanomolar range (22 nM in a biochemical assay)[209], and EPZ015666 was shown to decrease the expression of SmD3me2s in a concentration-dependent manner and to bind specifically to PRMT5 *in vitro*. The *in vivo* studies for EPZ015666 were designed as follows: EPZ015666 was applied on severe combined immunodeficiency mice bearing subcutaneous Z-138 and Maver-1 xenografts and were administered oral doses twice-daily (BID), with four groups administered different doses used (25, 50, 100, and 200 mg per kg of body weight). Tumour samples were collected after 21 days of treatment. The results showed that treatment with 200 mg kg

$^{-1}$ BID induced tumour stasis in Z-138 cells, with > 93% tumour growth inhibition (TGI) after 21 days, whereas the Maver-1 cells showed > 70% TGI. In addition, the inhibitor was well tolerated in all models. The co-crystal structure of EPZ015666 with PRMT5:MEP50 and SAM is shown in Figure 1.9A. The compound binds to the peptide-binding site, including the pocket occupied by the arginine residue of the substrate in the presence of SAM. This finding is consistent with the enzymatic data, indicating that EPZ015666 is competitive with the peptide substrate for a K_i value of 5 ± 0.3 nM and is uncompetitive with SAM[209].

SAM competitive inhibitors: Bonday et al. initially identified the potent and selective PRMT5 inhibitor LLY-283[210]. The molecule is an analogue of SAM, with the methionine moiety replaced by a phenyl group. LLY-283 exhibits potent inhibitory activity against the PRMT5 enzyme with an IC50 value of 20 nM. LLY-283 inhibited the methylation of SmBB with an IC50 of 25 nM in MCF-7 cells, and inhibited MDM4 splicing with an IC50 of 40 nM in A375 cells. The co-crystal structure of the PRMT5:MEP50 complex was also determined, and the results showed that the adenine and ribose moieties adopt very similar conformations and interactions with Asp419, Met420, Glu392, and Try324 (Figure 1.9B). The phenyl group occupies the position of the side chain of Phe327, a residue-specific to PRMT, which contributes to the high selectivity of LLY-238 for PRMT5. Although LLY-283 exhibits anti-proliferative activity in tumour cell lines and anti-tumour effects in A375 mouse xenografts, its

regulation of histone arginine methylation was not evident *in vitro*[210].

To date, three PRMT5 inhibitors, GSK3326595, JNJ-64619178, and PF-0693999915, are in clinical trials[211]. GSK3326595 is a substrate competitive inhibitor that is an improvement from EPZ015666, and JNJ64619178 is a SAM mimetic/competitive inhibitor. The structural information for the inhibitors PF-0693999915 and PRT54315 has not been disclosed. Notably, GSK3326595 was an improvement over EPZ015666. The aim of the phase 1 clinical trial for GSK3326595 is to assess the safety, pharmacokinetics (PK), pharmacodynamics (PD), and the preliminary clinical activity in subjects with advanced or recurrent solid tumours as well as the activity in subjects with a subset of solid tumours and non-Hodgkin's lymphoma. The phase 1 clinical trial, which was led by Janssen Research & Development, was started in July 2018. The purpose of the study was to identify the maximum tolerated dose (MTD) for JNJ-64619178 in participants with advanced solid tumours, relapsed or refractory B cell non-Hodgkin lymphoma (NHL), and to identify the recommended phase 2 dose(s) (RP2D). The tolerability of JNJ-64619178 in participants with lower-risk myelodysplastic syndromes (MDS) was also evaluated[191]. The phase 1 study for PF-06939999 was led by Pfizer and was started in March 2019. The study aimed to evaluate the safety, PK, and PD using escalating doses of PF06939999 in participants with advanced or metastatic non-small cell lung cancer,

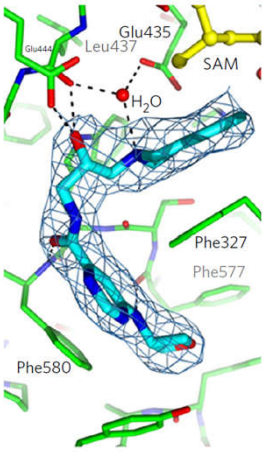
head and neck squamous cell carcinoma, oesophageal cancer, endometrial cancer, cervical cancer, and bladder cancer[211].

Although preclinical experiments for GSK3326595 have shown its preclinical activity with a low IC50 value in several MCL cell lines, a good selectivity profile, and animal toxicity results are available[209], several studies have reported a few concerns regarding the use of the PRMT5 inhibition model[212-215]. The inhibitor effectively inhibited the growth of many selected cell lines *in vitro*; however, its inhibition in these studies showed little correlation with 5-methylthioadenosine phosphorylase (MTAP) status, or with the PRMT5 expression level, raising the concern that this model of PRMT5 inhibition may lack selectivity in cancer cell lines, which may translate into greater cellular toxicity as the loss of PRMT5 leads to embryonic lethality. The discrepancy in effect size observed between the genetic depletion and enzymatic inhibition of PRMT5 indicates that the loss of MTAP leads to increased intracellular metabolite levels for methylthioadenosine (MTA), which in turn inhibits PRMT5 activity and confers heightened susceptibility to further depletion of PRMT5[212]. The loss of MTAP confers sensitivity to PRMT5 depletion, and offers a unique opportunity to target PRMT5 in diseased cells. For example, in malignant mesothelioma cells, shRNA silencing of *PRMT5* selectively led to increased cell death and clonogenic potential in MTAP- deleted malignant mesothelioma cells. PRMT5 may be a possible therapeutic target in MTAP-deleted malignant mesothelioma cells[213]. However, the

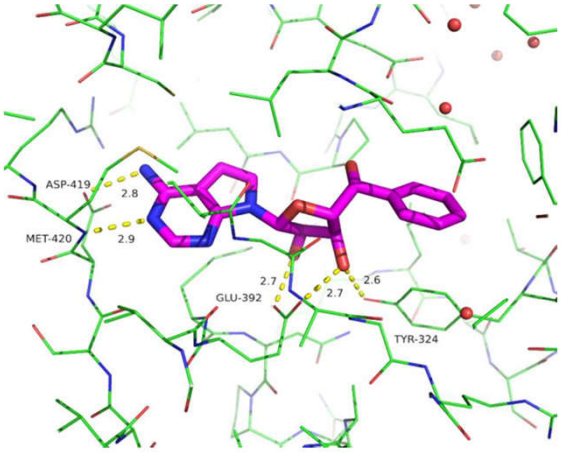
discrepancy also suggests the presence of other possible selective modifications to methylome depletion that function in an MTAP-independent manner, which need to be identified[214]. For the SAM competitive binding mode, the molecule has a highly conserved SAM-binding site within the PRMT family members as well as in other MTase domain-containing proteins, indicating high selectivity among MTases for the SAM mimetics. However, the PK may be a potential problem with SAM mimetics[215].

Figure 1.9 Comparison of two typical PRMT5 inhibitors

A



B



C

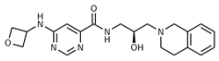
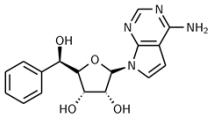
Compd	Formula structure	Binding site	Biochemical activity (nM)	Cellular activity (nM)
EPZ015666		substrate-binding site	IC50 = 22	IC50 = 96/Z-138 IC50 = 450/Maver-1
LLY-283		SAM-binding site	IC50 = 20	IC50 = 25/MCF7 IC50 = 40/A375

Figure 1.9 Comparison of two typical PRMT5 inhibitors. (A) Crystal structure of EPZ015666 (cyan) bound to PRMT5:MEP50 complex (green) in the presence of SAM (yellow; PDB accession 4X61)[209]. (B) Crystal structure of the PRMT5:MEP50 complex (green) bound to LLY-283 (purple). The key hydrogen bonds are indicated by dotted yellow lines as the ligand binds in the AdoMet pocket. Select residues are labelled[210]. (C) The table describes the characterization of the two compounds[209,210].

1.11 Research objectives

PRMT5 is a major type II arginine methyltransferase and plays a crucial role in tumorigenesis, including the regulation of gene expression through histone methylation, transcription factor binding, promoter binding, and signal transduction[147]. The over-expression of PRMT5 been observed in multiple tumour cell lines and primary patient samples derived from lymphomas, breast cancer, colorectal cancer, and lung cancer[157-163]. In addition to the upregulation of PRMT5 in patient samples and cancer cell lines, the knockdown of PRMT5 in cancer cell lines leads to an anti-proliferative effect[200,203]. In a survival analysis, a high level of PRMT5 was identified as an independent factor for poor clinical outcomes in patients with cancer[147]. These results indicate that PRMT5 may serve as a potential clinical target for anti-tumour therapy. Several studies have reported small molecular inhibitors of PRMT5 in the last past several years[208], and three are in clinical trials for the treatment of solid tumours and NHL[211]. The targeting of PRMT5 offers a new window in the treatment of cancers efficiently and selectively. However, studies on the mechanism of action underlying PRMT5 function are limited and various analyses need to be performed to better understand its therapeutic potential.

E2F is a family of master transcriptional regulators and plays an important role during tumorigenesis. The pRB-E2F1 axis contributes to essential steps in tumori-genesis, as aberrant pRB activity has been observed in a large number of cancer types[131,132]. In the classical view, pocket proteins are phosphorylated by cyclin D-

CDK4/6 and cyclin E-CDK2 in mid-to-late G1, and free E2F1 is released. The physical interaction between pRB and E2F1 facilitates transcriptional repression and cell cycle arrest, indicating that E2F1 may be an important physiological target for pRB[42,133-135]. PRMT5 methylates E2F1 on its arginine residues and the meR E2F1 mark is read by p100/TSN10, which recruits a chromatin-bound symR E2F1 complex on E2F1 target genes[190]. Besides, PRMT5-dependent methylation is unique and selective to E2F1[88], suggesting that PRMT5 function plays a pivotal role in E2F1 activity.

In general, we aimed to uncover the biological function of PRMT5 in association with E2F1 during tumorigenesis, to further correlate it with clinical outcomes, and to investigate the clinical efficiency of PRMT5 inhibitors. First, we used a highly selective small molecular inhibitor of PRMT5 with its anti-proliferative activity in tumour cells and effective regulation of histone arginine methylation in cell-based experiments, and together with the measurement of biochemical activity in enzyme assays, the experiments allowed us to study the biological function of PRMT5 in cells. Next, to evaluate the mechanisms underlying E2F1-mediated pathways, we used the CRISPR-Cas9 technology to functionally and stably knockout E2F1 in cells, which facilitated the assessment of the oncogenic mechanisms of E2F1. To identify novel E2F1 target genes participating in PRMT5-mediated regulation, we used RNA sequencing technology to analyse differential gene expression under specific conditions, and analysed the global map for downstream targets of PRMT5 and E2F1. The functional

study of downstream targets was performed and additional clinical studies of downstream targets correlated with gene expression in cancer types may help bridge the gap between basic research and clinical outcomes.

In conclusion, the targeting of PRMT5 offers a great opportunity to combat cancer efficiently and selectively. However, additional research on PRMT5 function is required to better understand its therapeutic potential. This study focuses on the biological function of the PRMT5-E2F1 axis in tumorigenesis. These findings would enrich the understanding of PRMT5 inhibition and E2F1 regulation in cancer cells, and further validate PRMT5 as an anti-cancer target.

Chapter 2: Materials and Methods

2.1 Cell culture

U2OS and HCT116 cell lines were obtained from the American Type Culture Collection (ATCC). They were maintained in Dulbecco's Modified Eagle Medium (DMEM) supplemented with 10% (v/v) fetal bovine serum (FBS) (Labtech) and 1% Penicillin-Streptomycin (Pen-Strep) (Life technologies). Cells were passaged every 3-5 days to maintain 40-60% confluency. During passage each time, cells were gently rinsed with phosphate-buffered saline (PBS) (Oxoid) and the solution was removed. Appropriate quantity (normally 1 ml/10cm^2) of Trypsin-EDTA (Lonza) was added to the side wall of the flask and the contents were gently swirled to cover the cell layer. After incubating at 37 °C for 2-3 minutes, fresh prepared medium containing FBS was added to neutralise trypsin activity. The medium was gently dispersed by pipetting over the cell layer surface several times to ensure recovery of >95% of cells. Cell suspension was transferred to tube and the tube was gently centrifuged at 300-1000 x g for 5 min. After removing the supernatant, the cell pellet was gently resuspended in pre-warmed fresh medium containing 10% FBS and 1% Pen-Strep. The remaining solution was diluted to the seeding density and appropriate volume was pipetted to the culture flask. The culture flask was placed in the incubator.

2.2 PRMT5 inhibitors

GSK591 was ordered from Sigma-Aldrich. J579-41, J579-43, J579-44, J578-65 and J578-68 were synthetized by Argonaut Therapeutics. All inhibitors were dissolved in dimethyl sulfoxide (DMSO) to the concentration of 10 mM and were stored in -20°C.

2.3 Western blotting and antibodies

For western blotting, cells were collected in microfuge tubes in radioimmunoprecipitation assay buffer (50 mM tris-HCl (pH 8), 150 mM NaCl, 1% Igepal CA-630, 0.5% sodium deoxycholate, 0.1% SDS, 0.2 mM sodium orthovanadate and protease inhibitor cocktails) and incubated on ice for 30 min. Microfuge tubes were centrifuged at 12000 x g for 10 min at 4°C. The supernatant was collected in fresh tube and placed on ice prior to SDS-polyacrylamide gel electrophoresis and transferred to nitrocellulose. The following antibodies were used in western blotting: β-actin (AC-74, Sigma-Aldrich), Cleaved-PARP (Cell Signaling Technology), E2F1 (C20, Santa Cruz Biotechnology, S-C-193, Dallas, TX, USA), E2F1 (Cell Signaling, 3742S, Danvers, MA, USA), p53 (DO-1, Santa Cruz Biotechnology, SC-126), H4R3 (Abcam plc), CTTN (H-222, Cell Signaling, 3503S) , SDMe (Cell Signaling, 13222S). Mouse and rabbit secondary antibodies were from GE Healthcare.

2.4 Bradford assay

To draw a calibration curve to measure the concentration of protein samples, 1ml

of Bradford assay solution was dispensed into 7 disposable plastic cuvettes. 0 µl, 1 µl, 2 µl, 5µl, 10 µl, 20 µl, 40 µl of 1 mg/ml BSA standard were added to each and OD_{595} was recorded with a spectrophotometer. 3 µl of the purified protein sample was added to 1 ml Bradford assay solution. The OD_{595} of each sample was measured to compare against the calibration curve to get the final concentration of each purified protein sample.

2.5 MTT assay

Cells were seeded in a 96-well plate and incubated overnight to settle cells down. Cells were further incubated with the appropriate stimulus for the desired time. Medium was removed and cells were gently rinsed with PBS and the solution was removed. MTT (3-(4,5-dimethylthiazol-2-yl)-2,5-diphenyltetrazolium bromide) made up in medium was added to a final concentration of 0.5 mg/mL. The 96-well plate was incubated for 30 minutes to 4 hours at 37°C, until intracellular purple formazan crystals were visible under microscope. MTT was removed and 10 µl solubilizing solution (20% SDS, 50% N,N-dimethylformamide and H2O) was added and triturated. The 96-well plate was incubated at 37°C for 30 minutes to 2 hours, until cells have lysed and purple crystals have dissolved. The absorbance was measured at 570 nanometers.

2.6 Determination of the IC50 of PRMT5 inhibitors

Cells were seeded in 96-well plate and incubated at 37°C overnight to settle cells down. Cells were treated with inhibitors to reach to concentrations (100 µM, 10 µM, 1 µM, 0.1 µM, $1x10^{-2}$ µM, $1x10^{-3}$ µM, $1x10^{-4}$ µM and $1x10^{-5}$ µM). DMSO treated sample was set as the control group to calculate cell viability. After addition of compounds, assay plates were incubated for 2 days, 4 days and 6 days at 37 °C, 5% CO_2. The IC50 curves were generated by GraphPad Prism Version 8.4.0.

2.7 Enzyme assay of PRMT5 inhibitors

Half maximal effective concentration (EC50) of PRMT5 inhibitor was calculated through the PRMT5 Direct Activity Chemiluminescent Assay Kit (AMS Biotechnology). The key to the PRMT5 Chemiluminescent Assay Kit is a highly specific antibody that recognizes methylated R3 residue of Histone H4. With this kit, only three simple steps on a microtiter plate are required for methyltransferase detection. First, SAM was incubated with a sample containing assay buffer and methyltransferase enzyme for one hour. Next, primary antibody was added. Finally, the plate was treated with an HRP-labelled secondary antibody followed by addition of the HRP substrate to produce chemiluminescence that could then be measured using a chemiluminescence reader. EC50 curves were generated by GraphPad Prism Version 8.4.0.

2.8 Cell proliferation assay

Cells were seeded at a density of 50,000 cells in triplicate (day 1). The cell number was counted 2-6 days post seeding by Luna-II™ Automated Cell Counter (Logos Biosystems, Villeneuve d'Ascq, France) after stained cells with Trypan Blue dye for 5 minutes.

2.9 Colony formation assay

Cells were seeded at a density of 1000 cells per well in a 6-well plate and were incubated with the indicated compounds for 8 days as described previously[190]. The culturing media was gently aspirated and the plates were briefly rinsed with cold PBS. Crystal violet stain was applied to the cells for 2 min, followed by washing with deionized water and left to dry. Image scanning was performed with a Gelcount automated colony counter (Oxford Optronics, Oxford, UK).

2.10 Apoptosis and necrosis assay

Apoptosis and necrosis were measured through GFP CERTIFIED Apoptosis/Necrosis detection kit for microscopy and flow cytometry provided by Enzo Life Sciences (UK) Ltd. Grown cells and treated cells with appropriate agents were incubated for desired period of time. The protocol provided was followed and samples were analysed by using an BD Accuri™ C6 Plus Flow Cytometer and C6 flow software package (Becton Dickinson; Franklin Lakes, NJ, USA).

2.11 Flow cytometry assay

Cells were collected with trypsin in the front falcon tube and the tube was centrifuged at 1000 rpm for 1-5 mins. Supernatant was discarded and cells were rinsed by PBS. The tube was centrifuged at 1000 rpm for another 1-5 mins to pellet cells down. Supernatant was discarded and cells were fixed in ice cold 70% ethanol (ethanol in PBS) overnight at 4 °C. After cells were fixed, the tube was centrifuged at 1000 rpm for 1-5 mins and rinsed by PBS twice. Supernatant was decanted and fixed cells were resuspended in 100 μg/ml propidium iodide (Sigma) containing 200 μg/ml RNase A (Sigma) and incubated in the dark at 4°C for 1 h. Cell cycle analysis was performed by measuring fluorescence in the FL2 channel using an BD Accuri™ C6 Plus Flow Cytometer and C6 flow software package (Becton Dickinson; Franklin Lakes, NJ, USA). A minimum of 2 × 104 events were collected from triplicate samples.

2.12 Generation of stable CRISPR-Cas9 knockout cell lines

The generation of stable CRISPR-Cas9 knockout cell lines was based on the protocol (doi:10.1038/nprot.2013.143) developed by Feng Zhang[216].

Design of targeting genomic DNA sequence and the use of the CRISPR design web tool: the design of the genomic single guide RNA (sgRNA) primers was from online

CRISPR design web tool CHOPCHOP (https://chopchop.cbu.uib.no). The genomic sgRNA primers of E2F1 were listed as following:

Gene	Primer	Sequence
E2F1	forward	5'-CACCGGGAAACTGACCATCAGTACC-3'
	reverse	5'-AAACGGTACTGATGGTCAGTTTCCC-3'

Preparation of sgRNA expression construct: the plasmid-based procedure was performed to generate the sgRNA expression construct.

(i) Preparation of the sgRNA oligos inserts. Resuspended the forward and reverse stands of oligos for the sgRNA design to a final concentration of 100 μM. Prepared the following mixture for phosphorylating and annealing the sgRNA oligos:

Component	Amount (μl)
sgRNA forward (100 μM)	1
sgRNA reverse (100 μM)	1
T4 ligation buffer, 10x	1
T4 PNK	1
ddH_2O	6
Total	10

(ii) Phosphorylated and annealed the oligos in a thermocycler by using the following parameters: 37°C for 30 min; 95°C for 5 min; ramped down to 25°C at 5°C min^{-1}.

(iii) Diluted phosphorylated and annealed oligos 1:200 by adding 1μl of oligo to 199 μl of room temperature ddH2O.

(iv) Cloning the sgRNA oligos into pSpCas9(BB). Set up a ligation reaction of the sgRNA, as described below. We also set up a no-insert, pSpCas9(BB)-only negative

control for ligation.

Component	Amount (μl)
pSpCas9(BB), 100 ng	x
Diluted oligo duplex from Step (iii)	2
Tango buffer, 10x	2
DTT, 10 mM	1
ATP, 10mM	1
FastDigest *BbsI*	1
T7 ligase	0.5
ddH_2O	to 20
Total	20

(v) Incubated the ligation reaction for a total of 1 h.

(vi) Transformation. Added 2 μl of oligo sample and 0.85 μl β-mercaptoethanol into 50 μl XL1-Blue Supercompetent Cells for quick transformation. Incubated the mixture on ice for 20 min, heat-shocked it at 42°C for 45 s, incubated on ice for 2 min. Added 100 μl LB medium and shake it for 10 min. Added on LB plate and incubated it overnight at 37°C.

(vii) Picked up colonies. Inspected the plates for colony growth. On the negative control plates there were no colonies. There were tens to hundreds of colonies on the pSpCas9(sgRNA) cloning plates. From each plate, picked up 4 colonies to check for the correct insertion of sgRNA. A sterile pipette tip was used to inoculate a single colony into a 3ml culture of LB medium with 100 μg ml^{-1} ampicillin. Incubated the mixture and shake it at 37°C overnight.

(viii) Isolated the plasmid DNA from cultures by using a QIAprep spin miniprep kit according to the manufacturer's instructions (Qiagen, LLC).

(ix) Validation of CRISPR plasmid. Verified the sequence of each colony by sequencing from the U6 promoter using the U6-Fwd primer. The sequencing was conducted by Source BioScience PLC. BLAST (https://blast.ncbi.nlm.nih.gov/Blast.cgi) was used to check whether target sequence was cloned into CRISPR vectors.

(x) Transfection of CRISPR plasmid. Before transfection, seeded fresh HCT116 cells ahead to have sufficient cells for the day of transfection (0.5-1 x 10^5 cells in a 6-well plate per transfection), washed by PBS and added pre-warmed Opti-MEM I Reduced Serum Media (Thermo Fisher Scientific) to starve cells. The mixture of 200 µl Opti-MEM media and 5 µl GeneJuice (Novagen) was incubated at room temperature for 5 minutes. Added 1µg plasmid to the mixture and another 20 minutes for incubation at room temperature was followed. After the incubation was up, added the transfection mixture dropwise to the cells, making sure to cover the whole dish, agitated to mix. Left cells at 37°C overnight and topped up dished with DMEM with FBS to get the overall 10% FBS concentration. Cultured cells for 24h for the next step.

(xi) Puromycin selection. Puromycin selection could be applied at a concentration of 2 $\mu g.ml^{-1}$. Incubated cells with puromycin for 48h and changed to regular media. Cultured cells for 24 h.

(xii) Isolation of clonal cell lines by flow cytometer. Dissociated to single cells from transfected plates and counted the number of cells from each plate by flow cytometer. Serially diluted them in normal medium to a final concentration of 0.5 cells per 100 µl

to reduce the likelihood of having multiple cells per well. Plated two 96-well plates for each transfected population.

(xiii) Inspected the colonies for a clonal appearance 1 week after plating. Marked off the wells that may have been seeded with multiple cells. Returned the cells to the incubator and allow them to expand for 2-3 weeks.

(xiiii) Sequencing and off-target analysis. Designed the primers as following:

Gene	**Primer**	**Sequence**
E2F1	forward	5'-GACTCTCAGGCTATGTCCCC-3'
	reverse	5'-GCATTCTTCTTCTGGCTGGG-3'
DNML1	forward	5'-TGTGAGTTGGCAAGTTCCTCA-3'
	reverse	5'-CAGCTCCTCCAGTACTTTCATACT-3'
MACROD2	forward	5'-CAAGCAACTCAACCCTCTGT-3'
	reverse	5'-TCTTAGCCCACACCAAAGGT-3'
NR0B1	forward	5'-AAGTACTTGCCCTGCTTCCAG-3'
	reverse	5'-TCCCATGAAGGCACAAACTTTTC-3'

Extracted DNA from Cas9-targeted cells. Set PCR reaction as following:

Component	Amount (μl)
DNA	2
10 x PAQ5000 reaction buffer	2
Betaine	2
forward primer (10mM)	0.5
reverse primer (10mM)	0.5
dNTP (10mM)	0.5
PAQ5000	0.2
ddH_2O	12.3
Total	20

Performed the PCR with the following cycling conditions:

Cycle number	Denature	Anneal	Extend
1	95°C, 2 min		
2-30	95°C, 30 s	60°C, 1 min	72°C, 1 min
31			72°C, 5 min

Run 2 μl of PCR product on a 2% (wt/vol) agarose gel to check for single-band product. Purified PCRs by using the QIAQuick PCR purification kit (QIAGEN) and normalized the eluants to 20 ng/μl. PCR samples and forward primers for PCR were sent to perform Sanger sequencing analysis (Source BioScience PLC). Extracted protein of samples and performed a western blot to measure protein expression of Cas9 targeted cells.

2.13 Small interfering RNA (siRNA)

Cells were seeded as normal and left at 37°C overnight to settle cells down. Oligofectamine reagent (Invitrogen) and siRNA were incubated separately with Opti-MEM I Reduced Serum Media (Thermo Fisher Scientific) at room temperature for 5 minutes. The final concentration of siRNA should reach 25nM. The two mixtures should be combined and another 20 minutes for incubation at room temperature was followed. Media was removed from the dishes and Opti-MEM I Reduced Serum Media was added. After the incubation was up, transfection mixture was dropwise added to cells, making sure to cover the whole dish. The dishes were left at 37°C overnight and topped up with DMEM with FBS to get the overall 10% FBS concentration. Endoribonuclease-prepared siRNAs human CTTN was provided by Sigma-Aldrich (EHU093121).

2.14 RNA isolation and quantitative Polymerase Chain Reaction (qPCR)

RNA was isolated from cells using TRIzol (Thermo Fisher Scientific, Waltham, MA, USA) or the Direct-zol RNA MiniPrep kit (Zymo Research, Irvine, CA, USA) according to the manufacturer's instructions. One microgram of total RNA was used for complementary DNA synthesis. Reverse transcription with oligo(dT)20 primer (Invitrogen) was performed using SuperScript III Reverse Transcriptase (Invitrogen) as per the manufacturer's instructions. Quantitative reverse-transcription PCR was carried out in technical triplicate using the indicated primer pairs and the Brilliant III Ultra-Fast SYBR® Green QPCR Master Mix (Agilent, Santa Clara, CA, USA) on an AriaMX real-time qPCR instrument (Agilent). Results were expressed as average (mean) fold change compared with control treatments using the ΔΔCt method from three biological repeat experiments. Glyceraldehyde-phosphate dehydrogenase primer sets were used as an internal calibrator. Error bars represent SE unless otherwise indicated. The primer sequences used for qPCR were listed as below:

Gene	Primer	Sequence
CTTN	forward	5'-AGAGATGAAGAGGCTCCCCG-3'
	reverse	5'-AGAGCTCGCCCGGAAGTA-3'
FLII	forward	5'-ACCAGGATGTATCGTGTGTATGG-3'
	reverse	5'-TCCAGAGAGGTCCCCTTGAG-3'
AIF1L	forward	5'-AGAACCTTCCAGAAAAGCTCACA-3'
	reverse	5'-TCGCCTTCATTGTTCAGGTCA-3'
TLE2	forward	5'-GGCTCAATACCACAGCCTCA-3'
	reverse	5'-ATGTCGCTGCATTTCCGTCT-3'

ITGA3	forward	5'-GCGCAAGGAGTGGGACTTAT-3'
	reverse	5'-CTGCATCGTGTACCCAATATAGA-3'
GAPDH	forward	5'-TTCATTGACCTCAACTACAT-3'
	reverse	5'-GTGGCAGTGATGGCATGGA-3'

2.15 Transwell cell migration and invasion assay

Cells were detached from tissue culture plate using 0.25% Trypsin-EDTA solution. Cells were pelleted by centrifugation and the existing media was aspirated to leave pelleted cells. Cells were resuspended in serum free DMEM. For the 12-well transwell (Corning) insert, 5×10^5 - 1×10^6 cells/ml was used depending on the growth curve of cells. 100µl of cell solution was plated on top of the filter membrane and 2ml of medium containing 20% FBS was added in the lower well of transwell plate to make sure the medium in the lower well contact with the membrane in the upper well. Cells were incubated overnight at 37°C and 5% CO_2 to allow cells to settle down. Transwell insert was removed from the plate. Cotton-tipped applicators were used to carefully remove the media. 2ml of ethanol were added into transwell plate and transwell insert was placed into 70% ethanol for 10 minutes to allow cell fixation. Transwell insert was removed from the 12-well plate and transwell membrane was left to dry (typically 10-15 minutes). 2ml of 0.2% crystal violet was added for staining. Transwell membrane was incubated at room temperatures for 5-10 minutes. Crystal violet was removed from the top of the membrane with a pipette tip and membrane was dipped into distilled water to remove the excess crystal violet. After the transwell membrane got dried, the number of cells were counted in different fields of view to get an average sum of cells

that have migrated through the membrane and attached on the underside of the membrane.

The invasion assay was conducted the same as the migration assay. The only difference was precoated transwell membrane with 500 µl Matrigel and solidified in a 37°C incubator for 30 minutes to form a thin gel layer. Precoated transwell membrane was washed by PBS twice and cell solution was added on top of the Matrigel coating.

2.16 Cell adhesion, migration and invasion assays via xCELLigence real-time quantitative cell analysis (RTCA) instrument

Cells (100,000 cells) were seeded in 6 cm dishes and treated with 1 µM PRMT5 inhibitor for 48 h. Adhesion, migration and invasion assays were carried out according to the manufacturer's protocol using E-plates 16 and CIM plates 16 (Acea Biosciences, San Diego, CA, USA), respectively. All measurements were performed using an xCELLigence® RTCA DP Instrument. Briefly, for an adhesion assay Matrigel (prepared according to manufacturer's instructions by mixing with DMEM medium in a 1:1 ratio; concentration 50%) (Cell Applications, 126-2.5, San Diego, CA, USA) was added to the wells in the E-Plate and incubated for 3 h at 37 °C. The coated plates were washed with PBS and incubated with 0.1% bovine serum albumin for 30 min at 37 °C. After PBS washing, 100 µl of media without FBS (serum free) was added to each well and the background impedance was measured. Cells were collected by short

trypsinization, centrifuged and resuspended in serum-free media. Cells (25,000 cells) suspended in 100 µl of media were transferred to Matrigel-coated wells. As a positive control, non-treated cells suspended in FBS-containing medium were used. As a negative control, empty Matrigel-coated wells without cells were used. The measurement of cell adhesion was monitored every 10 s for 1 h.

For an invasion assay, the upper chamber of a CIM plate was coated with Matrigel and incubated for 3 h at 37 °C. Then, a CIM-Plate 16 was assembled (lower chamber contains media with FBS; upper chamber contains serum-free media), equilibrated at 37 °C for 1 h and the background measurement was taken. Preparation of cells was as described for the adhesion assay, although CIM plates were left for a 30 min to allow cells to settle. The measurement of cell invasion was monitored every 10 min for 72 h.

An identical protocol was used for the migration assay, but without the Matrigel coating step. The assay system expresses impedance in arbitrary Cell Index units $(R_n - R_b)/4.6$; where R_n is the cell-electrode impedance of the well when it contains cells and R_b is the background impedance of the well with the media alone. The rate of adhesion/migration/invasion was determined by analysing the slope of the line between two given time points in each biological repeat ($n = 3$).

2.17 Chromatin immunoprecipitation (ChIP)

Cells were seeded in 55 cm^2 dishes and were incubated overnight. DMSO and

J579-44 was added to the dishes and the final concentration of each plate was 1 µM. After 2 days incubated at 37°C and 5% CO_2, formaldehyde was added to a final concentration of 1% and incubated at room temperature with invert occasionally to mix for 15 minutes to form DNA-protein cross-links. Glycine was added to a final concentration of 0.125 M to neutralise the formaldehyde and cross-linking activity. Cells were collected in appropriate 15 ml Falcon tube and samples were centrifuged at 1000 rpm in 4 °C to pellet cells down. Cells were spun down and washed in 2.5 ml ice cold PBS. Cells were spun down and resuspended in 1 ml lysis buffer I (5mM Tris-Cl pH 8.0, 85mM KCl, 0.5% Igepal and 1x protease inhibitor), followed by gently mixed with a pipette and let stand at room temperature for 10 mins. Samples were spun down and cells were re-suspend in 1 ml lysis buffer II (10 mM Tris-Cl pH 7.4, 150 mM NaCl, 1 mM EDTA, 1% Igepal, 1% DOC, 0.1% SDS and 1 x protease inhibitor), followed by mixed thoroughly with a pipette and stand on ice for 10 mins. Samples were sonicated for 10 times 12 for 10 seconds with intervals of 30 seconds on the sonifier (Branson 250 Analog Ultrasonic Sonifier). Samples were kept on ice during intervals. Samples were transferred to a new 1.5 ml Eppendorf tube and centrifuged at 14000 rpm for 10 minutes. Supernatant was transferred to a new Eppendorf tube and centrifuged again at 14000 rpm for 10 minutes. Crude soluble chromatin was contained in supernatant.

The preparation of beads for ChIP was as following: approximate 1.25 ml dead volume of protein A and 1.25 ml protein G sepharose were mixed and washed twice in

ChIP dilution buffer (20 mM Tris-Cl pH 8.0, 500 mM NaCl, 2 mM EDTA, 0.1% SDS, 1% Triton X-100). Mixture was resuspended to 5 ml in ChIP dilution buffer and 1 mg/ml BSA (284 µl of 20 mg/ml BSA in TE buffer), 400 µg/ml sonicated salmon sperm DNA (217 µl of 10 mg/ml stock) and 1x protease inhibitors were added. The beads were rotated at 4°C for 3 hours. The beads were spun down and washed in ChIP dilution buffer. The beads were spun down again and resuspended to 5 ml in ChIP dilution buffer and kept at 4°C for storage.

60 µl protein A/G beads and 3 µg of appropriate IgG control antibody were added into sample. The sample was rotated at 4°C for 3-4 hours to continue to immunoprecipitation process.

The beads were spun down and supernatant was taken to a fresh 1.5 ml Eppendorf and separated into the appropriate number of Eppendorf tubes (1 per antibody to be used). The volume was topped up to 1 ml with lysis buffer II. Appropriate amount (2-3 µg) of specific antibody and control IgG were added and samples were incubated rotating overnight at 4°C.

On the following day, 60 µl protein A/G beads were added into samples with a further 2 hours incubation at 4°C. The sample was spun down and 500 µl of supernatant was taken from the IgG control IP sample to use as input. The other sample was spun down and the supernatant was discarded. Next, the beads were washed twice with low

salt wash buffer (20 mM Tris-Cl pH 8.0, 150 mM NaCl, 2 mM EDTA, 0.1% SDS, 1% Triton X-100, 1x protease inhibitor), four times with LiCl buffer (10 mM Tris-Cl pH 8.0, 250 mM LiCl, 1 mM EDTA, 1% Igepal, 1% DOC, 1x protease inhibitor), switched to new 1.5 ml Eppendorfs and continue washed twice with TE buffer. The beads were eluted with 250 µl elution buffer (1% SDS, 0.1 M $NaHCO_3$) on a 65°C hot block for 15 mins. During elution process, the sample was vortexed every 3 mins. The sample was spun down and supernatant was collected to a new 1.5 ml Eppendorf tube. This elution process was repeated again as above with a further 250 µl elution buffer and the eluate was pooled with the first collected one. 20 µl 5 M NaCl, 25 µl 200 mM EDTA, 20 µl 1 M Tris pH 6.5, and 1 µl RNAse A were added to each sample and the sample was incubated at 55 °C for 2-3 hours, followed by overnight reversed crosslink at 65°C.

The third day, 10 µl of 10 mg/ml proteinase K was added and the sample was incubated at 55°C for 2-3 hours. DNA was purified by transferring to a 15 ml falcon tube and 5 times volumes of PB buffer from the Qiagen DNA purification kit was added to falcon tube. 750 µl of buffer was loaded a time onto pink Qiagen spin column. The column was spun through at 13,000 rpm for 1 min. The sample was washed with 750 µl PE buffer and spun through at 13,000 rpm for 1 min. The sample was spun again to remove traces of PE buffer. The column was transferred to a clean 1.5 ml Eppendorf tube and 50 µl EB buffer was added. The sample was left for 5 mins and spun at 13,000

rpm for 1 min to collect DNA. DNA was stored at -20°C to qPCR analysis as previous listed.

Gene	Primer	Sequence
CTTN	forward	5'-AGAGATGAAGAGGCTCCCCG-3'
	reverse	5'-AGAGCTCGCCCGGAAGTA-3'
actin	forward	5'-ATCGTGCGTGACATTAAGGAGAAG-3'
	reverse	5'-CTGGAAGCAGCCGTGGCCATCTCTTG-3'
CDC6	forward	5'-GGCCTCACAGCGACTCTAAGA-3'
	reverse	5'-CTCGGACTCACCACAAGC-3'

2.18 RNA sequencing (RNA-Seq) analysis

HCT116 p53-/- wild-type (WT) *E2F1* and HCT116 p53-/- *E2F1* CRISPR cells were treated with DMSO or J579-44 for 48h. Concentration performed was 1 µM. Total RNA was isolated using Direct-zol RNA MiniPrep kit (Zymo Research) according to the manufacturer's instructions. Three biological replicates of each sample were collected. RNA-Seq was performed by BGI Genomics. Quality of samples was evaluated through NanoDrop™ before sending to BGI Genomics for analysis. Briefly, an Agilent 2100 Bioanalyzer (Agilent RNA 6000 Nano Kit) was used for RNA sample quality control purposes (RNA concentration, RIN value, 28S/18S, and the fragment length distribution). mRNAs were isolated from total RNA using the oligo(dT) method. mRNAs were fragmented, and first strand/second strand cDNA were synthesized. cDNA fragments were purified and resolved with EB buffer for end reparation and single nucleotide A (adenine) addition. Subsequently, the cDNA fragments were linked

with adapters, those cDNA fragments with suitable size were selected for the PCR amplification. Agilent 2100 Bioganlyzer and ABI StepOnePlus Real-Time PCR System were used in quantification and qualification of those libraries. The RNA-Seq was carried out using Illumina HiSeq Platform. Maximum reads per run was 400 million, the reads length was 2 × 150 bp.

Reads were trimmed to remove adapters and low-quality bases with TrimGalore v.0.4.3 (http://www.bioinformatics.babraham.ac.uk/projects/trim_galore/).The trimmed reads were aligned to the human reference genome build hg19 with STAR aligner v.2.7 with two mismatches allowed. Differential gene expression analysis was performed with DESeq2 R Bioconductor package (v.1.25.17), using read counts data provided by the aligner. Genes were considered differentially expressed if the adjusted *P*-value, calculated using the Benjamini-Hochberg method in order to minimize the false discovery rate, was less than 0.01. We further filtered significantly differentially expressed gene sets using a 30% or 2-fold change in absolute expression level.

2.19 Parametric gene set enrichment analysis (PGSEA)

The parametric gene set enrichment analysis was performed with the R PGSEA package (v. 1.58) on the collections of curated gene sets (c2, c5) derived from KEGG pathway database and Gene Ontology (GO) vocabulary, respectively, available from the Broad Institute's Molecular Signatures Database (v 6.2). The expression matrix

used in these analyses was normalised and rlog-transformed with DESeq2 R package. Gene sets with less than 10 genes and more than 10,000 genes were excluded from the analyses. A linear model was applied employing the limma package (v.3.44.0) followed by empirical Bayesian analysis to determine concepts associated with significant differences between treated and untreated samples. Differences were considered significant if the adjusted *P*-value, calculated using the Benjamini-Hochberg method in order to minimize false discovery rate, was less than 0.005.

2.20 Xena browser functional genomics analysis

For the analysis of *E2F1*, *PRMT5* and *CTTN* expression levels in human cancers, Xena browser (University of California) was used (https://xena.ucsc.edu/). The TCGA TARGET GTEx data set was selected, which contained transcript expression data from The Cancer Genome Atlas (TCGA; cancer tissue) and Genotype-Tissue Expression (GTEx; healthy tissue) samples. Box plots show the inter-quartile range (box) and median (solid line). The whiskers show lowest and highest datum still within 1.5 × inter-quartile range of the lower and upper quartiles. Outliers are shown as black dots.

2.21 Kaplan-Meier survival analysis

Kaplan-Meier plots of overall survival (OS) and progression-free survival (PFS) were generated from Xena browser (https://xena.ucsc.edu/) in TCGA cohort. For each

analysis, patients were divided into two groups: one with high expression (above or equal to the mean gene expression of all patients; red line) or one with low expression (below the mean gene expression of all patients; blue line).

2.22 ENCODE ChIP sequencing (ChIP-Seq) data analysis

CTTN promoter characterization was performed utilizing bioinformatics tools present in UCSC Genome Browser (https://genome.ucsc.edu; GRCh37/h19 assembly) and analysing ChIP-Seq data for E2F1 tracks from the ENCODE project (http://genome.ucsc.edu/ENCODE/).

2.23 Statistical analysis

All quantitative data were presented as mean ± SD unless otherwise indicated. Differences between experimental groups were evaluated for statistical significance using Student's *t*-test for unpaired two group comparison. *P* values less than 0.05 were considered to be statistically significant.

Chapter 3: J579-44 is an effective small-molecule inhibitor of PRMT5 in cell-based and enzyme assays

3.1 Introduction

PRMTs are a class of enzymes that transfer either one or two methyl groups to the nitrogen atoms of the guanidinium side chains of arginine residues using SAM as the methyl donor[141-145]. PRMT5 is the predominant type II PRMT that is responsible for symmetric demethylation, and it acts as an oncoprotein with a crucial role in tumorigenesis, which includes the regulation of gene expression through histone methylation, transcription factor binding, promoter binding, and signal transduction[147]. Therefore, PRMT5 may serve as a potential clinical target for antineoplastic therapy.

Small-molecule chemical probes that selectively inhibit the catalytic activity of PRMT5 are valuable tools for deciphering unknown regulatory mechanisms that may be enabled due to protein arginine methylation. A selective and effective PRMT5 inhibitor in cell-based and enzyme assays may serve as a key to deciphering the mechanisms underlying PRMT5 function. Therefore, we aimed to find an effective chemical probe for PRMT5 and its less active analogue probe via a battery of cellular and biochemical assays.

3.2 The IC50 values of PRMT5 inhibitors identified by MTT assays

Six small-molecule inhibitors of PRMT5 (GSK591, J579-41, J579-43, J579-44, J578-65, and J578-68) were studied. All samples were dissolved in DMSO to prepare a 10 mM stock solution. The structural formula of each compound is provided in Figure 3.1.

We used six candidate PRMT5 inhibitors in the human osteosarcoma cell line U2OS to assess the cytotoxic effects of each compound using the MTT assay. As all the compounds tested were dissolved in DMSO, the percentage of cell viability was normalised relative to DMSO-treated cells. U2OS cells were treated for 2, 4, and 6 days with each inhibitor using a concentration gradient of 10 pM to 100 μM (10 pM, 100 pM, 1 nM, 10 nM, 100 nM, 1 μM, 10 μM, and 100 μM). Based on the MTT cytotoxic assay, the IC50 curves of all six candidate compounds were generated (Figure 3.2A-F), and these values are listed in Figure 3.2G.

The results from the MTT assay showed the time and concentration-dependent effect of the various compounds in the cells. J579-44 had the strongest inhibitory activity (IC50=0.0161 ± 0.0029 μM), whereas J578-68 exhibited the lowest cytotoxic effect in cells (IC50=2.7700 ± 0.3422 μM), and can be used as a less potent analogue inhibitor.

Next, we treated U2OS cells with 32 nM DMSO, 2x the IC50 of each compound,

and 32 nM etoposide as a positive control for six days. Poly (ADP-ribose) polymerase (PARP) is a highly abundant nuclear enzyme involved in DNA repair that synthesises poly ADP ribose from NAD+ in response to damaged DNA. When cells are exposed to a critical level of DNA damaging agents, cellular apoptosis is induced through an intracellular signalling cascade. Activation of the caspase family of apoptosis-specific proteases results in the cleavage of PARP by caspase-3[217]. Therefore, cleaved-PARP is regarded as a biomarker of apoptosis in cells. We performed western blotting to examine the levels of cleaved PARP and E2F1 (Figure 3.2H) and observed a high level of apoptosis induced by J579-44. PRMT5 regulates transcription and many downstream events through the methylation of transcription factors such as E2F1, and our results showed an increase in the expression level of E2F1 upon treatment with J579-44 (Figure 3.2H). Thus, J579-44 is a selective PRMT5 inhibitor that induces cellular apoptosis and activates the release of the PRMT5 target protein E2F1 in U2OS cells.

J579-44 was found to impair colony formation in a clonogenic assay on HCT116 cells (Figure 3.2I). A series of incremental concentrations was used (1.6 nM, 8 nM, 40 nM, 200 nM, and 1000 nM), with the J578-68 treated samples used as controls. The total treatment was 8 days. The results showed that in comparison with J578-68, cells treated with J579-44 lost reproductive capacity, and a concentration-dependent cytotoxic effect was observed.

To investigate the effect of J579-44 on the catalytic activity of arginine methyltransferases for various substrates, we measured the expression level of SDMe in HCT116 cells after 6 days of treatment. We found that the global level of SDMe was considerably decreased after treatment with J579-44 at a concentration of 40 nM, while its less active analogue J578-68 led a slight decrease at a concentration of 1 μM (Figure 3.2J). Thus, J579-44 inhibited the catalytic ability of PRMT5 methyltransferase in cells and altered the cellular methylation levels of SDMe.

Figure 3.1 Characterisation of candidate PRMT5 inhibitors

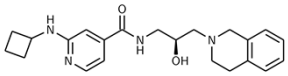
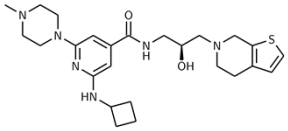
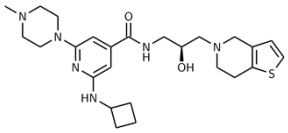
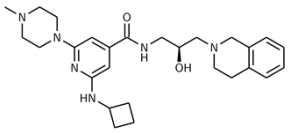
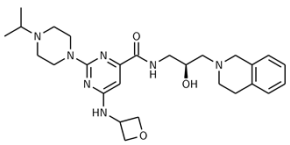
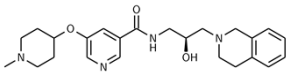
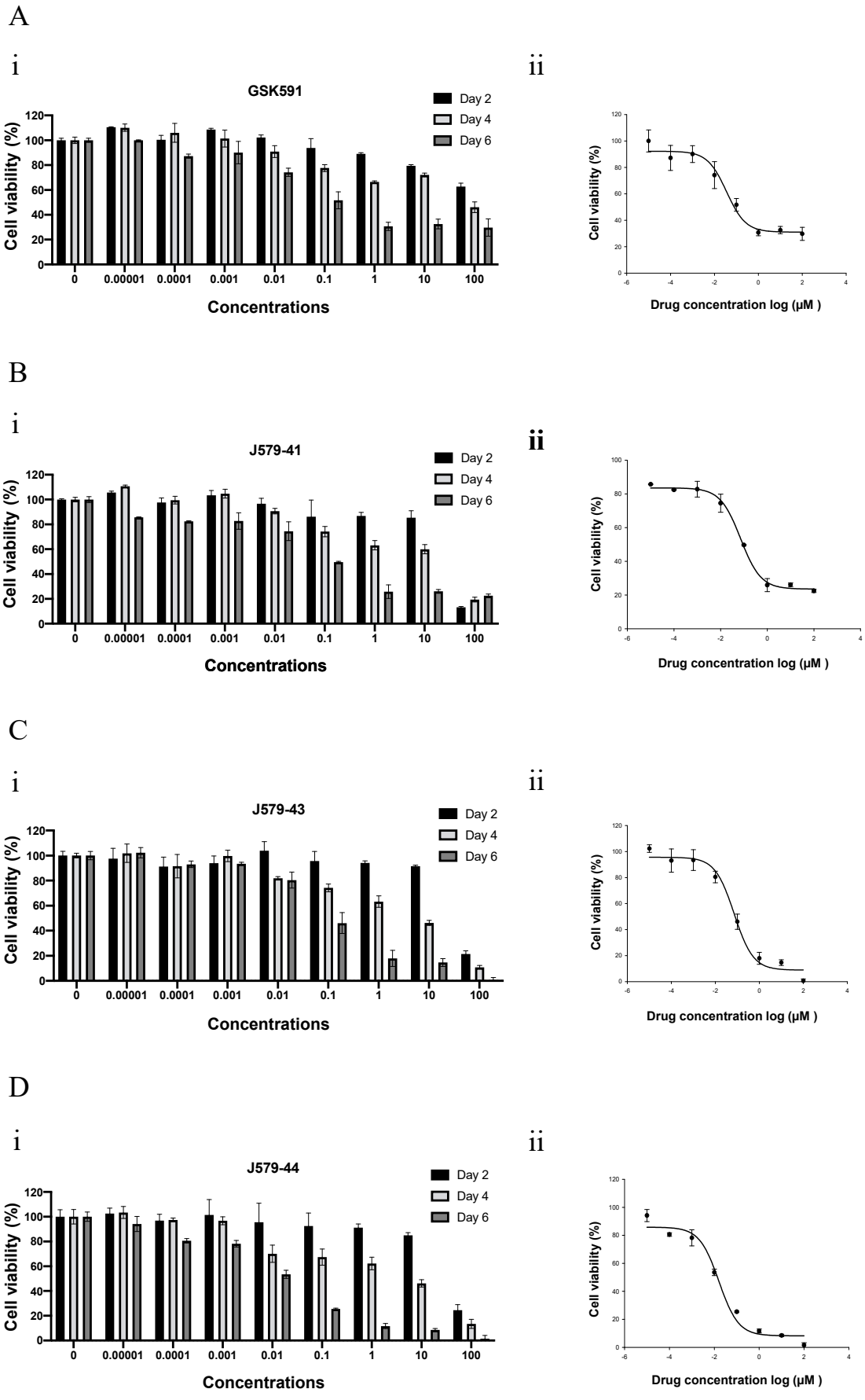
Compound	Formula structure	Molecular formula	Molecular weight
GSK591		**C22H28N4O2**	**380.20**
J579-41		**C25H36N6O2S**	**484.66**
J579-43		**C25H36N6O2S**	**484.66**
J579-44		**C27H38N6O2**	**478.63**
J578-65		**C27H39N7O3**	**509.64**
J578-68		**C24H32N4O3**	**424.54**

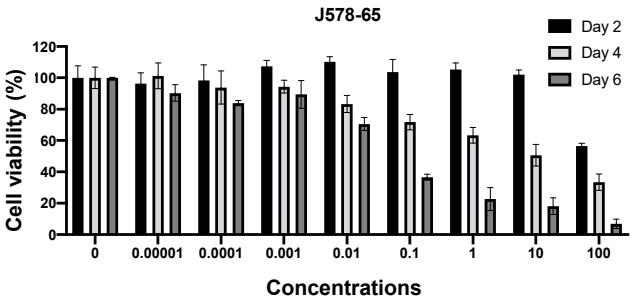
Figure 3.1 Characterisation of candidate PRMT5 inhibitors. The chart shows the structural formulas of the six small-molecular inhibitors of PRMT5 studied, including GSK591, J579-41, J579-43, J579-44, J578-65, and J578-68. The molecular weight of each compound is indicated. All compounds were dissolved in DMSO to prepare a 10 mM stock solution.

Figure 3.2 The selection of the PRMT5 inhibitor via the MTT assay

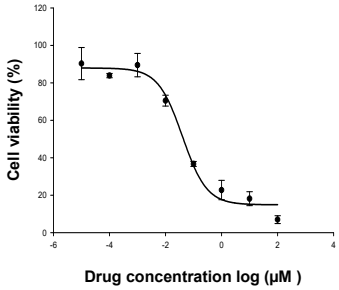


E

i

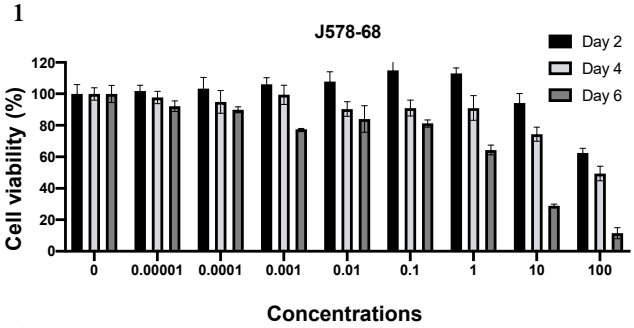


ii

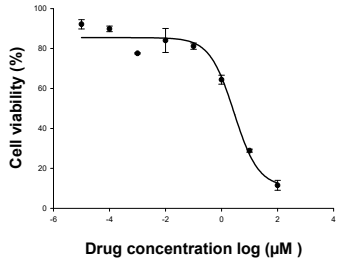


F

i



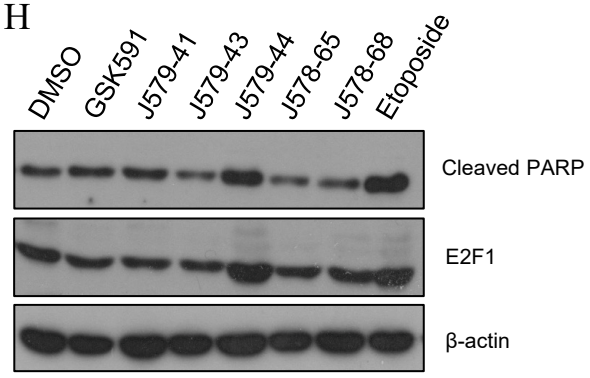
ii



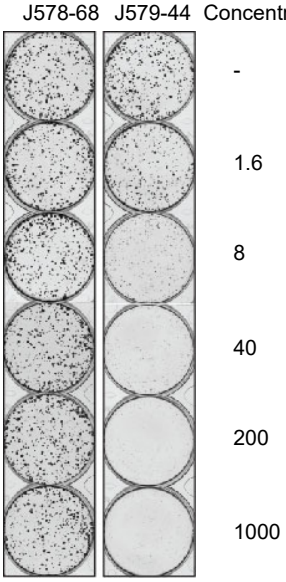
G

Compounds	IC50 (μM)
GSK591	0.1155 ± 0.0567
J579-41	0.0917 ± 0.0297
J579-43	0.0914 ± 0.0717
J579-44	0.0161 ± 0.0029
J578-65	0.0700 ± 0.0146
J578-68	2.7700 ± 0.3422

H

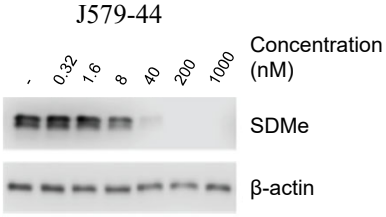


I



J

i



ii

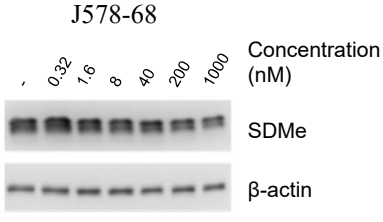


Figure 3.2 The selection of the PRMT5 inhibitor via the MTT assay. The MTT assay was performed to assess the cytotoxic effects of each PRMT5 inhibitor. All compounds tested were dissolved in DMSO, and the group of DMSO treated cells was set as the control. A concentration gradient of 10^{-5} μM, 10^{-4} μM, 10^{-3} μM, 10^{-2} μM, 10^{-1} μM, 1 μM, 10 μM, and 100 μM for each compound was used in U2OS cells. (i) The cell viability (%) of cells tested with each inhibitor normalized to DMSO treated cells after 2, 4, and 6 days of treatment. (ii) The IC50 curve after 6 days of treatment with each compound. The compounds used from (A) to (F) are GSK591, J579-41, J579-43, J579-44, J578-65, and J578-68. (G) The IC50 of the six PRMT5 inhibitors. Data are presented as mean ± SD; n=4. (H) Western blot showing the presence of cleaved PARP and E2F1. J579-44 was selected for use as a PRMT5 inhibitor as it induced cell apoptosis and activated the release of E2F1 in U2OS cells. U2OS cells were treated with 32 nM DMSO, 2x the IC50 of each compound, and 32 nM etoposide as control for six days. The data shown are representative of two experiments. (I) A colony formation assay in HCT116 cells was performed for 8 days using increasing concentrations of J579-44 and its less active analogue J578-68, as indicated. (J) Western blots demonstrating SDMe levels in HCT116 cells after 6 days of treatment with increasing concentrations of (i) J579-44, and (ii) its less active analogue J578-68. (I) and (J) were conducted by Dr. Wojciech Barczak.

3.3 Measurement of the EC50 of PRMT5 inhibitors via enzyme assays

To investigate the influence of J579-44 on PRMT5 enzymatic activity, we used the PRMT5 Chemiluminescent enzyme kit. The kit contained a 96-well plate pre-coated with the peptide substrate for histone H4, anti-methylated H4R3 antibody, the secondary HRP-labelled antibody, SAM, methyltransferase assay buffer, and the purified PRMT5 enzyme (expressed in HEK293 cells). Importantly, the kit has a highly specific antibody that recognises methylated H4R3. Methyltransferase detection was performed as per manufacturer's instructions: SAM was incubated with samples containing the assay buffer and methyltransferase enzyme, the primary antibody was added, and the plate was treated with an HRP-labelled secondary antibody followed by addition of the HRP substrate to produce chemiluminescence. The positive control for detection contained PRMT5, the HMT assay buffer, and SAM without the test inhibitor, whereas the substrate control contained PRMT5 and the HMT assay buffer alone. A negative control containing the HMT assay buffer and SAM was used. Samples were imaged in a luminometer or microtiter plate capable of reading chemiluminescence. Figure 3.3A describes the reactions being executed with the use of the PRMT5 enzyme kit.

Next, we tested the chemiluminescence of samples using several different concentrations (10^{-7} mM-1 mM) of J579-44, and the EC50 curves were generated (Figure 3.3B). J579-44 inhibited the enzymatic activity of PRMT5 in a dose-dependent manner. The corresponding EC50 value was 0.804 μM, indicating that J579-44 directly

inhibited the methyltransferase activity of PRMT5. In comparison, the EC50 value of the analogue J578-68 was 41.37 μM. Thus, our results showed that J579-44 inhibits the methyltransferase activity of PRMT5.

Figure 3.3 Enzymatic assays using J579-44 and the analogue J578-68

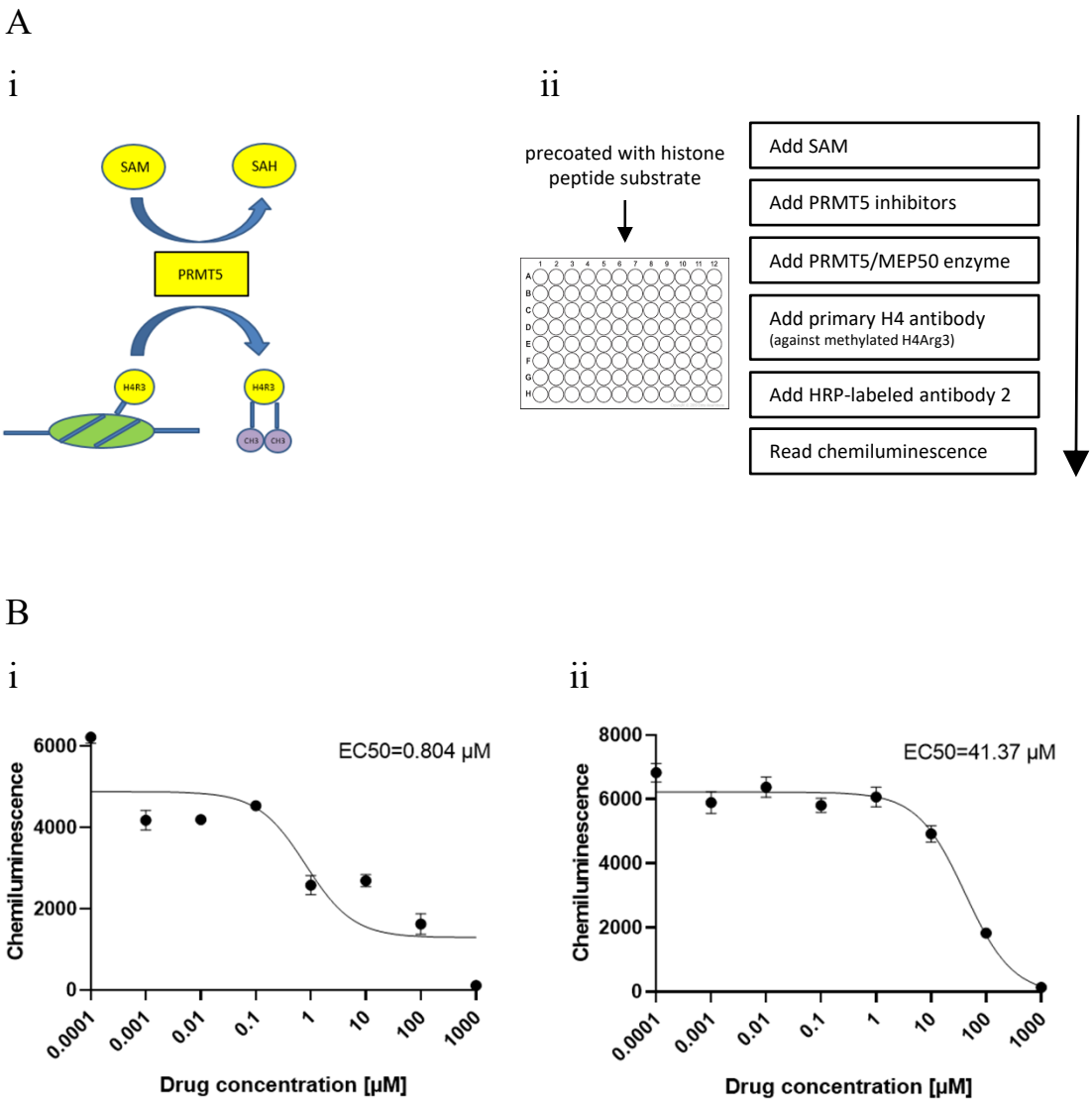


Figure 3.3 Enzymatic assays using J579-44 and the analogue J578-68. (A) The outline of the PRMT5 inhibitor activity assay. (i) The PRMT5 enzyme catalyses histone arginine methylation, where SAM is the methyl donor. (ii) The activity of different PRMT5 inhibitors was identified using the PRMT5 Direct Activity Chemiluminescent Assay Kit. The kit has a highly specific antibody that recognizes the methylated R3 residue of Histone H4. (B) The EC50 of (i) J579-44, and (ii) J578-68 was calculated as 0.804 µM and 41.37 µM, respectively. n=3.

3.4 Chapter summary

In this chapter, we sought to identify an effective PRMT5 inhibitor that could be used as a powerful chemical probe to inhibit the activity of PRMT5 and enable the study of its biological mechanisms in cancer cells. The pharmacological activity of PRMT5 inhibitors were evaluated in cell-based and enzymatic assays.

The results from the cell-based assays indicate that J579-44 shows a strong cytotoxic effect in U2OS cells, with an IC50 value as low as 16 nM. It induced cellular apoptosis and activated the release of the PRMT5 target E2F1. Further, J579-44 exhibited significant anti-proliferation effects and altered the cellular methylation levels in HCT116 cells. The results from the enzymatic assays showed that J579-44 inhibited PRMT5 methyltransferase activity with an EC50 value of 0.804 μM.

To summarise, we screened a total of 6 inhibitors of PRMT5 and identified J579-44 as having a low IC50 in cells and a low EC50 in enzymatic assays. Additionally, the inhibitor J578-68, a close analogue of J579-44, was also analysed in this experiment as a control for further studies. Figure 3.4 describes the characteristics of J579-44 and J578-68. Taken together, our results showed that J579-44 is an effective chemical probe that can be used to query the biological mechanisms underlying PRMT5 function.

Figure 3.4 Characterisation of the PRMT5 inhibitor J579-44 and its analogue J578-68

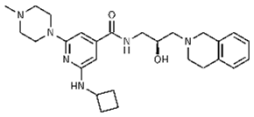
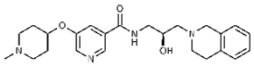
Compound	Formula structure	Molecular formula	MW	IC50 (μM)	EC50 (μM)
J579-44		C27H38N6O2	478.63	0.0161	0.804
J578-68		C24H32N4O3	424.54	2.77	41.37

Figure 3.4 Characterisation of the PRMT5 inhibitor J579-44 and its analogue J578-68. The chart shows the formula structure, molecular formula, molecular weight, IC50, and EC50 value of J579-44 and J578-68.

Chapter 4: PRMT5 inhibition induces cellular responses through E2F1

4.1 Introduction

In Chapter 3, we described the identification and characterisation of a small-molecule inhibitor of PRMT5, which can be used as a chemical tool for the exploration and study of the biological mechanisms underlying the role of PRMT5 in tumorigenesis. Additionally, we studied the biological functions of PRMT5, including its role in anti-proliferation, regulation of the cell cycle, DNA damage, apoptosis, cell migration, and invasion. The transcription factor E2F1 plays an important role in PRMT5 related pathways, as PRMT5 directly methylates E2F1 at the R111 and R113 residues[177]. We generated *E2F1* CRISPR knockout cells using the CRISPR-Cas9 technology, and altered the activity of PRMT5 to analyse the association of E2F1 with PRMT5 in multiple cellular processes.

4.2 PRMT5 inhibition triggers cell apoptosis and induces cell accumulation in the sub-G1 phase

Previously, we have shown that the expression of apoptotic effector cleaved-PARP was increased in the J579-44 treated U2OS cells (Figure 3.2H). We identified cells undergoing early apoptosis using an apoptosis detection kit to detect the phospholipid-binding protein Annexin V that binds specifically to phosphatidylserine. Labelled Annexin V was used to detect apoptotic cells via flow cytometry as the display of phosphatidylserine on the extracellular face of the plasma membrane is a hallmark of early apoptosis and Annexin V is not permeable into cells.

We treated a subset of two cell lines, HCT116 p53+/+ and HCT116 p53-/-, with J579-44 and J578-68, using three concentrations (0.1, 1, and 10 μM of each inhibitor), with DMSO-treated cells used as controls. We tested for early apoptosis at three-time points, i.e., day 2, day 4, and day 6 (Figure 4.1A, Figure 4.1B). Our results showed that J579-44 induced apoptosis in the two cell types at all three concentrations used (Figure 4.1C, Figure 4.1D) and that the percentage of cells undergoing apoptosis was increased in a time-dependent manner (Figure 4.1E, Figure 4.1F). Additionally, we observed apoptosis at day 2, indicating that PRMT5 inhibition activated the apoptosis pathways and triggered early cell death. Interestingly, we found a higher incidence of apoptosis in p53-/- cells compared to p53+/+ cells. Figure 4.1G shows the results of the apoptosis assay in two subsets of cells treated with J579-44 at three concentrations after day 6 (the *p*-values for the comparison of p53-/- relative to p53+/+ cells using concentrations

of 0.1, 1, and 10 μM for J579-44 were 0.0087, 0.00052, and 0.00017, respectively), indicating that the existence of p53 attenuates the PRMT5 induced apoptotic response in cells.

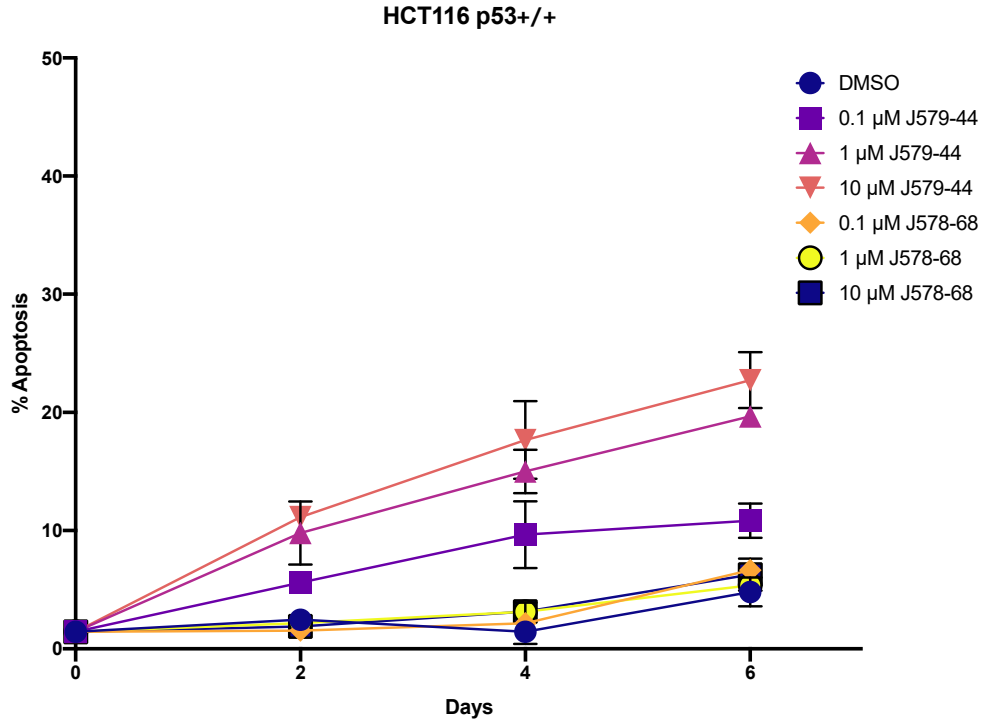
Next, we examined the effect of PRMT5 inhibition on cell cycle progression using flow cytometry. We treated HCT116 p53+/+ and HCT116 p53-/- cells with DMSO as a control, and J579-44 or J578-68 at a concentration of 1 μM each, and obtained the cell cycle phase distribution. In both cell types, we observed a significant decrease in the G1 population and a marginal increase in the S and G2/M populations after treatment with J579-44 (Figure 4.2A and 4.2B). Both subtypes did not progress from the sub-G1 phase between day 1 to day 6 (Figure 4.2C and 4.2D). Interestingly, we observed a much higher percentage of cells in the sub-G1 phase in p53-/- cells compared to p53+/+ cells (42.62 ± 3.15% vs. 13.89 ± 0.73%; p <0.0001; Figure 4.2E). Treatment with J579-44 led to an increase in the percentage of cells in the sub-G1 phase in both p53+/+ and p53-/- cells, indicating that the absence of p53 augments the accumulation of cells in this phase.

Next, we treated p53 +/+ and p53-/- cells with DMSO, or 1 μM each of J579-44, J578-68, and etoposide for 6 days. The cells treated with etoposide were used as the control group. Western blotting was performed using anti-E2F1, anti-cleaved PARP, and anti-p53 antibodies. Our results showed that treatment with J579-44 upregulated the expression of cleaved-PARP in p53-/- cells relative to p53+/+ cells (Figure 4.2F). J579-44 also increased the expression of p53, indicating that PRMT5 inhibition triggers

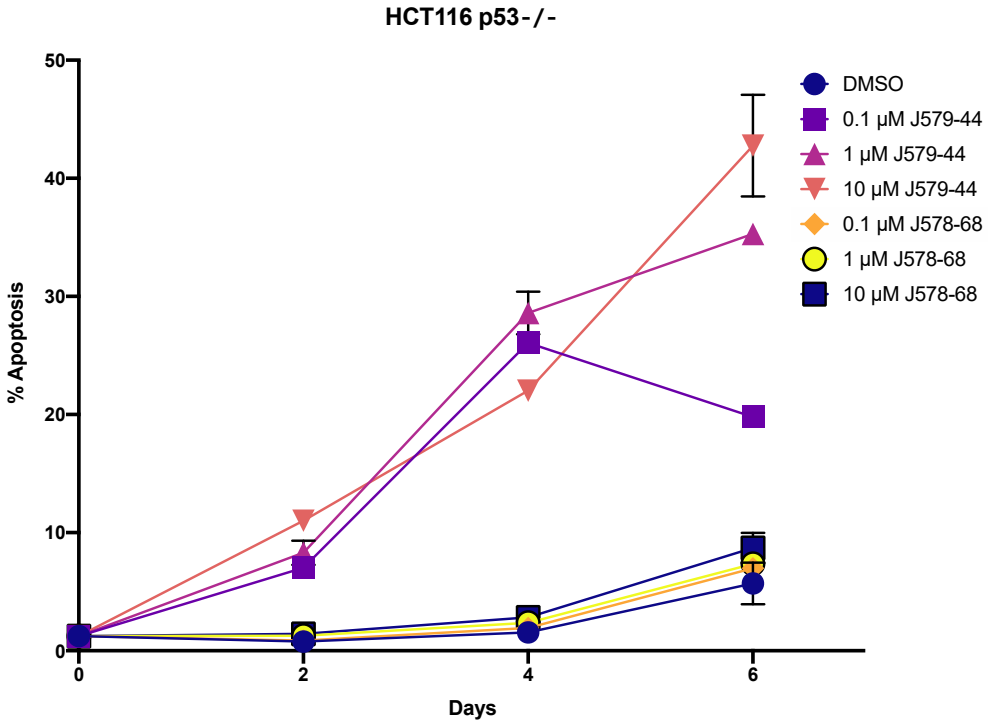
a p53 response in HCT116 cells. Arginine methylation is a part of the p53 response as PRMT5 monomethylates p53 within its oligomerization domain on a "GRG$^{R}/_{K}$" sequence similar to that found in histones, which modestly influences p53 tetramer formation and its target selection[176]. Therefore, cells with p53 mutations were more susceptible to PRMT5 inhibition than p53+/+ cells.

Figure 4.1 PRMT5 inhibition triggers cellular apoptosis

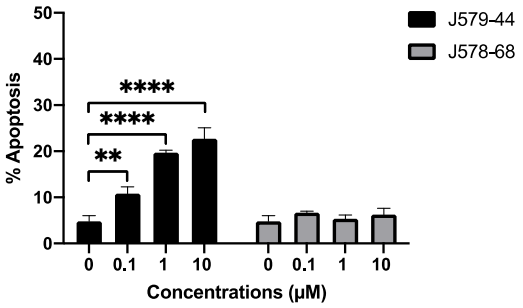
A



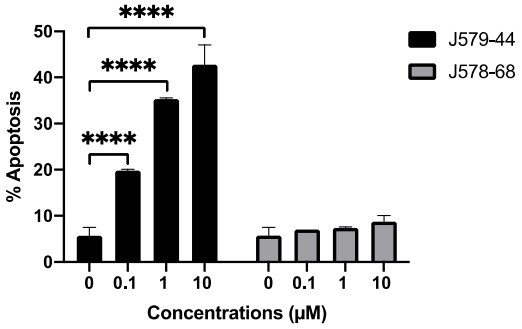
B



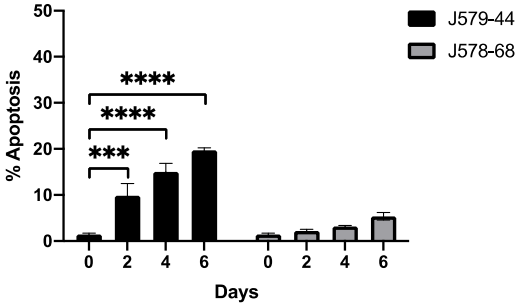
C


J579-44
J578-68
% Apoptosis
50
40
30
20
10
0
****
****
**
0 0.1 1 10 0 0.1 1 10
Concentrations (μM)

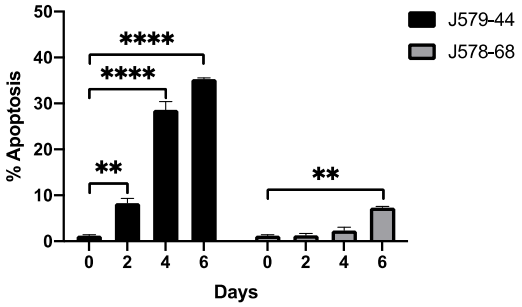
D


J579-44
J578-68
% Apoptosis
50
40
30
20
10
0
****
****
****
0 0.1 1 10 0 0.1 1 10
Concentrations (μM)

E


J579-44
J578-68
% Apoptosis
50
40
30
20
10
0
****
****
***
0 2 4 6 0 2 4 6
Days

F


J579-44
J578-68
% Apoptosis
50
40
30
20
10
0
****
****
**
**
0 2 4 6 0 2 4 6
Days

G

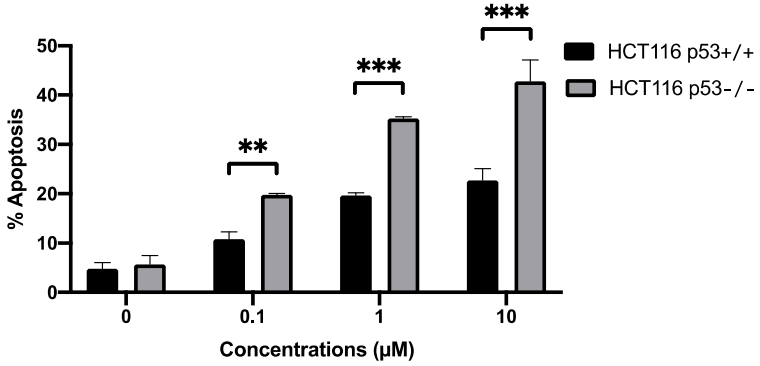

HCT116 p53+/+
HCT116 p53-/-
% Apoptosis
50
40
30
20
10
0
***
***
**
0 0.1 1 10
Concentrations (μM)

Figure 4.1 PRMT5 inhibition triggers cellular apoptosis. (A) HCT116 p53+/+, and (B) HCT116 p53-/- cells were treated with J579-44 and J578-68 using three concentrations including 0.1, 1, and 10 μM, with DMSO treated cells used as control. Early apoptosis was assayed at three-time points, i.e., at days 2, 4, and 6, with n=3. (C-D) J579-44 induced cell apoptosis was analysed in a concentration-dependent manner. The data was obtained from (A) and (B) is shown, using p53+/+ cells or p53-/- cells treated with the three concentrations of J579-44 for 6 days. (C) The *p*-value comparing the 0.1, 1, and 10 μM groups relative to the control was 0.0094, <0.0001, and <0.0001. (D) The *p*-value comparing the 0.1, 1, and 10 μM groups relative to the control was <0.0001, <0.0001, <0.0001. (E-F) J579-44 induced cellular apoptosis in a time-dependent manner. The data were obtained from the results of (A) and (B), that represented both subtypes of cells that were treated with 1 μM J579-44 for 0, 2, 4, and 6 days. (E) The *p*-values comparing the results at days 2, 4, and 6 relative to day 0 was 0.00069, <0.0001, <0.0001. (F) The *p*-values comparing the results at days 2, 4, and 6 relative to day 0 was 0.0096, <0.0001, <0.0001. (G) p53 attenuated the PRMT5 induced cellular apoptotic response. The data obtained from (C) and (D) were evaluated to identify the effect of p53 on the PRMT5 induced cellular apoptotic response. The *p*-values for the comparison between p53-/- cells and p53+/+ cells on using 0.1,1 and 10 μM of J579-44 were 0.0087, 0.00052, and 0.00017, respectively. Data are presented as mean ± SD, and the error bars indicate the SD for biological replicates. Statistical analyses were performed using a two-tailed, unpaired Student's *t*-test. A *p*-value of < 0.05 was considered as significant and is indicated using $*p < 0.05$, $**p < 0.01$, $***p < 0.001$, and $****p < 0.0001$.

Figure 4.2 PRMT5 inhibition induces cell accumulation in the sub-G1 phase

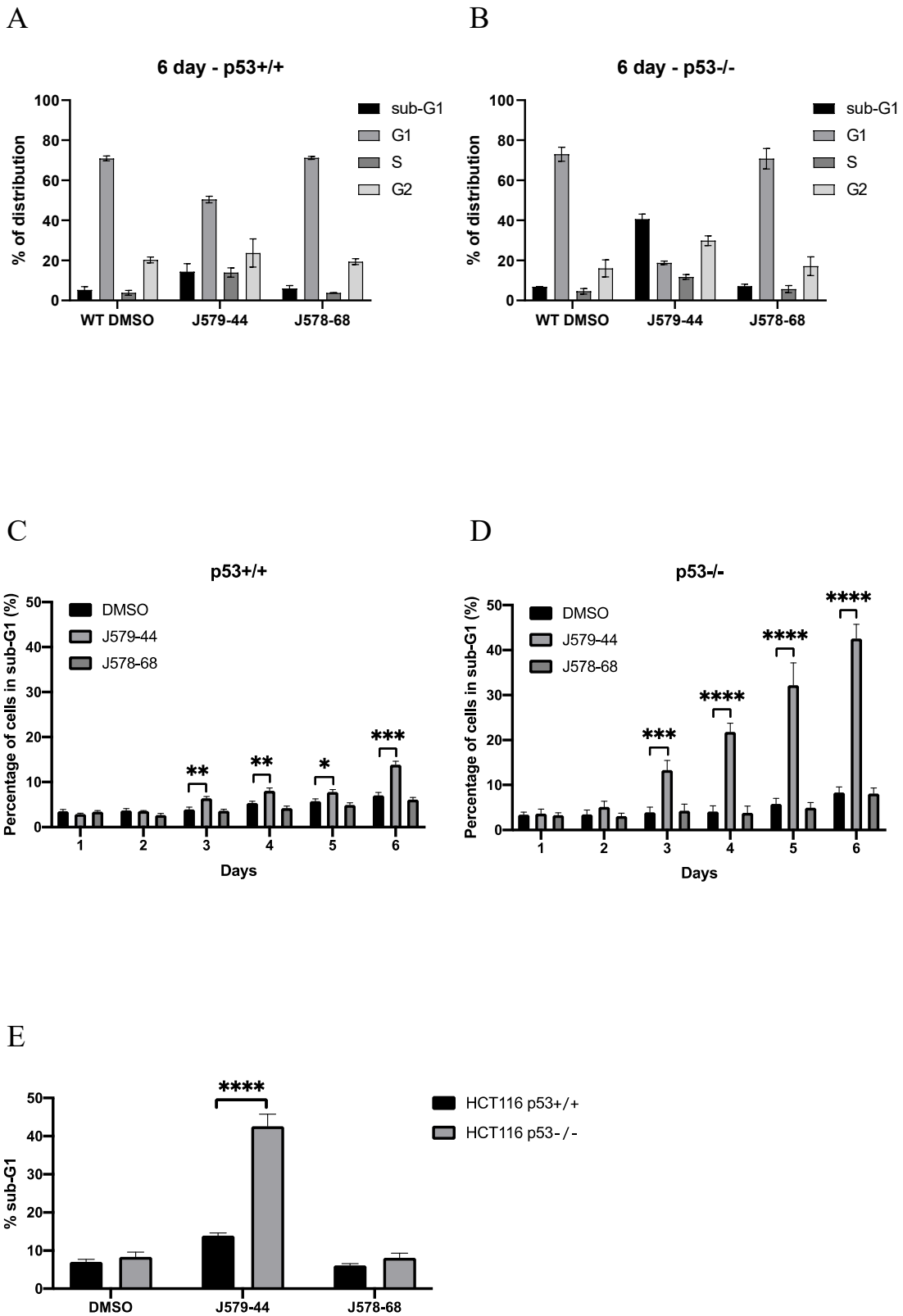


Figure 4.2 PRMT5 inhibition induces cell accumulation in the sub-G1 phase. (A) HCT116 p53+/+, and (B) HCT116 p53-/- cells were treated with DMSO as control, and a concentration of 1 μM each of J579-44, and J578-68, and the cell cycle phase distribution after 6 days was obtained (n=4). (C) HCT116 p53+/+ cells treated with J579-44 remained in the sub-G1 phase of the cell cycle between day 1 to day 6, with a proportion of 6.41% ± 0.37%, 8.08% ± 0.63%, 7.83% ± 0.52%, and 13.89% ± 0.73% cells, respectively. The corresponding proportion of DMSO treated cells were 3.93% ± 0.48%, 5.36% ± 0.38%, 5.76% ± 0.51%, and 7.05% ± 0.64%, respectively. The corresponding *p*-values for the comparison between treatment with J579-44 and the DMSO control were 0.0066, 0.0098, 0.0297, and 0.0004 respectively (n=4). (D) HCT116 p53-/- cells treated with J579-44 remained in the sub-G1 phase of the cell cycle between day 1 to day 6 with a proportion of 13.31% ±2.16%, 21.84% ± 1.87%, 32.21% ± 4.96%, and 42.62% ± 3.15%, respectively, whereas the corresponding proportion of cells treated with DMSO that remained in the sub-G1 phase from day 3 to day 6 was 3.95% ± 1.1%, 4.13% ± 1.26%, 5.82% ± 1.22%, and 8.35% ± 1.22%, respectively. The corresponding *p*-values of 0.0002, <0.0001, <0.0001, and <0.0001 were obtained for the comparison between the treated and the control samples, respectively (n=4). (E) A percentage of p53+/+ (13.89% ± 0.73%) and p53-/- (42.62% ± 3.15%) cells remained in sub-G1 after treatment for 6 days ($p < 0.0001$; n=4). (F) Western blots were developed using anti-E2F1, anti-cleaved PARP, and anti-p53 antibodies, and β-actin was used as a loading control. All cells were treated using the same experimental conditions, i.e., 1 μM of J579-44 or J578-68, and DMSO was used as a control. The data are shown as mean ± SD, and error bars indicate the SD of biological replicates. Statistical analyses were performed using a two-tailed, unpaired Student's *t*-test. The *p*-values of < 0.05 were considered significant and are indicated as $*p < 0.05$, $**p < 0.01$, $***p < 0.001$, and $****p < 0.0001$.

4.3 PRMT5 inhibition impairs cell proliferation and viability

We performed cell count assays to analyse the effect of PRMT5 inhibition on cell growth. Both HCT116 p53+/+ and HCT116 p53-/- cells were treated with DMSO, or 1μM each of J579-44, and J578-68. We calculated cell numbers at four different time points, i.e., days 2, 4, 6, and 8. Day 0 was set as control, which represented samples has been treated. Cells were stained with the Trypan Blue dye for 5 min and the cell numbers were estimated using the Luna-II™ Automated Cell Counter.

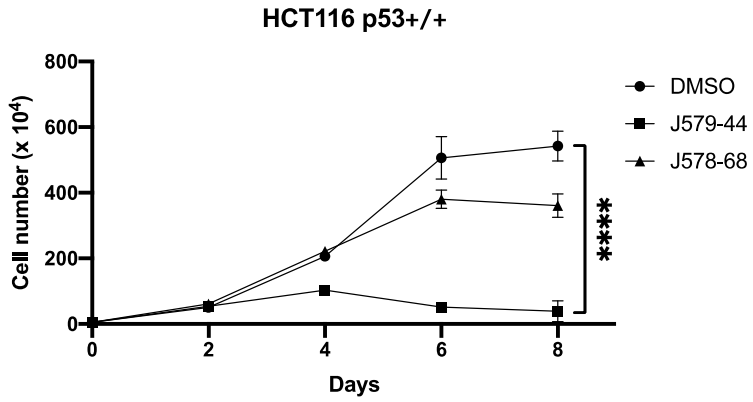
We found that PRMT5 inhibition decreases cell proliferation. A significant decrease in the number of cells in p53+/+ (mean number of DMSO-treated group was 542.33 $\times 10^4$; mean number of J579-44 treated group was 38.67 $\times 10^4$; $p < 0.0001$; Figure 4.3A) and p53-/- cells (mean number of DMSO treated group was 600.33 $\times 10^4$; mean number of J579-44 treated group was 20 $\times 10^4$; $p < 0.0001$; Figure 4.3B) upon treatment with J579-44 for 8 days, confirming previous results for colony formation (Figure 3.2I). However, the difference in the response to treatment with J579-44 for proliferation comparing p53+/+ and p53-/- was not significant (mean number for p53+/+ was 38.67 $\times 10^4$; the mean number for p53-/- cells was 20 $\times 10^4$; $p = 0.2192$; Figure 4.3C).

We determined the effect of PRMT5 inhibition on cell viability via the MTT assay. Data from the previously conducted MTT assay (Figure 3.2D, Figure 3.2F) were used to re-analyse. U2OS cells were treated with J579-44 and J578-68 at concentrations of 0.1, 1, and 10 μM for 2, 4, and 6 days (Figure 4.3D), and DMSO treatment was used

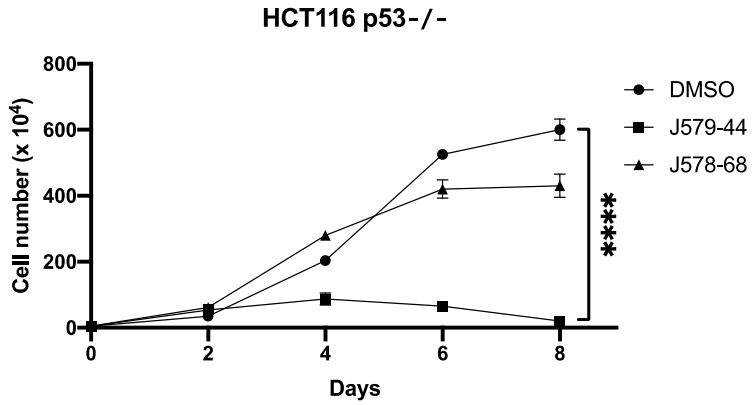
as a control. J579-44 treatment was found to decrease cell viability in a concentration-dependent manner. The percentage of viable cells in the 0.1, 1, and 10 μM group treated with J579-44 relative to DMSO control after 6 days was 84.97%, 46.18%, and 8.49%, with corresponding *p*-values of 0.0016, <0.0001, and <0.0001, respectively. Similarly, in the comparison of treatment with J578-68 relative to the DMSO control, the cell viability was 94.26%, 74.34%, and 28.86%, respectively, and the corresponding *p*-values were 0.634, 0.0019, and <0.0001, respectively (Figure 4.3E). For the estimation of the time dependence, the percentage of viable cells after days 2, 4, and 6 upon treatment with 1 μM J579-44 relative to day 0 were 89.17%, 62.23%, and 11.67%, respectively, with the corresponding *p*-values of 0.0017, <0.0001, and <0.0001, respectively. Similarly, the percentage of viable cells upon treatment with 1 μM J578-68 were 113.05%, 91.02%, and 64.41%, respectively, and the corresponding *p*-values of 0.625, 0.317, and 0.002, respectively, were obtained (Figure 4.3F).

Figure 4.3 PRMT5 inhibition impairs cell proliferation and viability

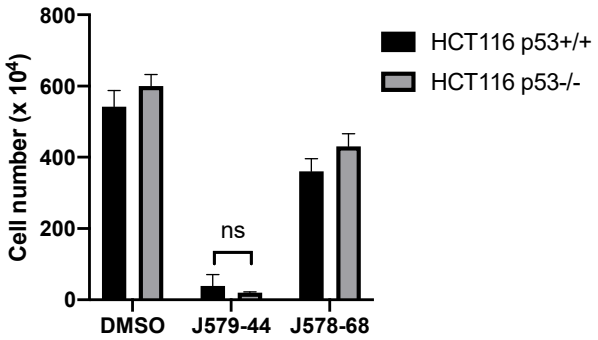
A



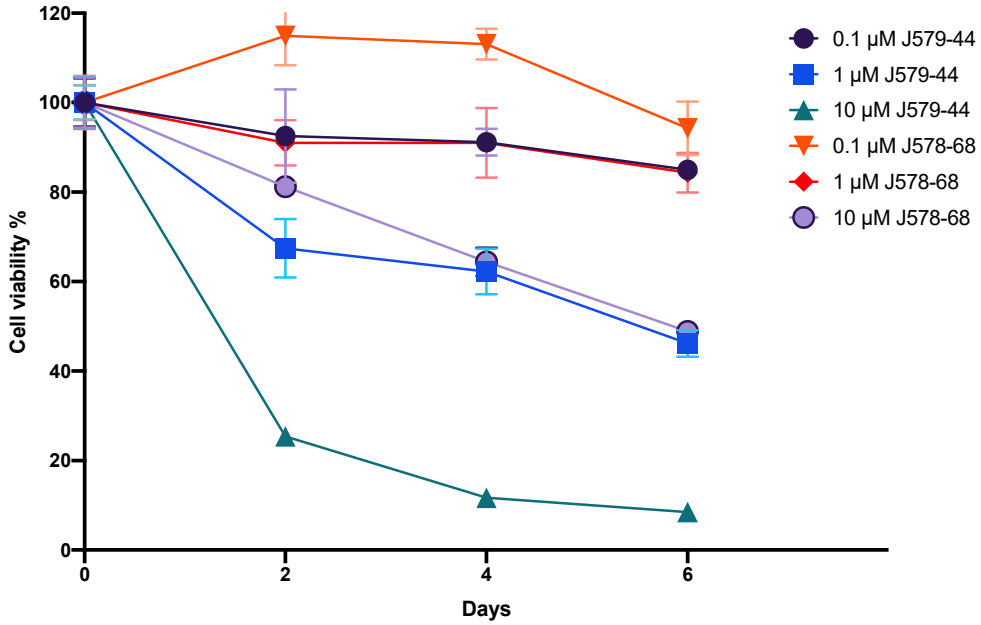
B



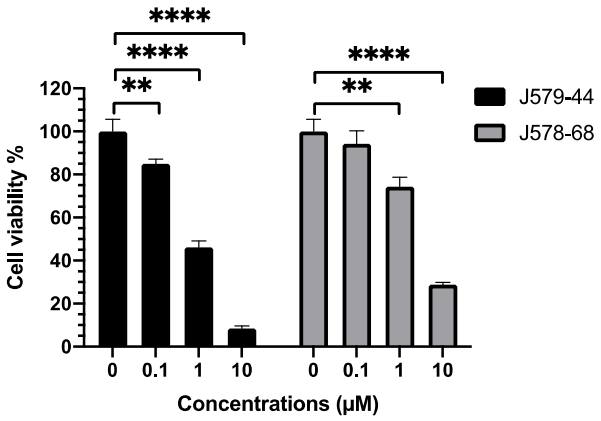
C



D


Cell viability %
120
100
80
60
40
20
0
0
2
4
6
Days
0.1 μM J579-44
1 μM J579-44
10 μM J579-44
0.1 μM J578-68
1 μM J578-68
10 μM J578-68

E


****
****
**
****
**
Cell viability %
120
100
80
60
40
20
0
0
0.1
1
10
0
0.1
1
10
Concentrations (μM)
J579-44
J578-68

F

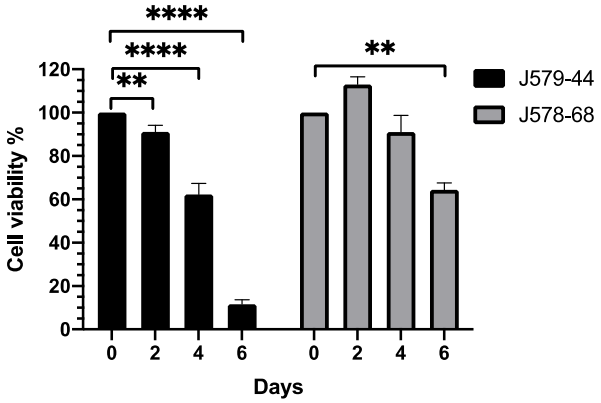

****
****
**
**
Cell viability %
120
100
80
60
40
20
0
0
2
4
6
0
2
4
6
Days
J579-44
J578-68

Figure 4.3 PRMT5 inhibition impairs cell proliferation and viability. (A) HCT116 p53+/+ cells were treated with DMSO, and with 1μM J579-44 or J578-68, and the cell number was measured using the Luna-II™ Automated Cell Counter at four-time points, i.e., at 2, 4, 6 and 8 days. After day 8, the cell numbers of the DMSO, J579-44, and J578-68 treated groups was identified as 542.33 ± 45.43 $\times 10^4$, 38.67 ± 32.34 $\times 10^4$, and 360.67 ± 35.33 $\times 10^4$ cells, respectively, with a corresponding *p*-value of <0.0001 (n=4). (B) In similar experimental conditions for HCT116 p53-/- cells, the mean number of cells in the DMSO, J579-44, and J578-68 treated groups after 8 days were 600.33 ± 32.33 $\times 10^4$, 20 ± 2.5 $\times 10^4$, and 430.67 ± 35.33 $\times 10^4$ cells, respectively, with a corresponding *p*-value of <0.0001 (n=4). (C) The difference in response to J579-44 treatment for proliferation in cells that were p53+/+ and p53-/- was not significant. The number of HCT116 p53 +/+ cells was 38.67 ± 32.34 $\times 10^4$, and for HCT116 p53-/- cells was 20 ± 2.5 $\times 10^4$ ($p = 0.2192$, n=4). (D) PRMT5 inhibition impairs cell viability. The effect of PRMT5 inhibition on cell viability was assessed via MTT assay in U2OS cells treated with J579-44 and J578-68 using the concentrations of 0.1, 1, and 10 μM for 2, 4, and 6 days (n=3). (E) J579-44 treatment decreased cell viability in a concentration-dependent manner. The percentage of viable cells after treatment with 0.1 μM, 1 μM and 10 μM J579-44 compared to the DMSO control after 6 days were 84.97% ± 2.18%, 46.18% ± 2.97%, and 8.49% 1.19%, respectively, with corresponding *p*-values of 0.0016, <0.0001, and <0.0001, respectively (n=3). (F) J579-44 treatment decreased cell viability in a time-dependent manner. The percentage of viable cells at 2, 4, and 6 days upon treatment with 1 μM J579-44 treatment was 89.17% ± 3.01%, 62.23% ± 5.09%, and 11.67% ± 1.99%, respectively, with corresponding *p*-values of 0.0017, <0.0001, and <0.0001, respectively, when compared to day 0 (n=3). Data are presented as mean ± SD. Error bars indicate the SD of biological replicates. Statistical analyses were performed using a two-tailed, unpaired Student's *t*-test. The *p*-values < 0.05 were considered as significant and are indicated as $*p < 0.05$, $**p < 0.01$, $***p < 0.001$, and $****p < 0.0001$. NS indicates not significant.

4.4 PRMT5 inhibition decreases cell migration and invasion

Cell migration is related to metastatic progression in cancer research. Cancer cells first migrate and invade tissues via the ECM, intravasate into the blood circulation, attach to a distant site, and eventually extravasate to form distant foci[52]. To investigate the effect of PRMT5 inhibition on cell migration and invasion, we performed a Transwell assay to assess cell migratory behaviour with and without inhibitory treatment for PRMT5. Additionally, we investigated the ability for cell invasion by adding a layer of ECM on top of the transwell membrane to mimic the process of ECM invasion and extravasation.

We treated HCT116 p53-/- cells with 1 μM J579-44 for 24 h, with DMSO used as the control treatment. The number of migrated cells could be quantified by counting crystal violet stained cells using a microscope. The invasion assay was modified from the migration assay. Cells were treated with 1 μM J579-44 and DMSO for 48 h. We precoated ECM materials on top of the transwell membrane and added the treated cells on top of the pre-coated ECM membrane.

Our results showed that PRMT5 inhibition decreases the cell migration and invasion of J579-44 treated cells significantly, and the mean number of migrated cells relative to the control-treated cells was 64.2 (p = 0.0074; Figure 4.4A). Similarly, the mean number of invaded cells relative to the control-treated cells was 51.44 (p = 0.0019; Figure 4.4 B). The data indicated that PRMT5 may play an important role in regulating

cell migration, invasion, and tumour metastasis. Furthermore, as the migration and invasion assays were performed using cells treated with J579-44 for 24 h and 48 h, respectively, the results indicate that the PRMT5 inhibitor impaired both cell migration and invasion at a very early stage.

Figure 4.4 PRMT5 inhibition decreases cell migration and invasion

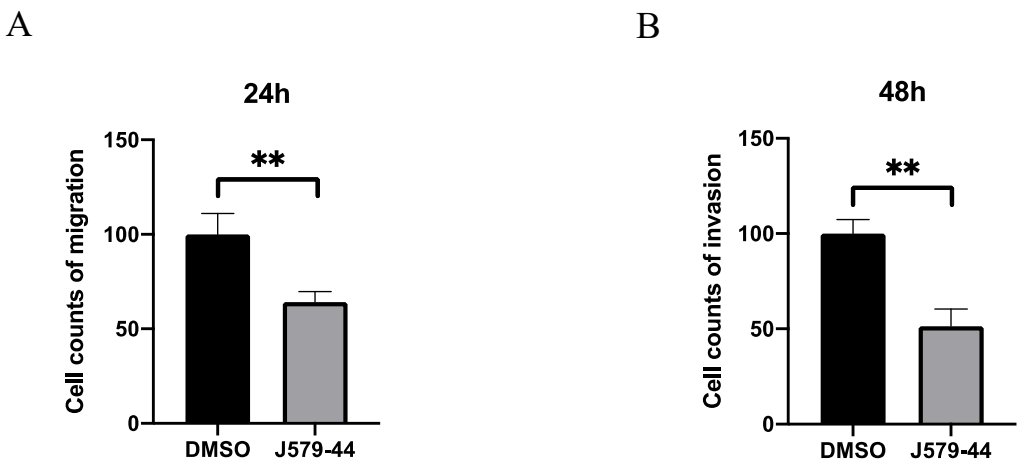


Figure 4.4 PRMT5 inhibition decreases cell migration and invasion. (A) J579-44 inhibited cell migration. HCT116 p53-/- cells were treated with 1 µM J579-44 or DMSO for 24 h. The number of migrated cells quantified relative to the DMSO control was 64.2 ± 5.43 (p = 0.0074; n=3). (B) J579-44 inhibited cell invasion. The invasion assay was performed similarly to the migration assay except that the membrane was precoated with ECM and the treatment was performed for 48 h. The number of invaded cells on treatment with J579-44 was 51.44 ± 8.91 (p = 0.0019; n=3). Data are presented as mean ± SD. Error bars indicate the SD of biological replicates. Statistical analyses were performed using the two-tailed, unpaired Student's t-test. The *p*-values < 0.05 were considered as significant and are indicated as *$p < 0.05$, **$p < 0.01$, ***$p < 0.001$, and ****$p < 0.0001$.

4.5 Generation of stable E2F1 CRISPR cells using CRISPR-Cas9 genome editing

As previously mentioned in Chapter 1.9, in addition to its ability to methylate histones, PRMT5 can influence global gene expression indirectly through the symmetric methylation of key transcription factors, thereby impacting cell growth, proliferation, and cell differentiation. PRMT5 can methylate p53 and modify its DNA-binding activity, which in turn triggers a modification in the p53-controlled gene expression cascade. PRMT5 directly controls the transcriptional activity of members of the E2F family, such as E2F1, via methylation of specific arginine residues R111 and R113, which can prevent cell apoptosis and promote cell proliferation[189,190,196].

To investigate the genomic functions of PRMT5, we knocked down *E2F1* in the HCT116 p53+/+ and HCT116 p53-/- cell lines using the CRISPR-Cas9 technology. The CRISPR system initially evolved as a nucleic acid-targeting bacterial defence mechanism capable of conferring resistance to viral infection and was introduced as a potent gene editing tool. By expressing the Cas9 nuclease and a suitable gRNA in mammalian cells, a double-strand break can be introduced at a target locus. Through combining a novel allele or transgene at the target site using its homology-directed repair system, the cell could repair the double-strand break. Sometimes, cell could also perform non-homologous end joining (NHEJ) to insert or delete mutations at the initial break sites (Figure 4.5). With its advantage in inducing permanent and stable non-revertible alterations, CRISPR-Cas9 technology facilitates cellular based analysis[216].

We validated the CRISPR-edited cells using western blotting and Sanger sequencing. Western blotting was used to demonstrate the presence of a functional protein knockout, whereas PCR amplification and subsequent Sanger sequencing were used to provide a quantitative assessment of the genome edits in the target sites and to examine the off-target effects via high throughput sequencing[216]. Western blot analysis of the p53+/+ *E2F1* CRISPR and p53-/- *E2F1* CRISPR cells showed that a functional knockout for *E2F1* was obtained (Figure 4.6A). Subsequently, a colony PCR amplification of the target sequence was performed, and the amplified DNA was analysed on an agarose gel to identify the band of the expected size. Further, the amplified PCR products were sequenced using Sanger sequencing and the sequencing data were aligned to the reference genome using BLAST software (https://blast.ncbi.nlm.nih.gov/Blast.cgi). The sequencing data from the two clonal cell types showed deletions and insertions in *E2F1* after NHEJ repair (Figure 4.6B, Figure 4.6C). We also examined the potential off-targets for the two *E2F1* CRISPR cell types, including for *DNM1L* (Figure 4.6D), *MACROD2* (Figure 4.6E), and *NR0B1* (Figure 4.6F), to identify the possible off-targets of *E2F1*.

We examined cell proliferation in the CRISPR/Cas9-edited *E2F1* knockout in HCT116 p53+/+ and HCT116 p53-/- cells by cell counting (Figure 4.7A). We compared the cell number after 6 days and observed a decrease in the number of HCT116 p53+/+ *E2F1* CRISPR cells compared to the HCT116 p53+/+ cells ($309.3 \pm 24.4 \times 10^4$ vs. $506.7 \pm 64.7 \times 10^4$; $p = 0.0078$; Figure 4.7B), and in HCT116 p53-/-

E2F1 CRISPR cells compared to HCT116 p53 -/- cells (306 ± 18 × $x10^4$ vs. 525.3 ± 32.3 $x10^4$; $p = 0.0005$; Figure 4.7.C). Thus, the CRISPR/Cas9-edited *E2F1* knockout in cells led to a decrease in proliferation. The disruption of *E2F1* resulted in a decline in cell proliferation compared to its control, reinforcing that *E2F1* plays an important role in regulating cell proliferation.

Figure 4.5 An outline of CRISPR-Cas9 genome editing

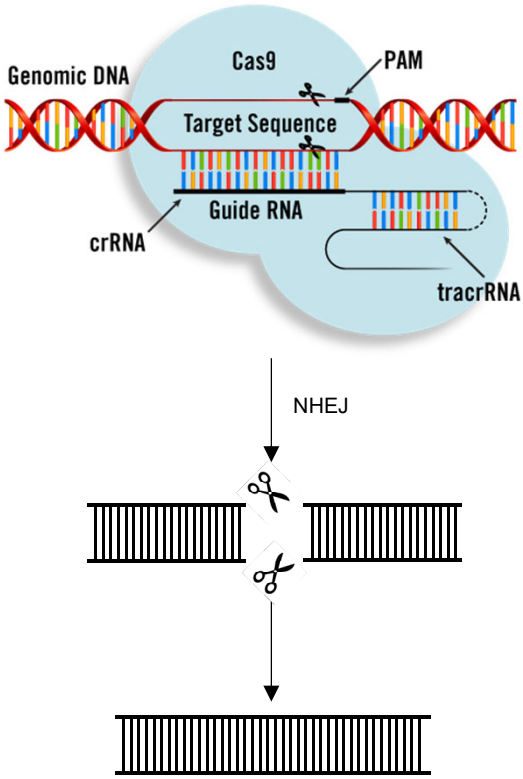
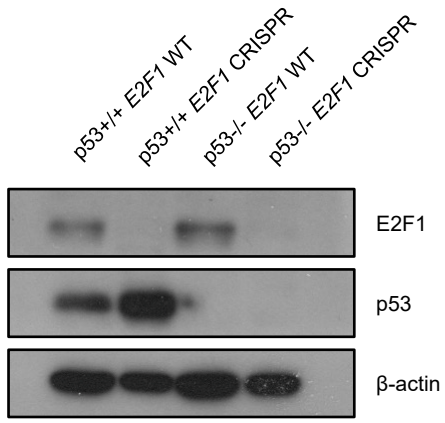


Figure 4.5 An outline of CRISPR-Cas9 genome editing. The Cas9 endonuclease (blue) is targeted to DNA by a guide RNA which can be supplied as a two-part system consisting of crRNA and tracrRNA or as a single guide RNA, where the crRNA and tracrRNA are connected by a linker (dotted line). Target recognition is facilitated by the protospacer-adjacent motif (PAM). Cleavage occurs on both strands (scissors) upstream of the PAM. Variable-length insertions and/or deletions (indels) can result near the DNA break due to errors in DNA repair by the endogenous non-homologous end joining (NHEJ) pathway. These indels frequently result in the disruption of gene function. Alternatively, by supplying a DNA repair template, defined deletions, insertions or modifications can be created by leveraging the homology-directed repair pathway[216].

Figure 4.6 Validation of *E2F1* CRISPR-edited cells using western blotting and Sanger sequencing

A



B

HCT116 p53+/+ *E2F1* CRISPR:

Homo sapiens E2F transcription factor 1 (E2F1), mRNA

Sequence ID: NM_005225.3 **Length:** 2690 **Number of Matches:** 1

Range 1: 382 to 475 GenBank Graphics ▼ Next Match ▲ Previous Match

Score	Expect	Identities	Gaps	Strand
169 bits(91)	2e-38	94/95(99%)	1/95(1%)	Plus/Plus

```
Query  1    GGTGAAGCGGAGGCTGGACCTGGAAACTGACCATCAGTTACCTGGCCGAGAGCAGTGGGC  60
            ||||||||||||||||||||||||||||||||||||| ||||||||||||||||||||||
Sbjct  382  GGTGAAGCGGAGGCTGGACCTGGAAACTGACCATCAG-TACCTGGCCGAGAGCAGTGGGC  440

Query  61   CAGCTCGGGGCAGAGGCCGCCATCCAGGAAAAGGT  95
            |||||||||||||||||||||||||||||||||||
Sbjct  441  CAGCTCGGGGCAGAGGCCGCCATCCAGGAAAAGGT  475
```

C

HCT116 p53-/- *E2F1* CRISPR:

Homo sapiens E2F transcription factor 1 (E2F1), mRNA

Sequence ID: NM_005225.3 **Length:** 2690 **Number of Matches:** 1

Range 1: 382 to 475 GenBank Graphics ▼ Next Match ▲ Previous Match

Score	Expect	Identities	Gaps	Strand
145 bits(78)	4e-31	89/94(95%)	2/94(2%)	Plus/Plus

```
Query  1    GGTGAAGCGGAGGCTGGACCTGGAAACTGACC-TG-GAAACTGGCCGAGAGCAGTGGGCC  58
            |||||||||||||||||||||||||||||||| || || ||||||||||||||||||||
Sbjct  382  GGTGAAGCGGAGGCTGGACCTGGAAACTGACCATCAGTACCTGGCCGAGAGCAGTGGGCC  441

Query  59   AGCTCGGGGCAGAGGCCGCCATCCAGGAAAAGGT  92
            ||||||||||||||||||||||||||||||||||
Sbjct  442  AGCTCGGGGCAGAGGCCGCCATCCAGGAAAAGGT  475
```

D

HCT116 p53+/+ *E2F1* CRISPR:

Homo sapiens dynamin 1 like (DNM1L), transcript variant 1, mRNA

Sequence ID: NM_012062.5 **Length:** 4514 **Number of Matches:** 1

Range 1: 2789 to 3085 GenBank Graphics ▼ Next Match ▲ Previous Match

Score	Expect	Identities	Gaps	Strand
549 bits(297)	3e-152	297/297(100%)	0/297(0%)	Plus/Plus

```
Query  1     AGCTTCTTTGCAGCCTTTGATGTGTTTTTAAGAAAGCTGAATGCACAAGAGGATCTGTGA  60
Sbjct  2789  AGCTTCTTTGCAGCCTTTGATGTGTTTTTAAGAAAGCTGAATGCACAAGAGGATCTGTGA  2848

Query  61    CACTGACATGGCTGTGGTGTGCATACTGTGTAGTTACATAGCCCTTCCAATTCTGGGTCC  120
Sbjct  2849  CACTGACATGGCTGTGGTGTGCATACTGTGTAGTTACATAGCCCTTCCAATTCTGGGTCC  2908

Query  121   ATTTGCACTAGCAAATTAAAATATGCTTTGATTCATACTTAAACCTGAAAGCAGGAATGC  180
Sbjct  2909  ATTTGCACTAGCAAATTAAAATATGCTTTGATTCATACTTAAACCTGAAAGCAGGAATGC  2968

Query  181   CTACATTAATTCCTACATTAAAAACAGCCATCTACCCTTGATTATCTAGAAAGACTTGGT  240
Sbjct  2969  CTACATTAATTCCTACATTAAAAACAGCCATCTACCCTTGATTATCTAGAAAGACTTGGT  3028

Query  241   AATGATGGTCAGTTCCTTTTAGATTTCAGAAAATCAAATGATGACCTAAATTTCCCT  297
Sbjct  3029  AATGATGGTCAGTTCCTTTTAGATTTCAGAAAATCAAATGATGACCTAAATTTCCCT  3085
```

HCT116 p53-/- *E2F1* CRISPR:

Homo sapiens dynamin 1 like (DNM1L), transcript variant 1, mRNA

Sequence ID: NM_012062.5 **Length:** 4514 **Number of Matches:** 1

Range 1: 2789 to 3085 GenBank Graphics ▼ Next Match ▲ Previous Match

Score	Expect	Identities	Gaps	Strand
549 bits(297)	3e-152	297/297(100%)	0/297(0%)	Plus/Plus

```
Query  1     AGCTTCTTTGCAGCCTTTGATGTGTTTTTAAGAAAGCTGAATGCACAAGAGGATCTGTGA  60
Sbjct  2789  AGCTTCTTTGCAGCCTTTGATGTGTTTTTAAGAAAGCTGAATGCACAAGAGGATCTGTGA  2848

Query  61    CACTGACATGGCTGTGGTGTGCATACTGTGTAGTTACATAGCCCTTCCAATTCTGGGTCC  120
Sbjct  2849  CACTGACATGGCTGTGGTGTGCATACTGTGTAGTTACATAGCCCTTCCAATTCTGGGTCC  2908

Query  121   ATTTGCACTAGCAAATTAAAATATGCTTTGATTCATACTTAAACCTGAAAGCAGGAATGC  180
Sbjct  2909  ATTTGCACTAGCAAATTAAAATATGCTTTGATTCATACTTAAACCTGAAAGCAGGAATGC  2968

Query  181   CTACATTAATTCCTACATTAAAAACAGCCATCTACCCTTGATTATCTAGAAAGACTTGGT  240
Sbjct  2969  CTACATTAATTCCTACATTAAAAACAGCCATCTACCCTTGATTATCTAGAAAGACTTGGT  3028

Query  241   AATGATGGTCAGTTCCTTTTAGATTTCAGAAAATCAAATGATGACCTAAATTTCCCT  297
Sbjct  3029  AATGATGGTCAGTTCCTTTTAGATTTCAGAAAATCAAATGATGACCTAAATTTCCCT  3085
```

E

HCT116 p53+/+ *E2F1* CRISPR:

Homo sapiens mono-ADP ribosylhydrolase 2 (MACROD2), transcript variant 1, mRNA

Sequence ID: NM_080676.6 **Length:** 4847 **Number of Matches:** 1

Range 1: 1400 to 1479 GenBank Graphics ▼ Next Match ▲ Previous Match

Score	Expect	Identities	Gaps	Strand
148 bits(80)	2e-32	80/80(100%)	0/80(0%)	Plus/Plus

```
Query  1     AGCTCCAGGCGAGGACACACCTAGGATGCCTGGGAAAAGTGAAGGCTCCAGTGACCTAGA  60
Sbjct  1400  AGCTCCAGGCGAGGACACACCTAGGATGCCTGGGAAAAGTGAAGGCTCCAGTGACCTAGA  1459

Query  61    AAATACTCCAGGTCCTGATG  80
Sbjct  1460  AAATACTCCAGGTCCTGATG  1479
```

HCT116 p53-/- *E2F1* CRISPR:

Homo sapiens mono-ADP ribosylhydrolase 2 (MACROD2), transcript variant 1, mRNA

Sequence ID: NM_080676.6 **Length:** 4847 **Number of Matches:** 1

Range 1: 1400 to 1479 GenBank Graphics ▼ Next Match ▲ Previous Match

Score	Expect	Identities	Gaps	Strand
148 bits(80)	2e-32	80/80(100%)	0/80(0%)	Plus/Plus

```
Query  1     AGCTCCAGGCGAGGACACACCTAGGATGCCTGGGAAAAGTGAAGGCTCCAGTGACCTAGA  60
Sbjct  1400  AGCTCCAGGCGAGGACACACCTAGGATGCCTGGGAAAAGTGAAGGCTCCAGTGACCTAGA  1459

Query  61    AAATACTCCAGGTCCTGATG  80
Sbjct  1460  AAATACTCCAGGTCCTGATG  1479
```

F

HCT116 p53+/+ *E2F1* CRISPR:

Homo sapiens nuclear receptor subfamily 0 group B member 1 (NR0B1), mRNA

Sequence ID: NM_000475.5 **Length:** 1813 **Number of Matches:** 1

Range 1: 894 to 1195 GenBank Graphics ▼ Next Match ▲ Previous Match

Score	Expect	Identities	Gaps	Strand
558 bits(302)	5e-155	302/302(100%)	0/302(0%)	Plus/Plus

```
Query  1     CTGCTGGGCGTCCCTGCTCATGCTTGAGCTGGCCCAGGACCGCTTGCAGTTCGAGACTGT  60
Sbjct  894   CTGCTGGGCGTCCCTGCTCATGCTTGAGCTGGCCCAGGACCGCTTGCAGTTCGAGACTGT  953

Query  61    GGAAGTCTCGGAGCCCAGCATGCTGCAGAAGATCCTCACCACCAGGCGGCGGGAGACCGG  120
Sbjct  954   GGAAGTCTCGGAGCCCAGCATGCTGCAGAAGATCCTCACCACCAGGCGGCGGGAGACCGG  1013

Query  121   GGGCAACGAGCCACTGCCCGTGCCCACGCTGCAGCACCATTTGGCACCGCCGGCGGAGGC  180
Sbjct  1014  GGGCAACGAGCCACTGCCCGTGCCCACGCTGCAGCACCATTTGGCACCGCCGGCGGAGGC  1073

Query  181   CAGGAAGGTGCCCTCCGCCTCCCAGGTCCAAGCCATCAAGTGCTTTCTTTCCAAATGCTG  240
Sbjct  1074  CAGGAAGGTGCCCTCCGCCTCCCAGGTCCAAGCCATCAAGTGCTTTCTTTCCAAATGCTG  1133

Query  241   GAGTCTGAACATCAGTACCAAGGAGTACGCCTACCTCAAGGGGACCGTGCTCTTTAACCC  300
Sbjct  1134  GAGTCTGAACATCAGTACCAAGGAGTACGCCTACCTCAAGGGGACCGTGCTCTTTAACCC  1193

Query  301   GG  302
Sbjct  1194  GG  1195
```

HCT116 p53-/- *E2F1* CRISPR:

Homo sapiens nuclear receptor subfamily 0 group B member 1 (NR0B1), mRNA

Sequence ID: NM_000475.5 **Length:** 1813 **Number of Matches:** 1

Range 1: 894 to 1195 GenBank Graphics ▼ Next Match ▲ Previous Match

Score	Expect	Identities	Gaps	Strand
558 bits(302)	5e-155	302/302(100%)	0/302(0%)	Plus/Plus

```
Query  1     CTGCTGGGCGTCCCTGCTCATGCTTGAGCTGGCCCAGGACCGCTTGCAGTTCGAGACTGT  60
             ||||||||||||||||||||||||||||||||||||||||||||||||||||||||||||
Sbjct  894   CTGCTGGGCGTCCCTGCTCATGCTTGAGCTGGCCCAGGACCGCTTGCAGTTCGAGACTGT  953

Query  61    GGAAGTCTCGGAGCCCAGCATGCTGCAGAAGATCCTCACCACCAGGCGGCGGGAGACCGG  120
             ||||||||||||||||||||||||||||||||||||||||||||||||||||||||||||
Sbjct  954   GGAAGTCTCGGAGCCCAGCATGCTGCAGAAGATCCTCACCACCAGGCGGCGGGAGACCGG  1013

Query  121   GGGCAACGAGCCACTGCCCGTGCCCACGCTGCAGCACCATTTGGCACCGCCGGCGGAGGC  180
             ||||||||||||||||||||||||||||||||||||||||||||||||||||||||||||
Sbjct  1014  GGGCAACGAGCCACTGCCCGTGCCCACGCTGCAGCACCATTTGGCACCGCCGGCGGAGGC  1073

Query  181   CAGGAAGGTGCCCTCCGCCTCCCAGGTCCAAGCCATCAAGTGCTTTCTTTCCAAATGCTG  240
             ||||||||||||||||||||||||||||||||||||||||||||||||||||||||||||
Sbjct  1074  CAGGAAGGTGCCCTCCGCCTCCCAGGTCCAAGCCATCAAGTGCTTTCTTTCCAAATGCTG  1133

Query  241   GAGTCTGAACATCAGTACCAAGGAGTACGCCTACCTCAAGGGGACCGTGCTCTTTAACCC  300
             ||||||||||||||||||||||||||||||||||||||||||||||||||||||||||||
Sbjct  1134  GAGTCTGAACATCAGTACCAAGGAGTACGCCTACCTCAAGGGGACCGTGCTCTTTAACCC  1193

Query  301   GG  302
             ||
Sbjct  1194  GG  1195
```

Figure 4.6 Validation of *E2F1* CRISPR-edited cells using western blot and Sanger sequencing. (A) Western blots showed the functional *E2F1* knockout in both HCT116 p53+/+ and HCT116 p53-/- cells. β-actin was used as the loading control. (B) Sequencing result for the *E2F1* target sequence obtained from the HCT116 p53+/+ *E2F1* CRISPR cells. (C) Sequencing result of the *E2F1* target sequence obtained from the HCT116 p53-/- *E2F1* CRISPR cells. (D-F) The sequencing results of potential off-targets in two *E2F1* CRISPR cell types, including (D) *DNM1L*, (E) *MACROD2*, and (F) *NR0B1*.

Figure 4.7 Growth curves for the two *E2F1* CRISPR cell types

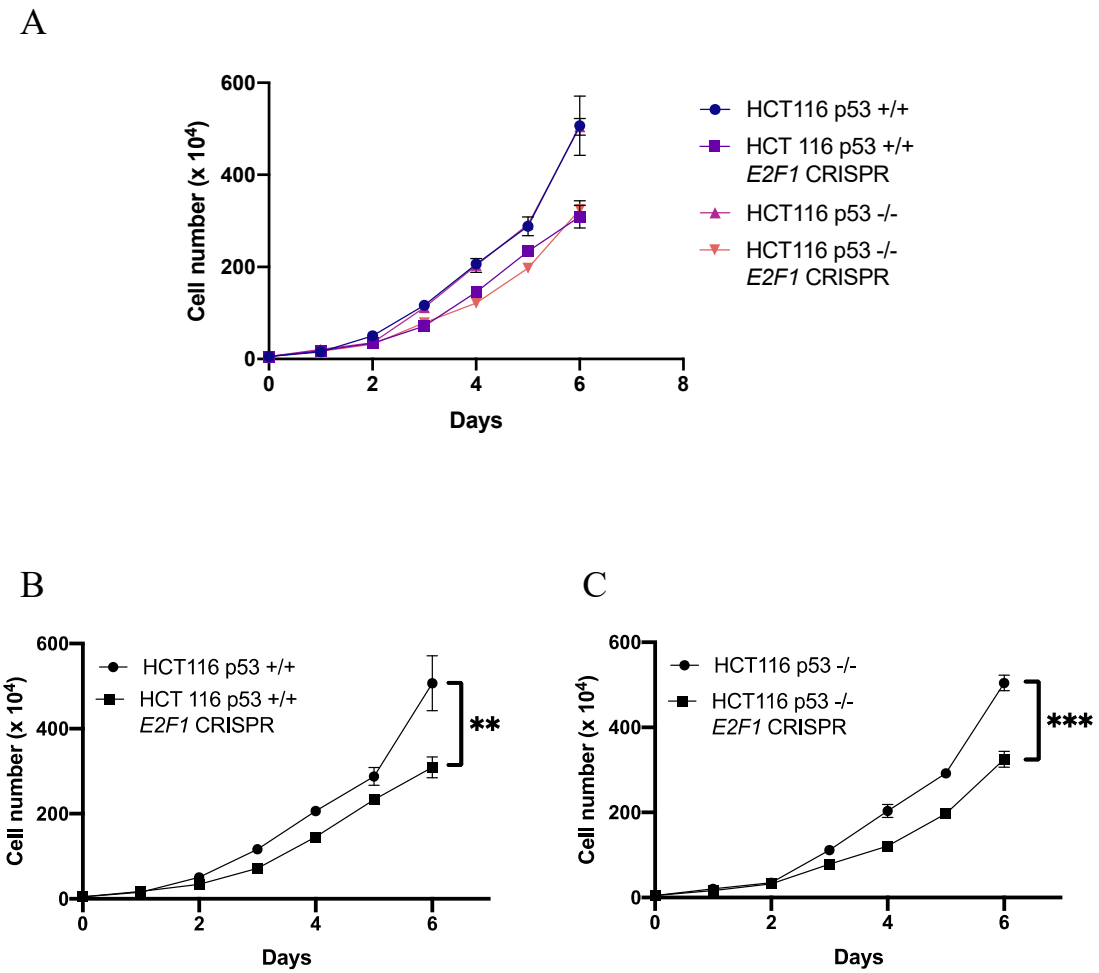


Figure 4.7 Growth curves for the two *E2F1* CRISPR cell types. (A) Growth curves for HCT116 p53+/+ *E2F1* CRISPR cells, HCT116 p53-/- *E2F1* CRISPR cells and their respective controls. Knockout of *E2F1* led to a decrease in cell proliferation. (B) Growth curves for HCT116 p53+/+ *E2F1* CRISPR cells and its control showed that the number of *E2F1* CRISPR cells and the control cells at day 6 was 309.3 ± 24.4 × 104 and 506.7 ± 64.7 × 104, respectively (p = 0.0078; n=3). (C) Growth curves for HCT116 p53-/- *E2F1* CRISPR cells and its respective control showed that the number of *E2F1* CRISPR cells and its control at day 6 was 306 ± 18 × 104 and 525.3 ± 32.3 × 104, respectively (p = 0.0005; n=3). Data are presented as mean ± SD. Error bars indicate the SD of biological replicates. Statistical analyses were performed using the two-tailed, unpaired Student's t-test. The p-values of < 0.05 were considered significant and are indicated as *$p < 0.05$, **$p < 0.01$, ***$p < 0.001$, and ****$p < 0.0001$.

4.6 PRMT5 inhibition regulates cell apoptosis through E2F1

Previously, we have shown that PRMT5 inhibition induced cellular apoptosis (Figure 4.1) and caused the accumulation of cells in the sub-G1 phase (Figure 4.2). Studies have demonstrated that E2F1 can induce proliferation and apoptosis in cells, that can be mediated via p53-dependent and independent pathways (Figure 1.5). E2F1 can stabilize p53 via transcriptional induction of p14/Arf. or directly up-regulates the expression of p53 apoptotic cofactors, including ASPP1, ASPP2, JMY and TP53INP1[86,115,116]. E2F1 can also activate many apoptotic genes in a p53-independent manner, such as through *p73* and *Apaf-1*[117,119]. E2F1 also transcriptionally induce other genes implicated in apoptosis, such as BH3 only proteins PUMA, BIM, NOXA, Hrk/DP-5 and several caspase family members CASP-3, CASP-7, CASP-8 and CASP-9[86,120,121]. Another mechanism of apoptosis induced by E2F1 is through survival signaling pathways, such as cell survival regulator NF-κB and anti-apoptotic Bcl-2 family members, including Bok, Bad, Bak and Bid1[122,123]. Therefore, several pathways mediate apoptotic activity, and the activities of p53 and E2F1 are integrated.

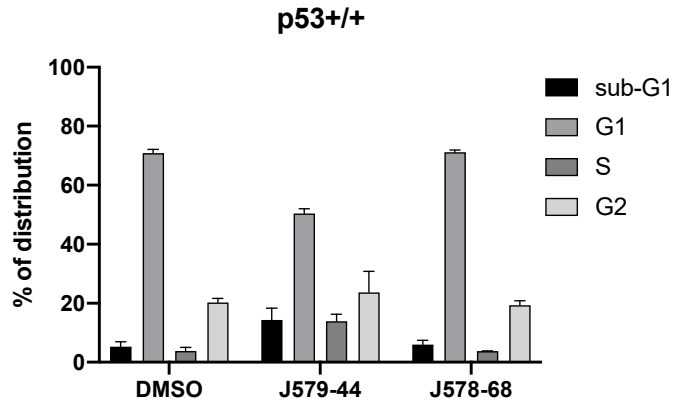
Further, we studied the inhibition of PRMT5 in HCT116 p53+/+ *E2F1* CRISPR, HCT116 p53 +/+, HCT116 p53-/- *E2F1* CRISPR, and HCT116 p53-/- cells to examine the involvement of PRMT5 in cellular apoptosis via flow cytometry (Figure 4.8A–E). In a comparison of the sub-G1 cell population, there was no significant difference between J579-44 treated HCT116 p53+/+ *E2F1* CRISPR cells and HCT116 p53+/+ cells (14.7% ± 1.67% vs. 15.3% ± 3.2%; $p = 0.872$; Figure 4.8E). The results indicate

that p53 masks the interplay between PRMT5 and E2F1. However, in the absence of p53, J579-44 induced a significant increase in the sub-G1 cell population in *E2F1* cells compared to *E2F1* CRISPR cells (39.87% ± 4.8% vs. 25.9% ± 2.7%; p <0.0001), indicating that apoptosis is induced by PRMT5 inhibition directly through manipulating the level and activity of E2F1. Next, western blotting was performed using the anti-E2F1, anti-p53, and anti-SDMe antibodies (Figure 4.8F). We observed an accumulation of p53 in the p53+/+ *E2F1* CRISPR cells and p53+/+ cells after treatment with J579-44. Taken together, the p53-dependent apoptosis pathways and the E2F1-dependent pathways were involved in PRMT5 inhibitor-induced apoptosis; however, the E2F1-dependent pathways played a crucial role in regulating the apoptotic response. Thus, these results highlight the role of PRMT5 in regulating cellular apoptosis through E2F1 activity.

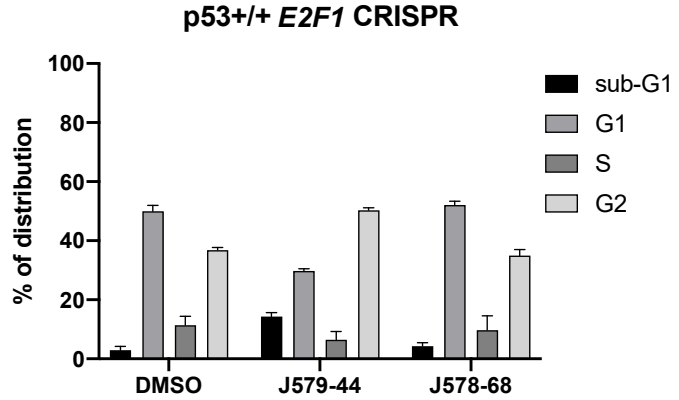
To examine whether the deregulation of E2F1 leads to a decrease in cell apoptosis upon PRMT5 inhibition, we conducted apoptosis experiments using the Apoptosis/Necrosis Kit to measure the early apoptosis induced by J579-44 on HCT116 p53-/- and the corresponding *E2F1* CRISPR cells. The experimental conditions were similar; i.e., cells were treated with DMSO, and 1 μM J579-44 or J578-68 for 6 days (Figure 4.8G). We observed a decrease in apoptosis in HCT116 p53-/- *E2F1* CRISPR cells relative to HCT116 p53-/- cells (25.4% ± 2.98% vs. 35.4% ± 0.58%; p = 0.0076). These results confirmed the importance of PRMT5 in regulating apoptosis by regulating the levels and activity of E2F1.

Figure 4.8 E2F1 plays a crucial role in regulating PRMT5 inhibition -induced apoptosis

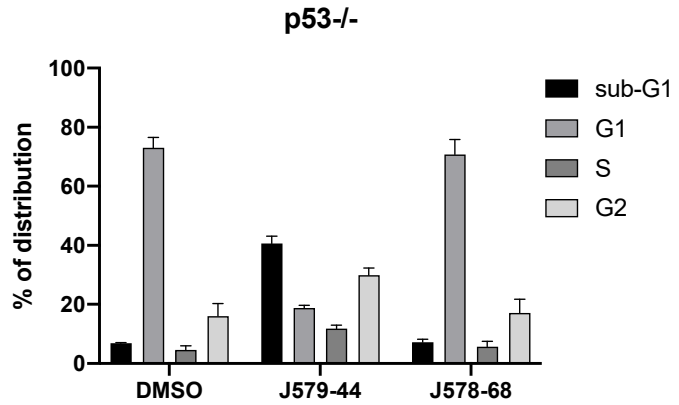
A



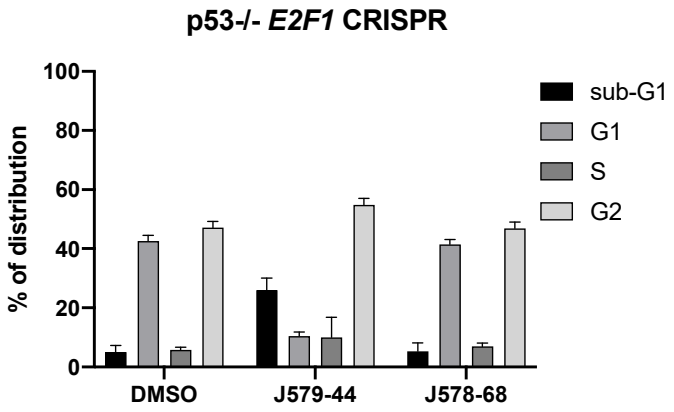
B



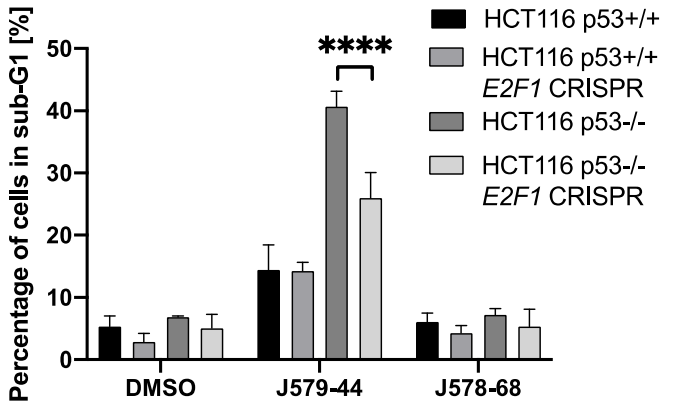
C



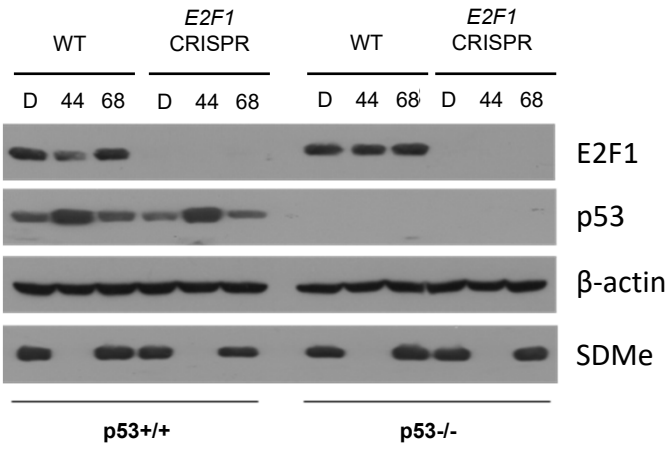
D


p53-/- E2F1 CRISPR
% of distribution
100
80
60
40
20
0
DMSO
J579-44
J578-68
sub-G1
G1
S
G2

E


Percentage of cells in sub-G1 [%]
50
40
30
20
10
0
****
DMSO
J579-44
J578-68
HCT116 p53+/+
HCT116 p53+/+ E2F1 CRISPR
HCT116 p53-/-
HCT116 p53-/- E2F1 CRISPR

F


WT
E2F1 CRISPR
WT
E2F1 CRISPR
D 44 68 D 44 68 D 44 68 D 44 68
E2F1
p53
β-actin
SDMe
p53+/+
p53-/-

G

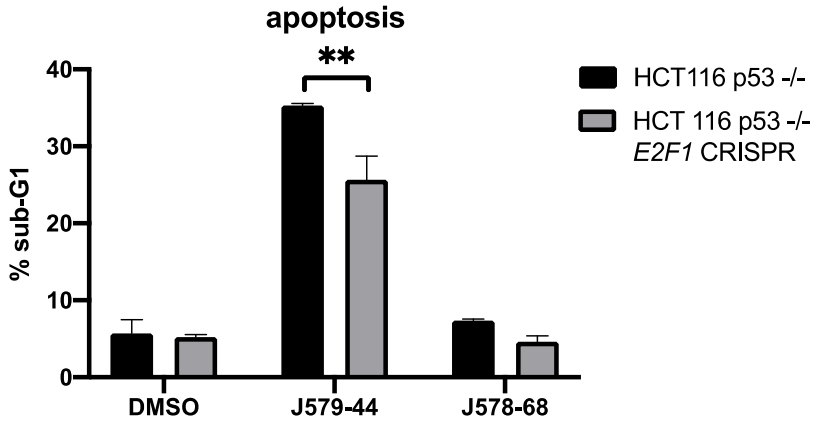


Figure 4.8 E2F1 plays a crucial role in regulating PRMT5 inhibition-induced apoptosis. We treated (A) HCT116 p53+/+ WT *E2F1* cells, (B) HCT116 p53+/+ *E2F1* CRISPR cells, (C) HCT116 p53-/- WT *E2F1* cells, and (D) HCT116 p53-/- *E2F1* CRISPR cells with DMSO, or 1μM each of J579-44 and J578-68, and analysed the percentage of cells in the sub-G1 phase by flow cytometry after 6 days (n=4). (E) The percentage of cells in the sub-G1 phase after treatment with the PRMT5 inhibitor in the 4 cell types examined. There was no significant difference between J579-44 treated HCT116 p53+/+ *E2F1* CRISPR cells and HCT116 p53+/+ cells (14.7% ± 1.67% vs. 15.3% ± 3.2%; p = 0.872; n = 4), whereas in p53-/- cells, J579-44 induced a significant increase in the sub-G1 cell population in cells containing *E2F1* relative to *E2F1* CRISPR cells (39.87% ± 4.8% vs. 25.9% ± 2.7%; p <0.0001; n=4). (F) Western blots were developed using the anti-E2F1, anti-cleaved PARP, and anti-SDMe antibodies, and β-Actin was used as a loading control. The western blots were conducted by Dr Wojciech Barczak. (G) Deregulation of *E2F1* leads to a decrease in cellular apoptosis upon PRMT5 inhibition. Apoptosis experiments were conducted using the Apoptosis/Necrosis Kit to measure the early apoptosis induced by J579-44 on HCT116 p53-/- and the corresponding *E2F1* CRISPR cells. J579-44 induced a decrease in apoptosis in HCT116 p53-/- *E2F1* CRISPR cells compared to the HCT116 p53-/- cells (25.4% ± 2.98% vs. 35.4% ± 0.58%; p = 0.0076, n = 3). Data are presented as mean ± SD. Error bars indicate the SD for biological replicates. Statistical analyses were performed using a two-tailed unpaired Student's *t*-test. The *p*-values of < 0.05 were considered as significant and are indicated as $*p < 0.05$, $**p < 0.01$, $***p < 0.001$, and $****p < 0.0001$.

4.7 Targeting PRMT5 activity inhibits cell migration and invasion in association with E2F1

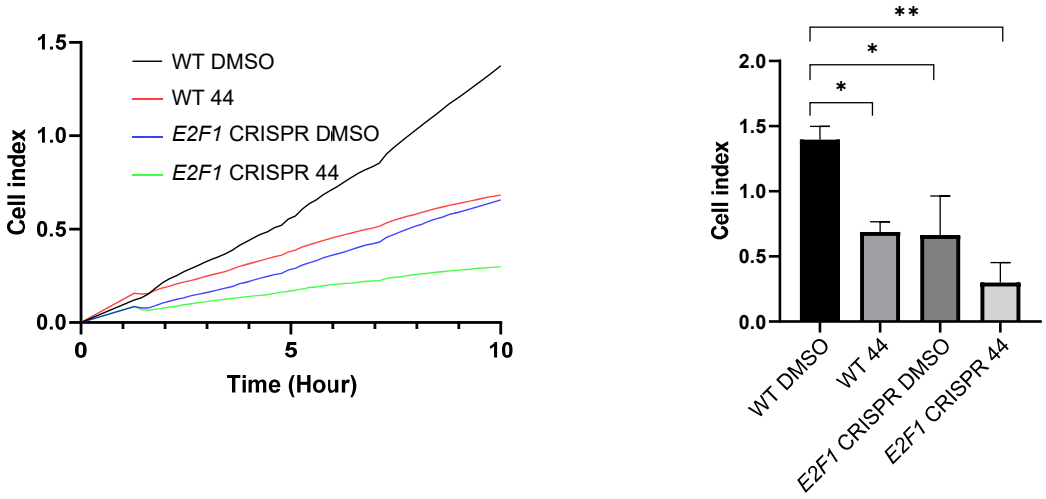
To study the role of E2F1 in PRMT5 inhibition regulated cell migration and invasion in cells, we used the xCELLigence RTCA system to analyse the migration and invasion of HCT116 p53-/- and HCT116 p53-/- *E2F1* CRISPR cells treated with 1 μM J579-44 for two days, and we obtained the cell index of samples from 0 h to 10 h (Figure 4.9A, Figure 4.9B). A western blot demonstrating input protein levels for H4R3 and E2F1 for the experiments displayed and β-actin included as a loading control (Figure 4.9C).

For the cell migration assay (Figure 4.9A), we compared the real-time cell index of WT *E2F1* cells treated with DMSO and J579-44. We found that the cell index of cells treated with J579-44 was significantly lower than that of DMSO-treated cells ($p = 0.019$). In the cell invasion assay (Figure 4.9B), the results were consistent with the migration assay, as J579-44 induced a decrease in the cell index relative to the DMSO control ($p = 0.026$). These results indicate that J579-44 inhibited cell migration and invasion in the HCT116 *E2F1* CRISPR cells. Further, we compared the cell index of DMSO-treated WT *E2F1* and DMSO-treated *E2F1* CRISPR cells. Our results showed that the knockout of *E2F1* directly induced a significant decrease in cell migration ($p = 0.022$) and invasion ($p = 0.014$). Cells treated with J579-44 or harbouring a knock out for *E2F1* showed similar anti-migration and anti-invasion effects. The use of J579-44 on *E2F1* CRISPR cells caused a marginal decrease in the cell index compared to

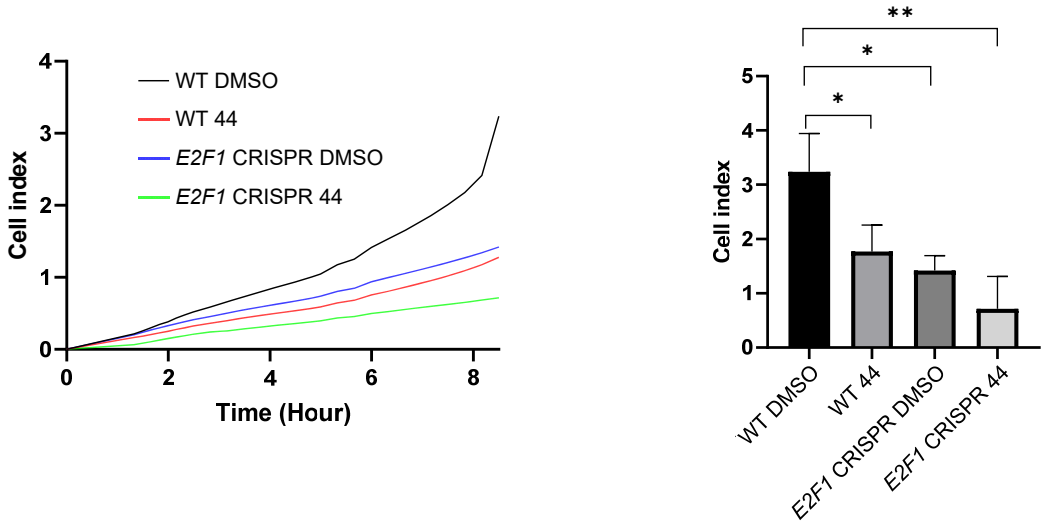
PRMT5 inhibition or an *E2F1* functional knockout, highlighting that *E2F1*-dependent anti-migratory and anti-invasive pathways play a pivotal role in PRMT5 regulated migratory activity.

Figure 4.9 J579-44 inhibits cell migration and invasion in association with E2F1

A



B



C

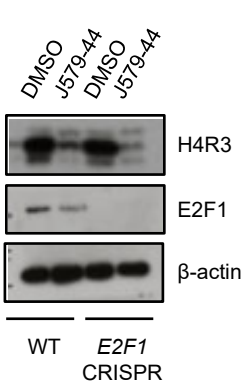


Figure 4.9 J579-44 inhibits cell migration and invasion in association with E2F1. We used the xCELLigence RTCA system to measure the real-time cell migration or invasion activity via the cell index for HCT116 p53-/- WT *E2F1* and HCT116 p53-/- *E2F1* CRISPR cells treated with 1 μM J579-44 for two days. DMSO treated cells were used as a control. (A) Cell index curves for cell migration activity. The PRMT5 inhibition (p = 0.019) and *E2F1* functional knockout (p = 0.022) decreased cell migration activity (n=3). The data shown are representative of three independent experiments. (B) Cell index curves for cellular invasion activity. The PRMT5 inhibition (p = 0.026) and *E2F1* functional knockout (p = 0.014) lead to a decrease in cell invasion activity (n=3). The data shown are representative of three independent experiments. (C) Western blots showing the input protein levels for H4R3 and E2F1, with β-actin used as a loading control. Error bars indicate the SD for biological replicates. Statistical analyses were performed using a two-tailed unpaired Student's *t*-test. The p-values of < 0.05 were considered as significant and are indicated as $*p < 0.05$, $**p < 0.01$, $***p < 0.001$, and $****p < 0.0001$.

4.8 Chapter summary

In this chapter, the outline for the biological function of PRMT5 in cell proliferation, cell viability, cell cycle progression, apoptosis, migration, and invasion have been discussed. We generated CRISPR-edited *E2F1* knockout cells to identify the association between PRMT5 and E2F1 in regulating various cellular processes, and showed that PRMT5 inhibition alters the methylation status of E2F1, leading to increased cell apoptosis, cell cycle arrest, and attenuated cell migration and invasion. Thus, the PRMT5-E2F1 axis regulates cellular apoptosis, cell migration, and invasion in cancer cells.

Chapter 5: RNA-Seq profiling reveals a cluster of E2F1 target genes involved in PRMT5 modulated cellular processes

5.1 Introduction

In the previous chapter, we showed that the PRMT5-E2F1 axis controls cell apoptosis, cell migration, and invasion. Our results highlighted the role of PRMT5 in manipulating cellular processes in association with E2F1. To identify potential E2F1 downstream targets and study the mechanism of the PRMT5-E2F1 axis in modulating cellular processes, we conducted a RNA-Seq study in the *E2F1* CRISPR-edited cell model and its control group, with and without J579-44 treatment, and characterised the potential E2F1 downstream targets.

5.2 RNA-Seq experimental design

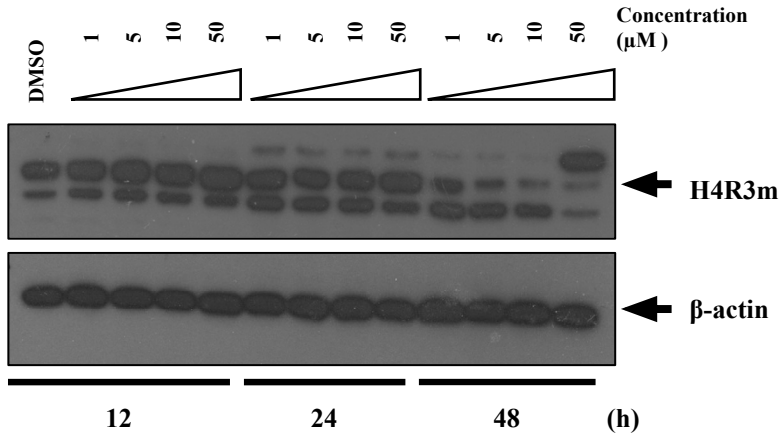
RNA-Seq is a high-throughput alternative to the traditional RNA/cDNA cloning and sequencing approach that utilises next generation sequencing (NGS) technology to study the entire transcriptome[218]. The process of RNA-Seq involves the reverse transcription of RNA into cDNA, and the sequencing of cDNA fragments performing on a high-throughput platform to obtain a large number of short reads. The reads are subsequently aligned to a reference genome, and the number of reads aligned to each gene or feature is evaluated[218-220]. RNA-Seq provides a precise measurement of transcriptomic complexity and detects expression levels of specific genes, differential splicing events, allele-specific expression of transcripts, enabling RNA-Seq study a useful tool to address multiple biological-related issues[221].

To determine the relevant experimental conditions for the RNA-Seq study, we performed a western blotting analysis. We treated HCT116 p53-/- cells with varying concentrations of J579-44 at 1, 5, 10, and 50 μM, and DMSO was used as a control. The cells were analysed after 12, 24, and 48 h of treatment. PRMT5 is known to catalyse the symmetric demethylation of H4R3[163]; therefore, the expression of the histone arginine methylation marker H4R3m was used to determine the pharmacological effect of the PRMT5 inhibitor J579-44 in cells. We observed a notable decrease in H4R3m levels after treatment with J579-44 for 48 h at a concentration of 1 μM (Figure 5.1A). Further, we generated the IC50 curve for HCT116 p53-/- cells treated with J579-44 to identify the optimal concentration to minimise noise effects,

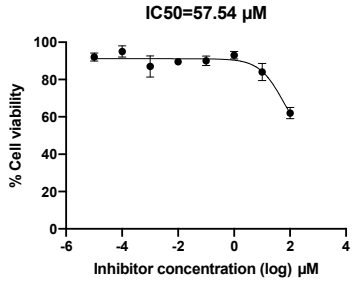
and our results showed that an IC50 = 57.54 μM was suitable for use (Figure 5.1B). To identify the set of E2F1 dependent differentially expressed genes (DEGs) upon PRMT5 inhibition, we designed a RNA-Seq experiment using four conditions: DMSO-treated HCT116 p53-/- cells, J579-44 treated HCT116 p53-/- cells, DMSO-treated HCT116 p53-/- *E2F1* CRISPR cells, and J579-44 treated HCT116 p53-/- *E2F1* CRISPR cells. Cells were treated with 1 μM of inhibitor for 48 h, with three independent biological replicates used. Figure 5.1C outlines the experimental design for the RNA-Seq sample preparation.

Figure 5.1 Experiment design of RNA-Seq preparation

A



B



C

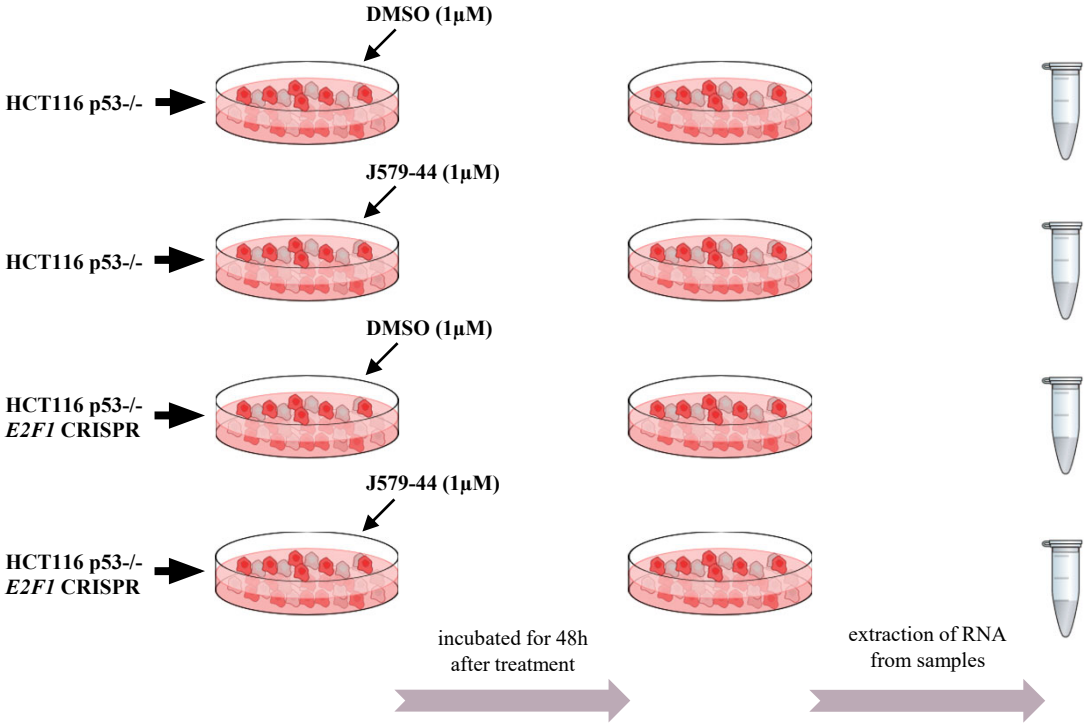


Figure 5.1 Experiment design of RNA-Seq preparation. (A) A western blot was developed using an anti-H4R3m antibody to determine the relevant useful experimental conditions. HCT116 p53-/- cells were treated with a concentration gradient of 1, 5, 10, and 50 μM of J579-44; DMSO cells treated for 12 h were set as control. The cells were analysed at 12, 24, and 48 h. (B) The dose-response curve for J579-44 in HCT116 p53-/- cells after 2 days of treatment. The percentage of cell viability was established by using the MTT assay. DMSO treated cells were used as the control. An IC50 of 57.54 μM was obtained from three independent experiments. (C) Flowchart of RNA sample preparation. HCT116 p53-/- and HCT116 p53-/- *E2F1* CRISPR cells were treated with DMSO or 1 μM J579-44 for 48 h. Subsequently, RNA was extracted from samples. Samples were analysed from three independent experiments to minimize noise effects.

5.3 Summary of results for RNA-Seq

A total of 12 RNA samples for sequencing were sent to BGI company (BGI Group) for RNA-Seq library preparation and analysis. The samples were sequenced using the Illumina HiSeq platform. Based on the transcriptome resequencing report provided by BGI, the mRNAs from each sample were isolated from total RNA using the oligo (dT) method. Next, the mRNAs were fragmented and the first and second-strand cDNAs were synthesised. The resulting cDNA fragments were purified using EB buffer, and used for end repair and single nucleotide (adenine) addition. Subsequently, the cDNA fragments were linked with adaptors and size selected for PCR amplification. The Agilent 2100 Bioanalyzer and ABI StepOnePlus Real-Timer PCR System were used for quantification and quality estimation of the prepared libraries. Figure 5.2A provides an outline of the sample preparation workflow for the sequencing library.

For the sequencing data analysis, the low-quality reads (> 20% of the base qualities lower than 10), reads with adaptors, and reads with unknown bases (N bases more than 5%) were filtered to obtain clean reads. Next, these cleaned reads were mapped onto the reference genome, and novel gene predictions were obtained. The DEGs were identified by comparing the relevant samples. The DEGs were used to perform the GO analysis and related pathway analysis. Figure 5.2 B outlines the transcriptome analysis pipeline.

The report from BGI also provided a detailed gene expression analysis and DEG detection. Reads were mapped to the reference genome using Bowtie2 (version: v2.2.5, http://bowtie-bio.sourceforge.net/Bowtie2/index.shtml), and gene expression levels

were calculated using the RSEM (version: v1.2.12). Next, the Pearson correlation was calculated between all samples, and samples were hierarchically clustered using the R package tools (version 2.20.0). A PCA analysis for all samples was performed using the *princomp* function, and the package ggplot2 was used to generate the various data plots in R. DEGs were detected using the NOIseq package, which utilized a noise distribution model.

We analysed four different conditions, including WT *E2F1* cells treated with DMSO or J579-44, and *E2F1* CRISPR cells treated with DMSO or J579-44, and the WT *E2F1* cells treated with DMSO were used as controls to identify differentially expressed E2F1 target genes. We used a top 30% change or two-fold change in expression level as the cut-off point with an adjusted p-value ≤ 0.01, and filtered the genes for those containing an E2F1 binding motif in their proximal promoter region (-900 to +100) based on ENCODE data, and analysed the overlap of DEGs as shown in the Venn diagrams, and generated the heatmap of DEGs (Figure 5.3).

Using the 30% cut-off, a large number of E2F1 target genes were identified as DEGs. In WT *E2F1* cells treated with J579-44, 216 *E2F1*-dependent genes were selectively upregulated, and this upregulation was absent in the *E2F1* CRISPR cells treated with DMSO or J579-44. In the DMSO-treated *E2F1* CRISPR group, 184 genes were upregulated. Interestingly, a set of 356 genes were upregulated in the *E2F1* CRISPR cells treated with J579-44. A similar analysis was performed on the downregulated DEGs. The expression of 307 genes was downregulated in WT *E2F1*

cells treated with J579-44, whereas a group of 141 genes were downregulated in the DMSO-treated *E2F1* CRISPR group. A set of 367 genes was downregulated in the *E2F1* CRISPR cells with J579-44 treatment. DEGs that are observed in different conditions represent the effects of different cellular behaviours. For example, the up or down-regulated DEGs specific for WT *E2F1* cells treated with J579-44 represented a set of genes that required both *E2F1* and PRMT5 for their expression, whereas the group of *E2F1* CRISPR cells upon treatment with J579-44 represented genes that were functional in the absence of *E2F1* and regulated by PRMT5 (Figure 5.3A, 5.3B).

To identify genes that overlapped between datasets using Venn diagrams, a cut-off with 2-fold expression level change was applied. The results showed that a set of 12 genes were upregulated, and 68 genes were downregulated in WT *E2F1* cells treated with J579-44. In the absence of *E2F1* and PRMT5 inhibition, 49 genes were upregulated and 146 genes were downregulated. Overall, these results defined different sets of differentially expressed *E2F1* targets, representing genes that are regulated by *E2F1* or PRMT5, and a third set that is regulated by both *E2F1* and PRMT5 (Figure 5.3C).

The list of DEGs was utilized to perform a functional analysis, and applied a PGSEA to test for enrichment of DEGs in KEGG-annotated pathways (Figure 5.4A) and GO vocabulary terms (Figure 5.4B), and to highlight the differences between J579-44 treated and control samples. The enriched GO and KEGG terms that were significantly different between J579-44 treatment and the control were related to

cellular adherence and migration, such as KEGG ‘Adherence Junction’, KEGG ‘Leukocyte Transendothelial Migration’, and GO ‘Filamentous actin’. Interestingly, previous studies have shown that targeting PRMT5 activity inhibits cell migration and invasion in an E2F1 dependent manner (Figure 4.9), which is consistent with the highly ranked term cellular adherence and migration terms that were enriched in the GO and KEGG analysis. Taken together, the cell-based migration and invasion assays and the functional analysis of DEGs highlighted a set of E2F1-dependent DEGs that regulate cell adherence and migratory patterns depending on the activity of PRMT5.

Next, we queried the list of DEGs for KEGG and GO terms, and identified the highly regulated DEGs in the RNA-Seq data sets. An example of one such gene was *CTTN*, which ranked as one of the top DEGs in the J579-44 treated WT *E2F1* cells. We performed a weighted correlation network analysis, which identified a co-expression cluster containing several genes associated with focal adhesions (highlighted in red in Figure 5.4C). Similar to *CTTN*, genes within the co-expression cluster (including genes connected with focal adhesion) were generally downregulated upon inhibition of PRMT5.

Taken the list of DEGs, the KEGG and GO analysis and the co-expression analysis showing genes with a coordinated expression pattern, a list of putative E2F1 targets related to PRMT5 regulated cellular processes were generated for further verification and functional studies (Figure 5.5).

Figure 5.2 Flowchart of RNA-Seq analysis

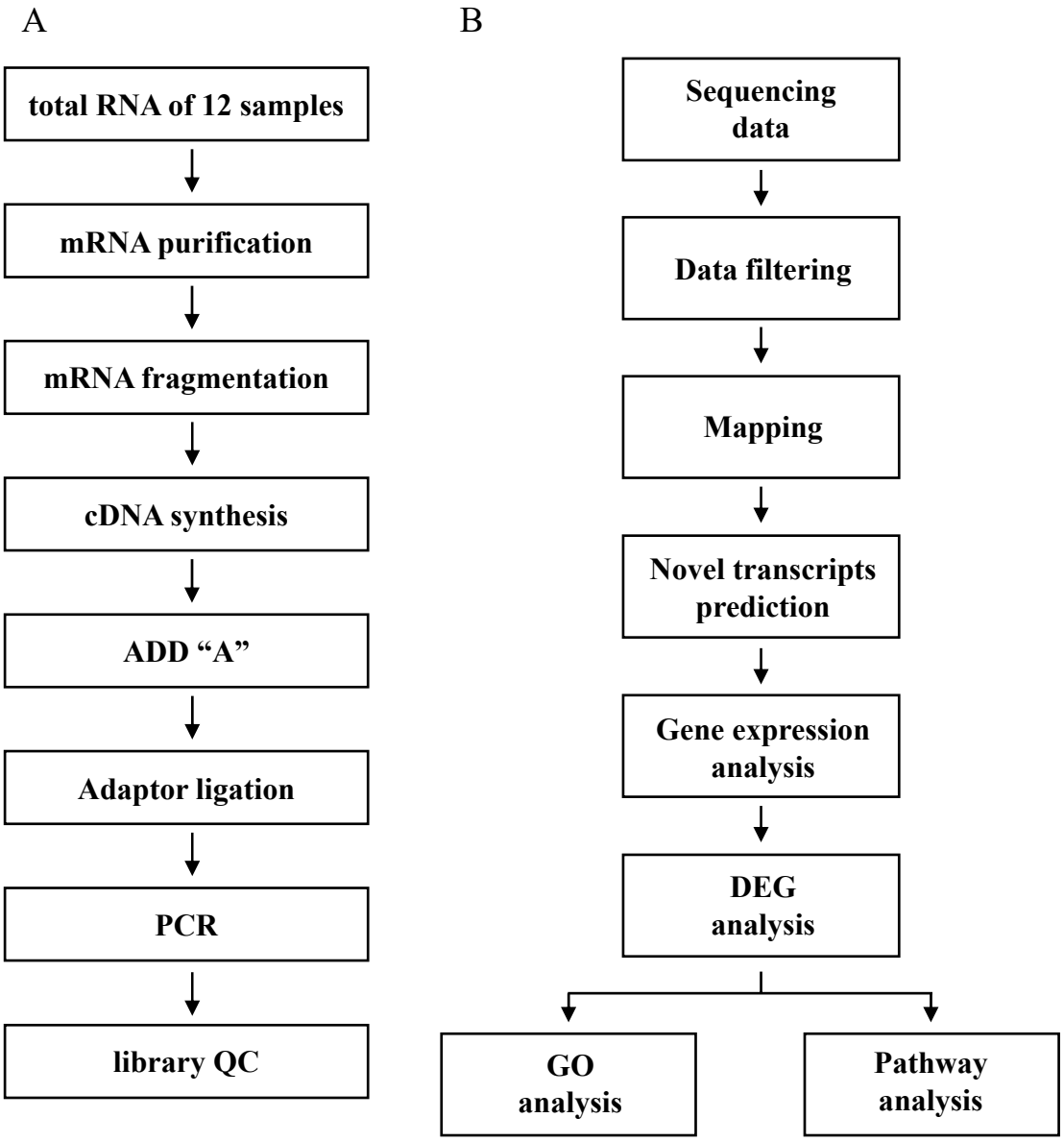
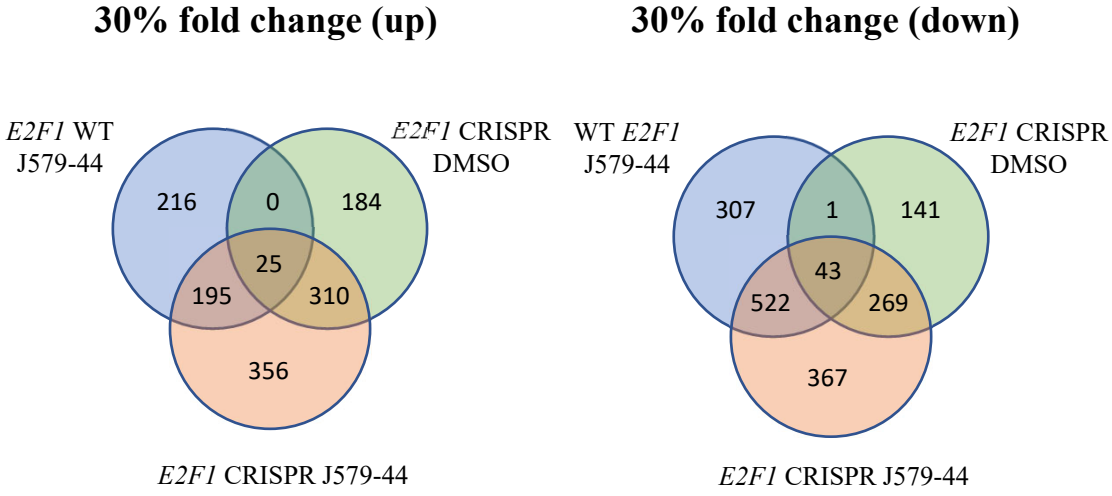


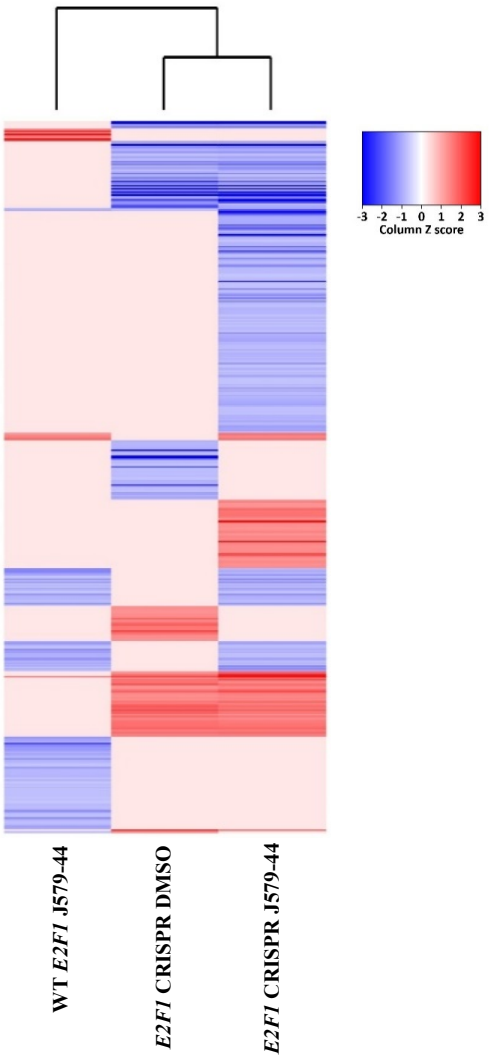
Figure 5.2 Flowchart of RNA-Seq analysis. (A) The workflow for sequencing library preparation. mRNAs were isolated from total RNA using the oligo (dT) method, and the mRNAs were fragmented. The first and second-strand cDNAs were synthesized, and cDNA fragments were purified using EB buffer for end repair and single nucleotide (adenine) addition. Subsequently, the cDNA fragments were linked with adapters and were size-selected for the PCR amplification. The Agilent 2100 Bioanalyzer and ABI StepOnePlus Real-Time PCR System were used for the quantification and estimation of library quality. (B) Transcriptome data analysis pipeline. The sequencing data was analysed and the reads obtained were filtered to get clean reads that were mapped onto the reference genome, and novel gene were identified. DEGs were identified by comparing the sequenced samples, and the GO analysis and related pathway analysis was based on the analysis of the DEGs.

Figure 5.3 Venn diagrams and heatmap of DEGs

A



B



C

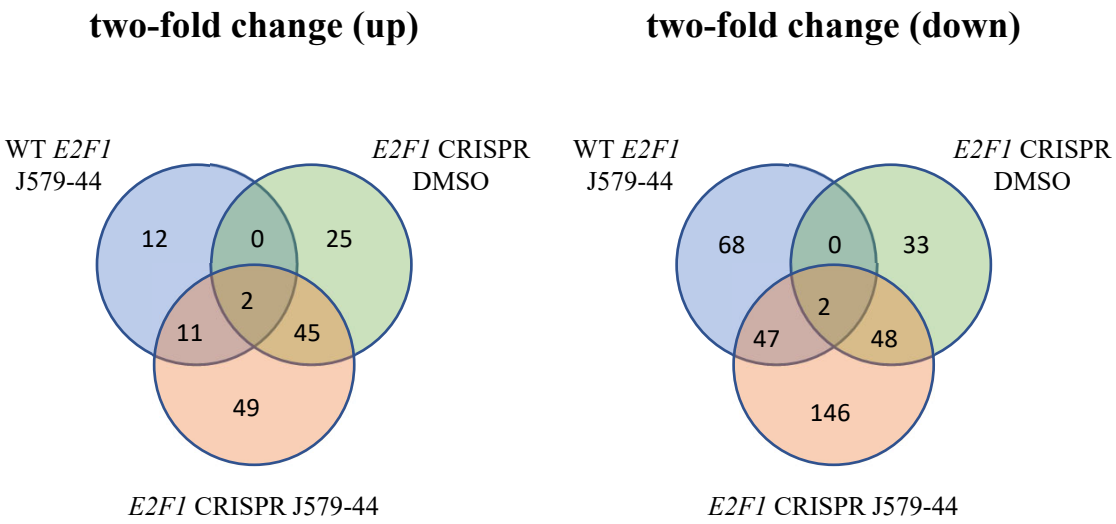


Figure 5.3 Venn diagrams and heatmap of DEGs. All samples were normalized to WT *E2F1* cells treated with DMSO. (A) Venn diagrams showing the up and down-regulated differentially expressed *E2F1* target genes under different conditions using a 30% cut-off. (B) Heatmap of DEGs (adjusted *p*-value ≤ 0.01; 30% change) in each treatment condition for DMSO treated WT *E2F1* cells. Increased expression levels are indicated with darker red colouring, whereas decreased expression levels are shown with darker blue colouring. The ivory colour represents no significant change. (C) Venn diagrams representing up and down-regulated differentially expressed *E2F1* target genes in different conditions at the two-fold change cut-off. Abbreviations: *E2F1* CRISPR DMSO: DMSO treated *E2F1* CRISPR cells; *E2F1* CRISPR J579-44: J579-44 treated *E2F1* CRISPR cells; WT *E2F1 J579*-44: J579-44 treated WT *E2F1* cells.

Figure 5.4 Functional analysis of DEGs

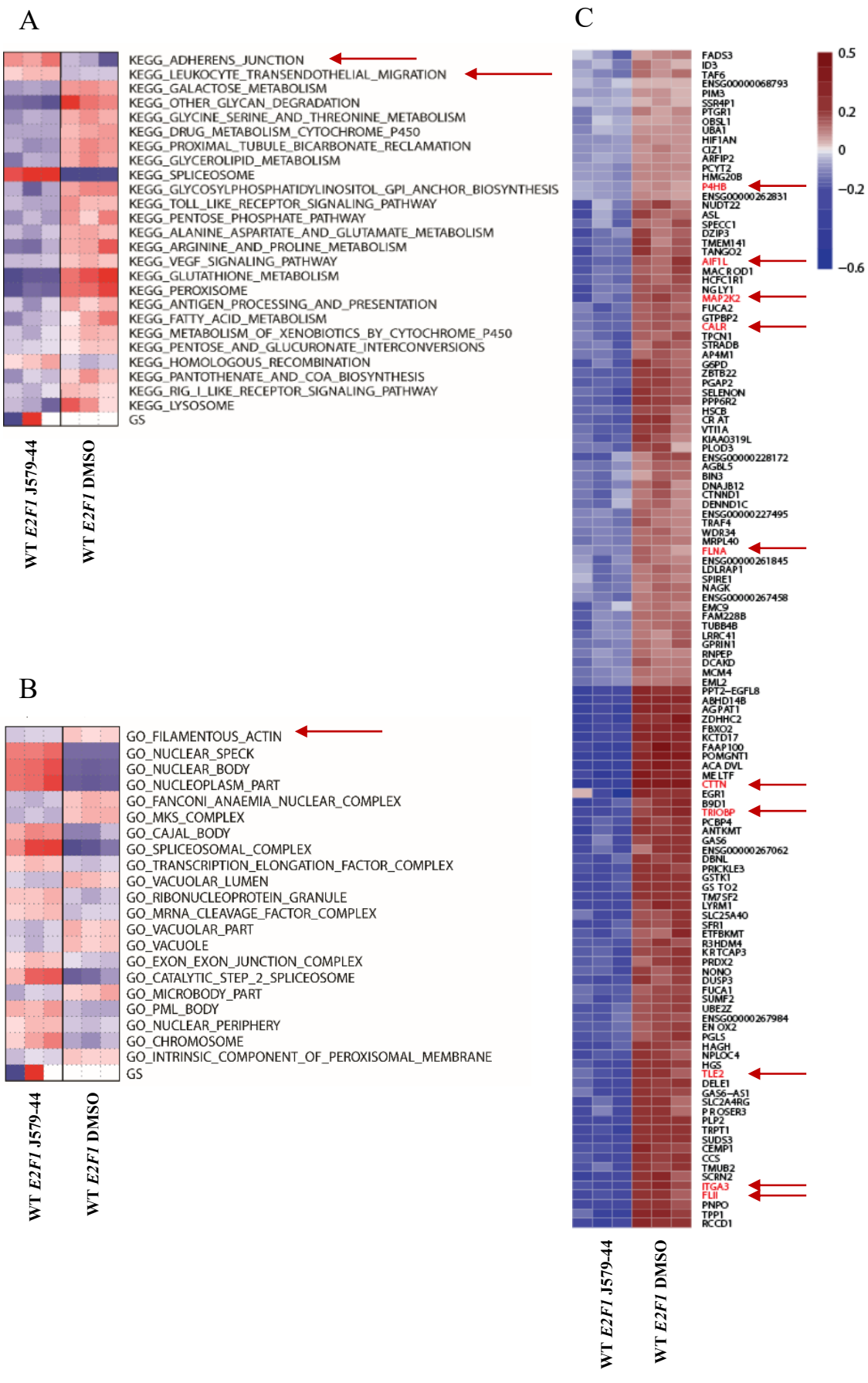


Figure 5.4 Functional analysis of DEGs. (A) Significantly enriched KEGG-annotated pathways and (B) GO terms, including cellular components that were associated with significant differences in expression upon J579-44 treatment (as compared to DMSO control) in HCT116 p53-/- WT *E2F1* cells. (C) Co-expression analysis associated with *CTTN* expression upon treatment with J579-44 relative to DMSO control in HCT116 p53-/- WT *E2F1*cells. Heatmaps show the PGSEA statistic (Z-score) which describes the mean fold-change for genes in a pathway or gene set that deviates from the mean for all genes in a comparison between J579-44 treatment and the control group. Blue indicates gene sets that showed decreased expression, whereas red corresponds to genes showing increased expression. The row labelled 'GS' indicates the colour range corresponding to the minimum and maximum value of the statistic. Potential related pathways or co-expressed genes are labelled by a red arrow. Co-expression analysis associated with *CTTN* and the corresponding heatmap were analysed and presented by Dr Wojciech Barczak.

Figure 5.5 List of adhesion related genes regulated by E2F1 and PRMT5 activity

Symbol	Log 2 fold change	*p* value	Description	Pathway
CTTN	-1.189542	1.86E-159	Cortactin	Actin dynamics signalling pathway; bacterial invasion of epithelial cells
P4HB	-0.218417	1.43E-05	Prolyl 4-Hydroxylase Subunit Beta	Protein processing in endoplasmic reticulum
AIF1L	-0.527159	5.12E-16	Allograft Inflammatory Factor 1 Like	Focal adhesion
MAP2K2	-0.496844	2.17E-22	Mitogen-Activated Protein Kinase Kinase 2	Actin dynamics signalling pathway
CALR	-0.432355	3.57E-17	Calreticulin	Adaptive immune system
FLNA	-0.314581	1.05E-14	Filamin A	Actin dynamics signaling pathway
TRIOBP	-0.954474	5.29E-17	TRIO And F-Actin Binding Protein	Actin filament organisation
TLE2	-0.611555	2.43E-13	TLE Family Member 2	Wnt signalling pathway
ITGA3	-0.701612	1.35E-20	Integrin Subunit Alpha 3	Actin dynamics signaling pathway
FLII	-0.658315	1.55E-29	FLII Actin Remodeling Protein	Actin filament severing

Figure 5.5 List of adhesion related genes regulated by E2F1 and PRMT5 activity. The table summarizes *CTTN* and its co-expressed genes, including the gene symbol, log2 fold change, the *p*-value used in RNA-Seq study (relative to DMSO control), the gene description, and the related pathways. Information for these genes was obtained from the GeneCards database (https://www.genecards.org).

5.4 RNA-Seq profiling reveals a cluster of adhesion related genes dependent on E2F1 and PRMT5 activity

The putative differentially expressed E2F1 target genes were verified by qPCR analysis in HCT116 cells using the same growth conditions as for the RNA sequencing analysis for biological triplicates. The expression levels of *CTTN*, *FLII*, *ITGA3*, *AIF1L*, and *TLE2* was reduced in cells treated with J579-44 compared to untreated cells. Next, we examined the expression level of these genes in HCT116 p53+/+ cells in the same experimental conditions as used for RNA sequencing analysis, and observed reduced expression levels of *CTTN*, *FLII*, *ITGA3*, *AIF1L*, and *TLE2* in J579-44 treated HCT116 p53+/+ cells relative to the DMSO control (Figure 5.6A). Interestingly, the gene expression effect of J579-44 was increased in p53-/- cells compared to p53+/+ cells, indicating that the effect of J579-44 on gene expression was marginally influenced by p53 status. Overall, the RNA-Seq profiling suggested that a cluster of adhesion related genes, including *CTTN* and its co-expressed genes, were downregulated by PRMT5 inhibition, thus modulating the cell adhesion and migratory phenotypes, resulting in a decrease in cellular metastasis and invasion.

Figure 5.6 Verification of *CTTN* and co-expressed genes

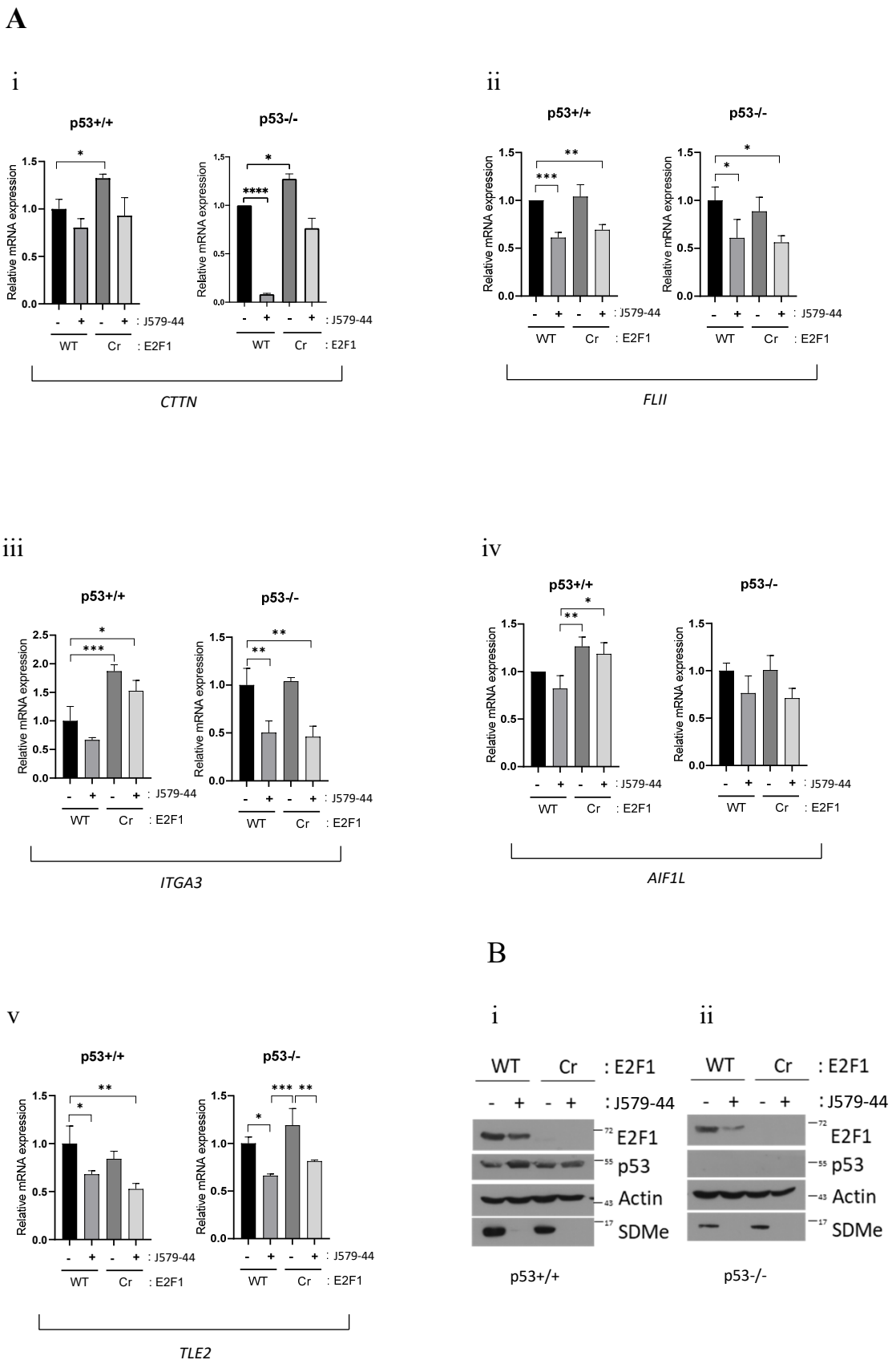


Figure 5.6 Verification of CTTN and co-expressed genes. (**A)** (i) qPCR for the *CTTN* gene in HCT116 p53+/+ WT *E2F1* and *E2F1* CRISPR cells, and HCT116 p53-/- and *E2F1* CRISPR cells that were treated for 2 days with 1 μM J579-44 or DMSO control, and (ii) as above, but qPCR was performed on *FLII*, (iii) *ITGA3*, (iv) *AIF1L*, (v) and *TLE2*. (**B)** Immunoblot for (i) p53+/+, and (ii) p53-/- cells to demonstrate the input protein levels for E2F1, p53 and SDMe; β-actin was used as a loading control. The qPCR analysis and western blots were presented by Dr Wojciech Barczak.

5.5 Chapter summary

RNA-Seq analysis shed light on putative E2F1 targets that were regulated by PRMT5. PGSEA was applied to test for the enrichment of KEGG-annotated pathways and GO terms, and highlighted the resulting differences between PRMT5 inhibitor-treated and control samples.

Enriched GO and KEGG terms that were significantly different between J579-44 treated and control cells were related to cellular adherence and migration. We analysed the list of DEGs for enrichment for KEGG and GO terms, and identified several highly regulated DEGs in the RNA-Seq data sets. Further, a co-expression analysis using *CTTN* in a weighted correlation network analysis identified a group of co-expressed genes containing *FLII*, *ITGA3*, *AIF1L*, and *TLE2*, and these results were verified by qPCR to show that their expression level was downregulated upon PRMT5 inhibition.

Studies on *CTTN* in the past decade have indicated that it encodes cortactin, which is a crucial regulator of actin cytoskeletal dynamics and plays a role in cellular migration and invasion thus acts as a key player in aggressive cancers[66,67,72]. Cortactin acts as an actin-nucleation-promoting factor that binds and activates the Arp2/3 complex, a seven-subunit complex that is responsible for the formation of branched F-actin, which directly regulates the polymerisation of actin during cell motility[66]. Cortactin is also essential for the formation and function of invadopodia. Invadopodia are actin-driven protrusions and are related to modulate cell migratory pattern in

invasive cancers. Overexpression of cortactin has also been linked to invasive cancers, including melanoma, colorectal cancer, and glioblastoma, metastatic breast carcinomas[72].

FLII encodes a protein with a gelsolin-like actin-binding domain and plays a role in the regulation of cytoskeletal rearrangements involved in cytokinesis and cell migration[222,223]. Another cell migratory gene, *ITGA3*, encodes a member of the integrin alpha chain family of proteins, which function as cell surface adhesion molecules[224]. *AIF1L* is an actin-binding protein that promotes actin filament binding[225], and *TLE2* acts as a transcriptional corepressor, and its overexpression has been observed in muscle-invasive bladder cancer[226]. Thus, these genes show a direct or indirect effect on actin networks or cell adhesion and migration.

Cell adhesion is related to the migration and invasion of cells during tumorigenesis and metastasis. Cell-cell adhesion determines the polarity and physiological function of cells within tissues[63]. In single cell, adhesion-related molecules prompt the interactions within the cell microenvironment, altering the cell phenotype, survival, differentiation, and cellular migratory pattern. As a consequence, change in cell adhesive model directly drive tumorigenesis and metastasis. In a developing tumour, the loss of stabilising cell adhesions between cells enables the cells to gain a migratory phenotype, facilitating tumour invasiveness and metastasis[63-65]. However, the invasive capacity of metastatic tumour cells depends on several factors, including efficient cell

adhesion during transit in the circulation, the colonisation of distant organs, and interactions with the extracellular matrix at secondary metastatic sites[227,228].

Taken together, RNA-Seq profiling indicated that a group of adhesion related genes regulated by E2F1 and PRMT5 activity modulate the cell adhesion and migratory phenotypes, resulting in a decrease in cellular metastasis and invasion, and highlighted the role of the PRMT5-E2F1 axis in the control of cell adhesion and migration.

Chapter 6: PRMT5 regulates cell adhesion and migration in an E2F1-dependent manner

6.1 Introduction

In the previous chapter, we reported that PRMT5 modulates cell adhesion and migration by regulating a group of adhesion related genes putatively dependent on E2F1. In this chapter, we examined the potential E2F1 binding sites and identified the underlying mechanisms controlling cell adhesion and migration upon PRMT5 inhibition. We also generated gene expression profiles of PRMT5, E2F1 and putative E2F1 target in different cancers, and performed a Kaplan Meier survival analysis to evaluate their clinical significance.

6.2 ChIP analysis indicates the presence of E2F1-binding site for *CTTN* near the transcription start site

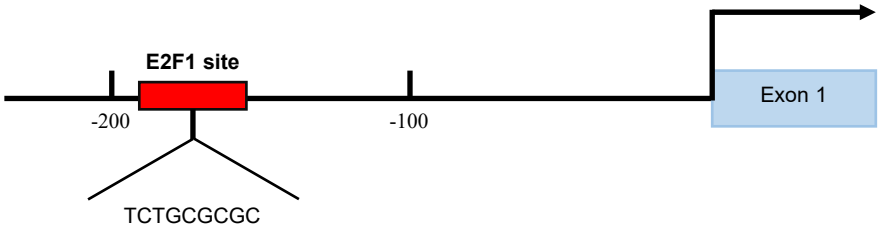
Integrating the DEGs analysis and qPCR results, we hypothesised that *CTTN* regulates cellular adhesion and migratory phenotype dependent on E2F1 and PRMT5 activity. Besides, compared to co-expressed genes, *CTTN* plays a pivotal role in PRMT5-dependent cell adhesion and migration signalling pathways. As a transcription factor, E2F1 is a key regulator of biological processes that function by binding to transcriptional regulatory regions (e.g., promoters, enhancers) to control the expression of their target genes. Location analysis may provide direct evidence that E2F1 has its cognate binding sites in target genes. Therefore, we conducted a motif-scan and analysed the Encyclopaedia of DNA Elements (ENCODE) that is based on the ChIP-Seq database to enable the prediction of the potential TF-DNA binding sites of *CTTN*, and verified the position of the DNA binding site via an E2F1 ChIP experiment.

We performed the motif scan for E2F1 using the JASPAR database; an open-access database for matrix models describing DNA-binding preferences for transcription factors and other DNA patterns (Figure 6.1A). We also examined the TF-DNA binding sites from ENCODE, which were based on ChIP-Seq data generated in MCF-7 cells (Figure 6.1B). Results using both databases indicated that the potential DNA binding sites were ~200 bp upstream of the first exon of *CTTN*.

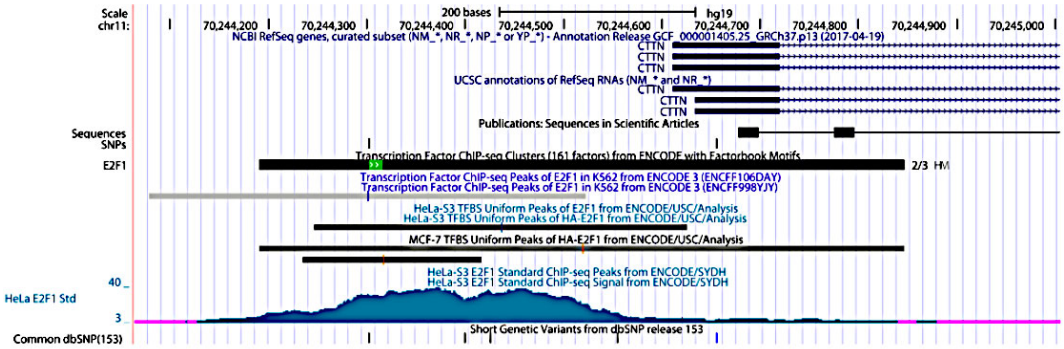
Next, we verified the DNA binding site by performing an E2F1 ChIP experiment. Western blots were performed to demonstrate the input protein levels for E2F1, p53 and SDMe. We observed that E2F1 localised to the promoter of *CTTN* in WT *E2F1* cells, and was undetectable in *E2F1* CRISPR cells (Figure 6.1C). We also conducted a ChIP analysis for E2F1 in HCT116 p53+/+ cells, and observed similar results as in p53-/- cells. Thus, E2F1 was found to associate with promoter DNA in both p53-expressing and p53-/- cells (Figure 6.1D).

Figure 6.1 Motif scan and ENCODE search suggest that *CTTN* is E2F1 target gene

A

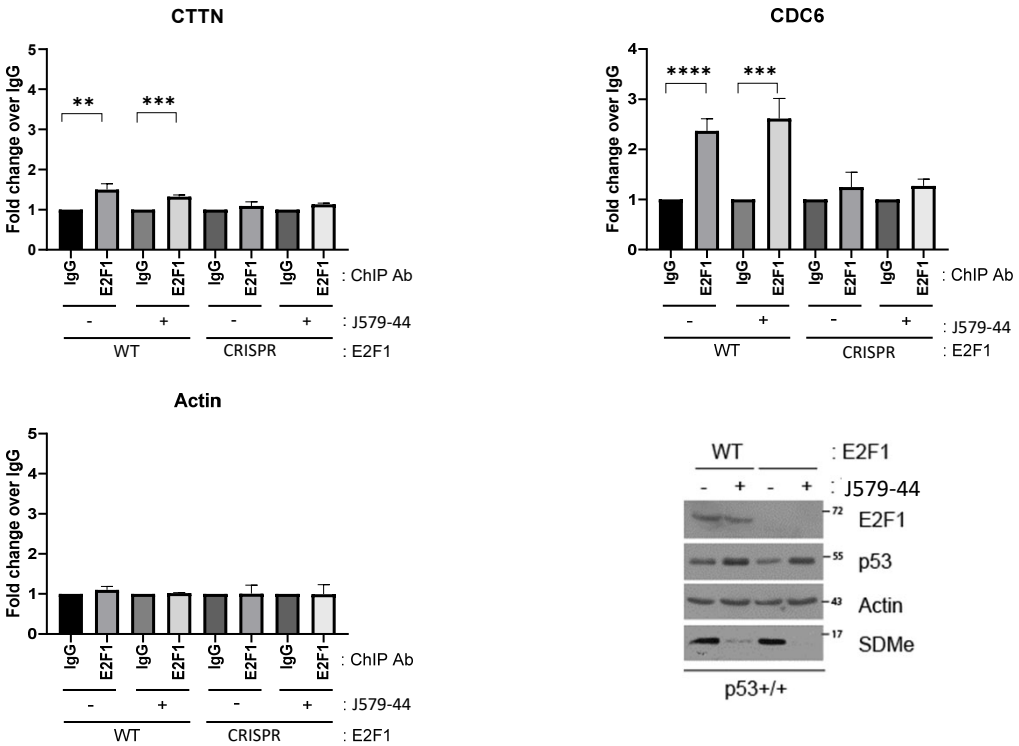


B



C

HCT116 p53+/+:



D

HCT116 p53-/-:

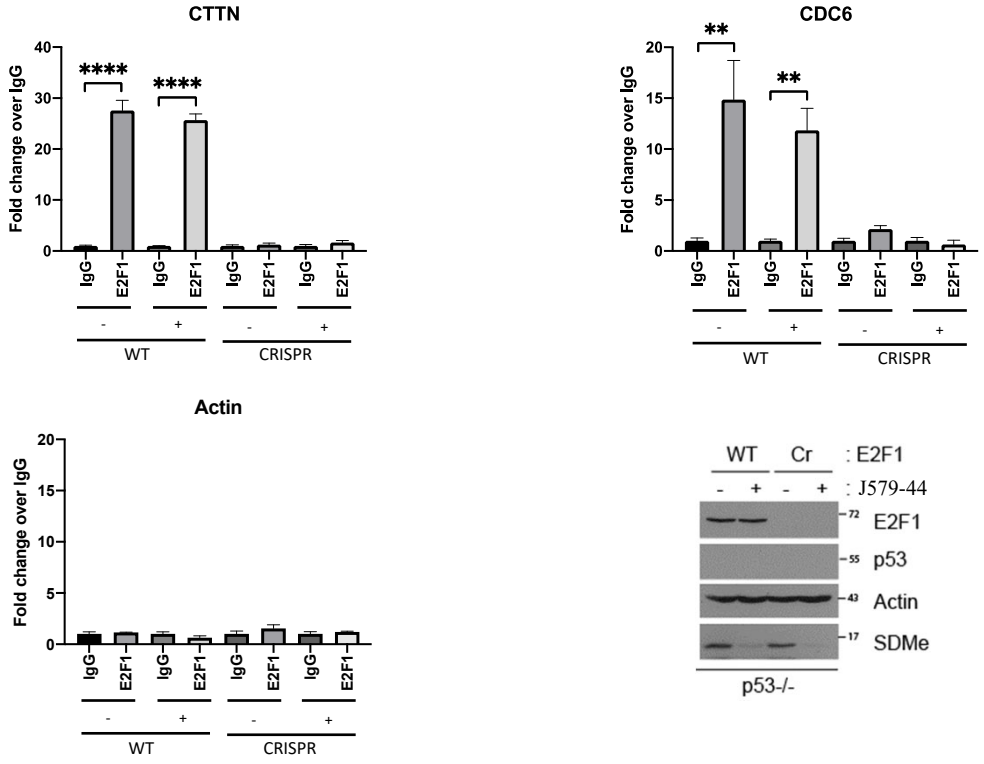


Figure 6.1 Motif scan and ENCODE search suggest that *CTTN* is E2F1 target gene. (A) The red area indicates the potential binding sites for E2F1 as determined from a motif scan analysis. (B) ENCODE analysis based on the ChIP-Seq database. The ENCODE analysis indicated that the binding sites for E2F1 may lie between 100-200 bp before the first exon of *CTTN*. ChIP for E2F1 was performed in (C) p53+/+, and (D) p53-/- WT *E2F1* and *E2F1* CRISPR HCT116 cell lines treated for 48 h with 1 μM J579-44 or with DMSO as a control. The experiment was analysed using primers spanning the E2F1 DNA binding site in the *CTTN* promoter, along with primers surrounding the known E2F1 motifs in the promoter of CDC6. Primers for the actin gene were used as a negative control. Western blots were performed to demonstrate the input protein levels for E2F1, p53 and SDMe, and actin was used as a loading control (n = 3). Error bars indicate the SD of biological replicates. (C) and western blots of (D) were conducted and analysed by Dr. Wojciech Barczak. Statistical analyses were performed using a two-tailed, unpaired Student's *t*-test. The *p*-values of < 0.05 were considered as significant and are indicated as $*p < 0.05$, $**p < 0.01$, $***p < 0.001$, and $****p < 0.0001$.

6.3 PRMT5 regulates cellular adhesion and migration by modulating the expression of *CTTN*

Results from previous studies indicate that the targeting of PRMT5 activity modulates the cell adhesion and migratory phenotypes by modulating the expression of E2F1 downstream targets, such as *CTTN*. We assessed the effect of *CTTN* silencing with and without PRMT5 inhibition in cells, and analysed cellular migration and invasion by using siRNA targeting *CTTN*, using cells transfected with siGFP as a control. The efficiency of siRNA-mediated silencing was confirmed by immunoblotting. Cell migration, invasion, and adherence were analysed via the Transwell and xCELLigence assays.

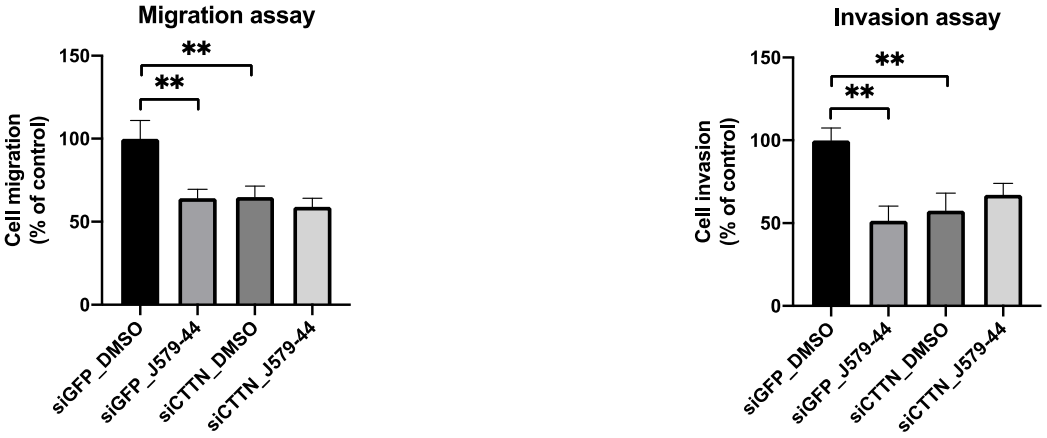
The results from the Transwell assays showed that cell migration and invasion activities were reduced in J579-44-treated cells compared to the control group. Silencing of *CTTN* also lead to a decrease in cellular migration and invasion. However, the combined treatment with PRMT5 inhibitor and using siRNA for *CTTN* did not result in any further significant reduction in cell migration and invasion (Figure 6.2A). These results suggest that PRMT5 and *CTTN* may have shared mechanisms to regulate cellular migratory phenotype and further affect invasive ability of cells.

The results obtained above were confirmed by real-time xCELLigence assays. PRMT5 inhibition leads to a 50% decrease in cellular migration and invasion capacity. A similar effect was observed in si*CTTN*-silenced cells. The combined treatment using

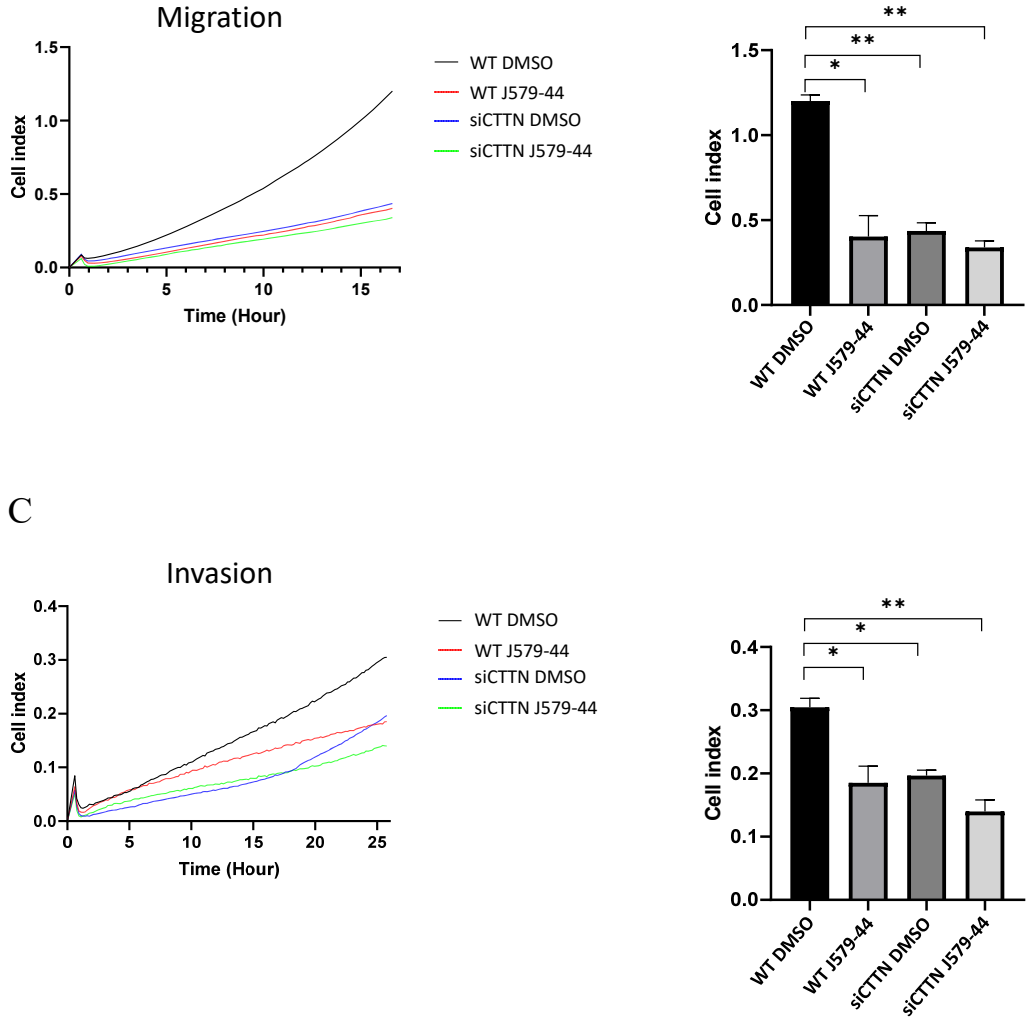
PRMT5 inhibition and siRNA silencing of *CTTN* did not result in a further decrease in cell migration and invasion (Figure 6.2B, Figure 6.2C). In contrast, both PRMT5 inhibition and the siRNA silencing treatment for *CTTN* enhanced cell adhesion. Similarly, the combination of the two treatments did not cause a further accumulation of physiological effects. To summarise, the siRNA knockdown of *CTTN* or its downregulation via treatment with the PRMT5 inhibitor led to the same expression pattern and physiological outcome. Together, both assays highlighted a cell adhesion-related and migration-related mechanism shared between PRMT5 and *CTTN*.

Figure 6.2 PRMT5 regulates cell adhesion and migration by modulating the expression of *CTTN*

A

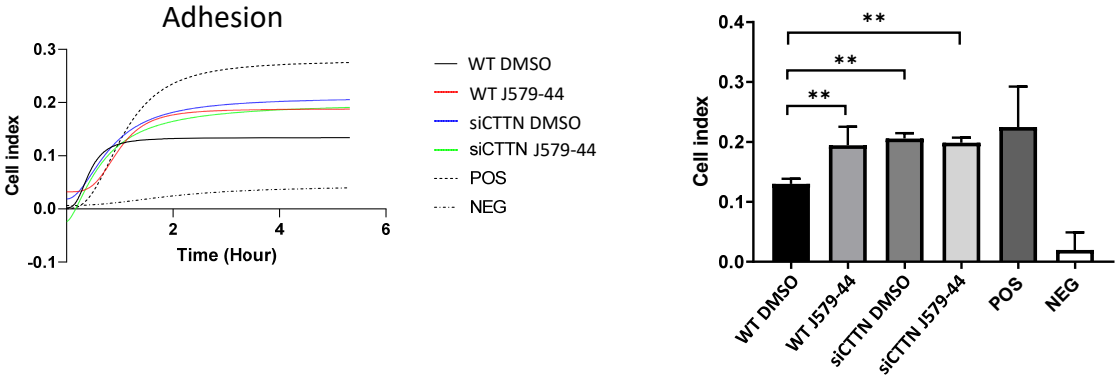


B



C

D



E

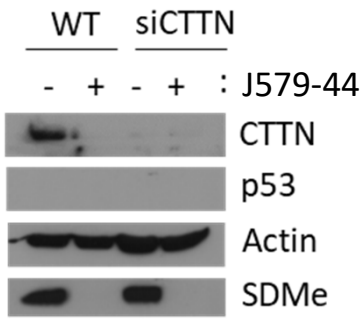


Figure 6.2 PRMT5 regulates cell adhesion and migration by modulating the expression of *CTTN*. HCT116 p53-/- cells were treated with siRNA treatment of *CTTN*, and siGFP was used as a control. After 24 hours post-transfection, the cells were treated with DMSO and 1 μM J579-44 for 2 days. (A) Transwell assays showed that PRMT5 inhibition or siRNA treatment of *CTTN* led to a decrease in cell migration and invasion (n=3). The xCELLigence RTCA assay showed similar results to the Transwell assays for (B) cell migration and (C) invasion (n=3). (D) The xCELLigence RTCA assay showed cell adhesion ability with different treatments, indicating that PRMT5 inhibition or siRNA treatment of *CTTN* led to the increase of cell-cell adhesion. n=3. (E) Immunoblot analysis depicted the input protein levels for CTTN, p53 and SDMe, with actin used as a loading control. From (B) to (E) were conducted and analysed by Dr. Wojciech Barczak. Error bars indicate the SD of biological replicates. Statistical analyses were performed using a two-tailed, unpaired Student's *t*-test. The *p*-values of < 0.05 were considered as significant and are indicated as $*p < 0.05$, $**p < 0.01$, $***p < 0.001$, and $****p < 0.0001$.

6.4 Gene expression profiling and survival analysis of *PRMT5*, *E2F1* and *CTTN*

We evaluated the prognostic and clinical significance of *PRMT5*, *E2F1*, and *CTTN* expression and validated the results using TCGA database (TCGA data were accessed and downloaded through the UCSC Xena Browser: https://xena.ucsc.edu). We compared the gene expression for the indicated candidates between normal and tumour tissues in 31 different primary sites in the TCGA database. Further, we evaluated the impact of these genes on the PFS and OS in the TCGA cohort, and generated the gene expression profiles for *PRMT5*, *E2F1*, and *CTTN* in different tumours.

Our results showed that *PRMT5* was overexpressed in multiple cancer types (cancer type was classified by its primary site), with *E2F1* concomitantly showing high expression in bladder cancer (n = 9 from normal tissues, n = 426 from tumour tissues; *p* (*PRMT5*) = 0.0449, *p* (*E2F1*) <0.0001), breast cancer (n = 179 from normal tissues, n = 1212 from tumour tissues; *p* (*PRMT5*) <0.0001, *p* (*E2F1*) <0.0001), cervical cancer (n = 10 from normal tissues, n = 309 from tumour tissues; *p* (*PRMT5*) = 0.0242, *p* (*E2F1*) <0.0001), colon cancer (n = 304 from normal tissues, n = 331 from tumour tissues; *p* (*PRMT5*) <0.0001, *p* (*E2F1*) <0.0001), oesophagus cancer (n = 649 from normal tissues, n = 195 from tumour tissues; *p* (*PRMT5*) <0.0001, *p* (*E2F1*) <0.0001), head and neck cancer (n = 248 from normal tissues, n = 1135 from tumour tissues; *p* (*PRMT5*) <0.0001, *p* (*E2F1*) <0.0001), liver cancer (n = 110 from normal tissues, n = 421 from tumour tissues; *p* (*PRMT5*) <0.0001, *p* (*E2F1*) <0.0001), lung cancer (n =

287 from normal tissues, n = 1122 from tumour tissues; *p* (*PRMT5*) <0.0001, *p* (*E2F1*) <0.0001), ovarian cancer (n = 88 from normal tissues, n = 426 from tumour tissues; *p* (*PRMT5*) <0.0001, *p* (*E2F1*) <0.0001), pancreatic cancer (n = 165 from normal tissues, n = 183 from tumour tissues; *p* (*PRMT5*) <0.0001, *p* (*E2F1*) <0.0001), prostate cancer (n = 100 from normal tissues, n = 548 from tumour tissues; *p* (*PRMT5*) <0.0001, *p* (*E2F1*) <0.0001), gastric cancer (n = 172 from normal tissues, n = 450 from tumour tissues; *p* (*PRMT5*) <0.0001, *p* (*E2F1*) <0.0001) (Figure 6.3A).

In two cancer types, there was a similar high expression of *CTTN* in tumour tissue relative to normal tissue. *CTTN* was overexpressed in head and neck cancer (n = 248 from normal tissues, n = 1135 from tumour tissues; $p = 0.0002$), and pancreatic cancer (n = 165 from normal tissues, n = 183 from tumour tissues; $p < 0.0001$) (Figure 6.3B). Interestingly, when comparing the expression level of *CTTN* among the subtypes of lung cancer, significantly higher expression of *CTTN* was observed in lung adenocarcinoma than in lung squamous cell carcinoma (n = 575 in adenocarcinoma, n = 553 in squamous cell carcinoma, $p = 0.0009$). Further analysis of the TCGA lung cancer cohort based on the clinical stage indicated no significant difference in the expression levels among the different clinical stages (Figure 6.3C).

PRMT5 overexpression lead to worse OS in breast cancer (n = 528 with low expression, n = 682 with high expression; $p = 0.02652$), head and neck cancer (n = 278 with low expression, n = 285 with high expression; $p = 0.003426$), and pancreatic cancer (n = 64 with low expression, n = 119 with high expression; $p = 0.0352$). Higher

PRMT5 expression was associated with worse PFS in bladder cancer (n = 206 with low expression, n = 220 with high expression; $p = 0.005994$), cervical cancer (n = 88 with low expression, n = 88 with high expression; $p = 0.008712$), lung cancer (n = 279 with low expression, n = 381 with high expression; $p = 0.007317$), pancreatic cancer (n = 64 with low expression, n = 119 with high expression; $p = 0.01699$), and prostate cancer (n = 158 with low expression, n = 226 with high expression; $p = 0.04931$) (Figure 6.3D). Therefore, *PRMT5* may serve as a promising prognostic and therapeutic target for the treatment of certain cancers.

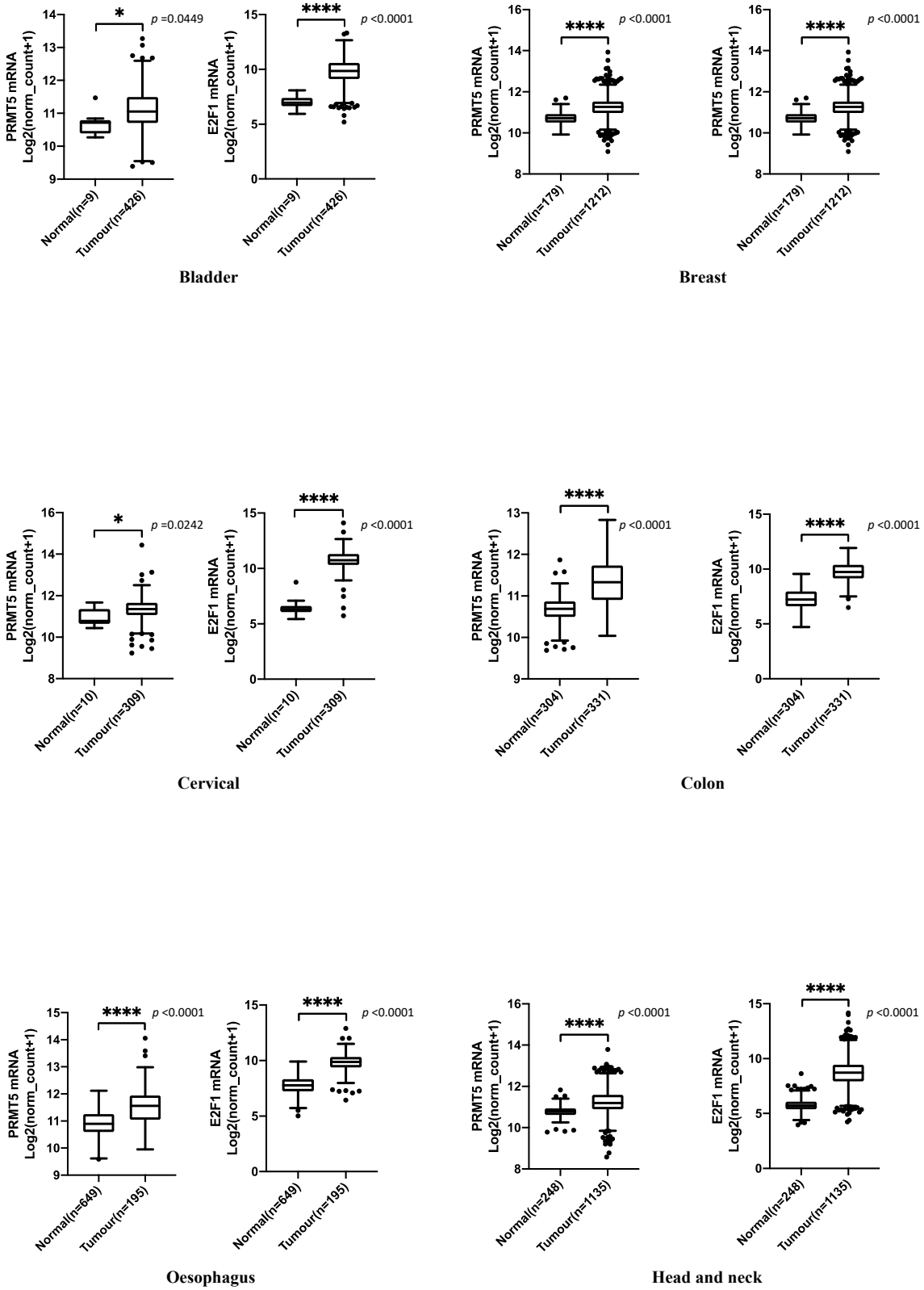
In the TCGA cohort, higher *CTTN* expression was associated with worse OS in head and neck cancer (n = 281 with low expression, n = 282 with high expression; $p = 0.0003878$), and pancreatic cancer (n = 39 with low expression, n = 144 with high expression; $p = 0.01157$). Higher *CTTN* expression was also associated with worse PFS in head and neck cancer (n = 281 with low expression, n = 282 with high expression; $p = 0.02208$), lung cancer (n = 291 with low expression, n = 369 with high expression; $p = 0.003557$), pancreatic cancer (n = 21 with low expression, n = 51 with high expression; $p = 0.01709$), and prostate cancer (n = 224 with low expression, n = 160 with high expression; $p = 0.0007568$) (Figure 6.3E).

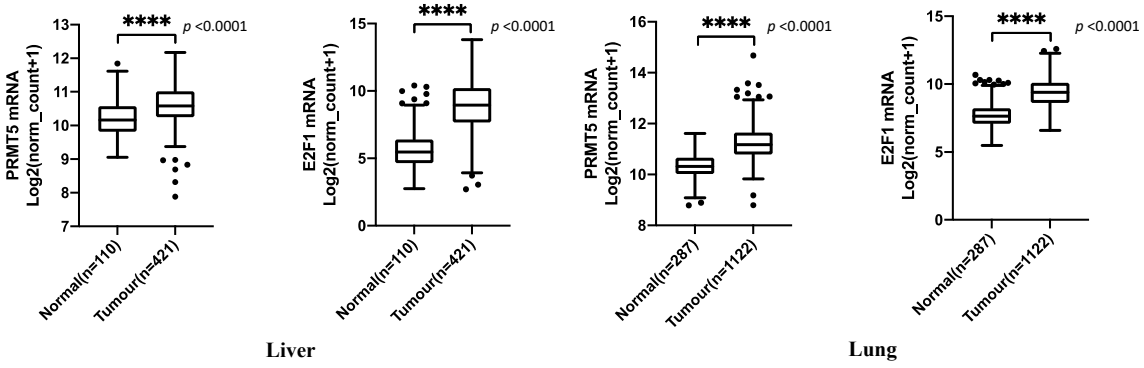
Taken together, we compared the gene expression profiles for 31 tumour samples and paired normal tissues from the TCGA database. *PRMT5* expression was confirmed to be significantly upregulated in the majority of tumour samples, and *E2F1* expression was upregulated in tumour samples. In samples for head and neck tumour and

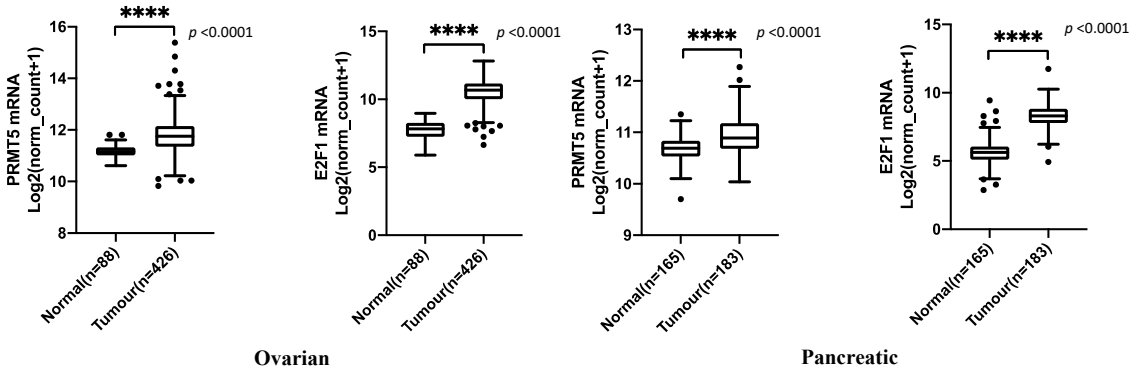
pancreatic tumour, *CTTN* was significantly upregulated relative to normal tissues. Additionally, the overexpression of *PRMT5* or *CTTN* leads to poor clinical outcomes in several cancer types. In head and neck cancer and pancreatic cancer, there was a similar high expression of *PRMT5*, *E2F1*, and *CTTN* in tumour tissues relative to normal tissue. Using Kaplan-Meier analysis curves, the levels of *PRMT5* and *CTTN* were linked to survival probability, and the high expression of *PRMT5* and *CTTN* was linked to poor OS and PFS.

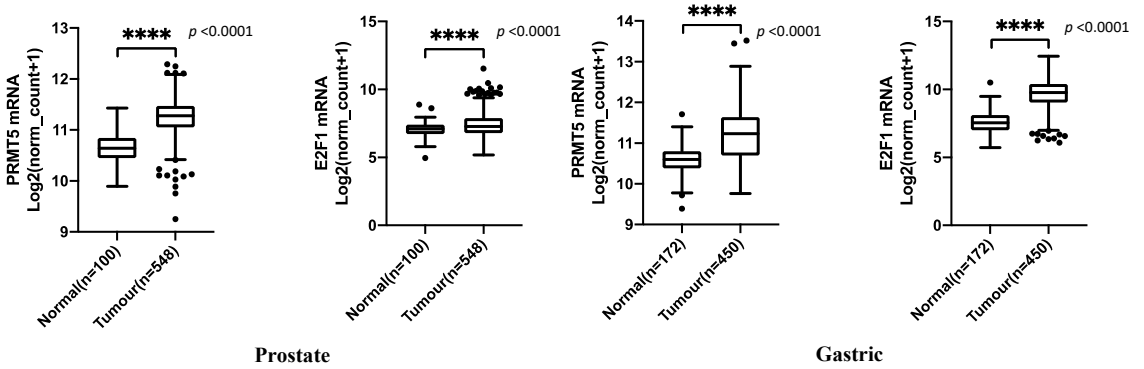
Figure 6.3 Gene expression profiling and survival analysis using expression data for *PRMT5*, *E2F1* and *CTTN* from the TCGA database

A

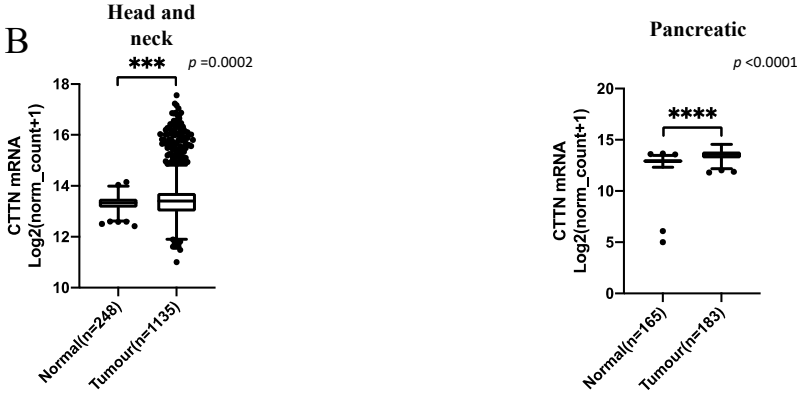



PRMT5 mRNA Log2(norm_count+1)
****
p <0.0001
Normal(n=110)
Tumour(n=421)
E2F1 mRNA Log2(norm_count+1)
****
p <0.0001
Normal(n=110)
Tumour(n=421)
Liver
PRMT5 mRNA Log2(norm_count+1)
****
p <0.0001
Normal(n=287)
Tumour(n=1122)
E2F1 mRNA Log2(norm_count+1)
****
p <0.0001
Normal(n=287)
Tumour(n=1122)
Lung

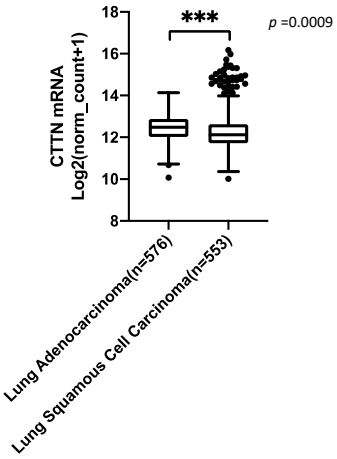

PRMT5 mRNA Log2(norm_count+1)
****
p <0.0001
Normal(n=88)
Tumour(n=426)
E2F1 mRNA Log2(norm_count+1)
****
p <0.0001
Normal(n=88)
Tumour(n=426)
Ovarian
PRMT5 mRNA Log2(norm_count+1)
****
p <0.0001
Normal(n=165)
Tumour(n=183)
E2F1 mRNA Log2(norm_count+1)
****
p <0.0001
Normal(n=165)
Tumour(n=183)
Pancreatic

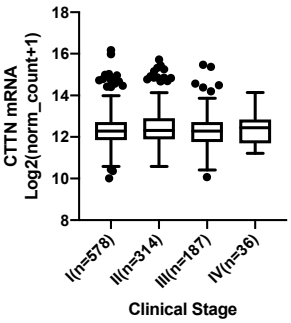

PRMT5 mRNA Log2(norm_count+1)
****
p <0.0001
Normal(n=100)
Tumour(n=548)
E2F1 mRNA Log2(norm_count+1)
****
p <0.0001
Normal(n=100)
Tumour(n=548)
Prostate
PRMT5 mRNA Log2(norm_count+1)
****
p <0.0001
Normal(n=172)
Tumour(n=450)
E2F1 mRNA Log2(norm_count+1)
****
p <0.0001
Normal(n=172)
Tumour(n=450)
Gastric

B

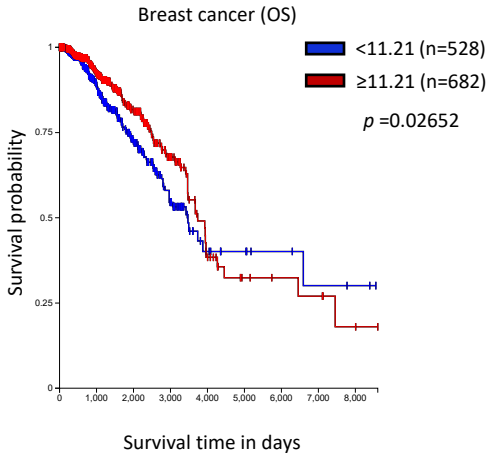

Head and neck
***
p =0.0002
CTTN mRNA Log2(norm_count+1)
Normal(n=248)
Tumour(n=1135)
Pancreatic
p <0.0001
****
CTTN mRNA Log2(norm_count+1)
Normal(n=165)
Tumour(n=183)

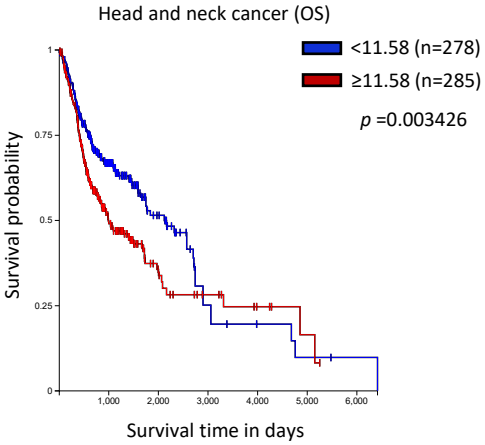
C

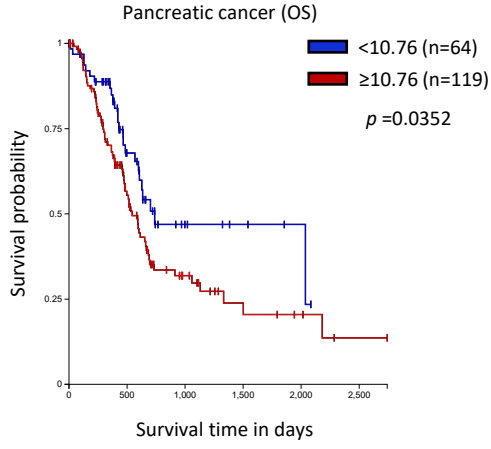

***
p =0.0009
CTTN mRNA
Log2(norm_count+1)
18
16
14
12
10
8
Lung Adenocarcinoma(n=576)
Lung Squamous Cell Carcinoma(n=553)

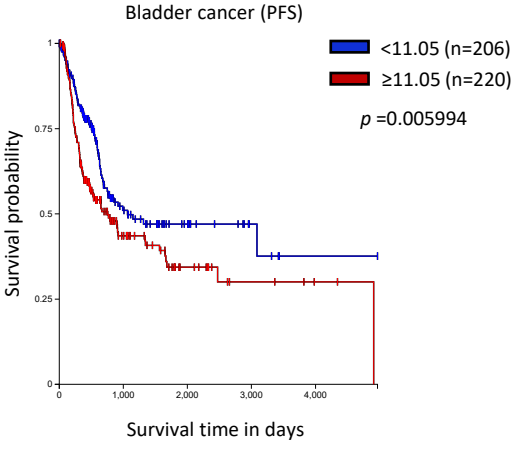

CTTN mRNA
Log2(norm_count+1)
18
16
14
12
10
8
I(n=578)
II(n=314)
III(n=187)
IV(n=36)
Clinical Stage

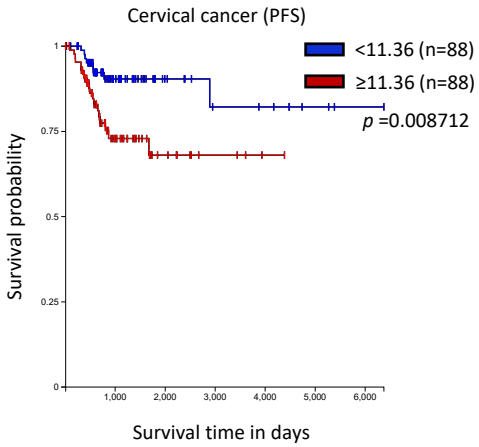
D

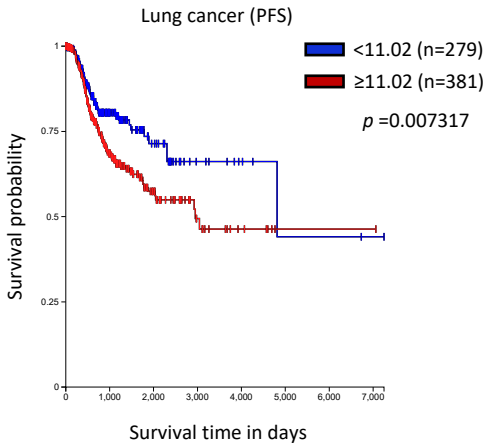

Breast cancer (OS)
<11.21 (n=528)
≥11.21 (n=682)
p =0.02652
Survival probability
1
0.75
0.5
0.25
0
0
1,000
2,000
3,000
4,000
5,000
6,000
7,000
8,000
Survival time in days

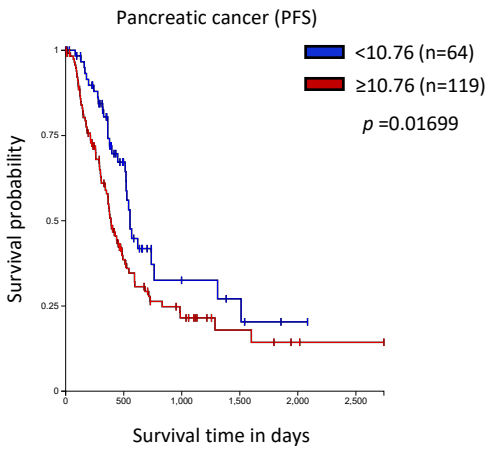

Head and neck cancer (OS)
<11.58 (n=278)
≥11.58 (n=285)
p =0.003426
Survival probability
1
0.75
0.5
0.25
0
1,000
2,000
3,000
4,000
5,000
6,000
Survival time in days

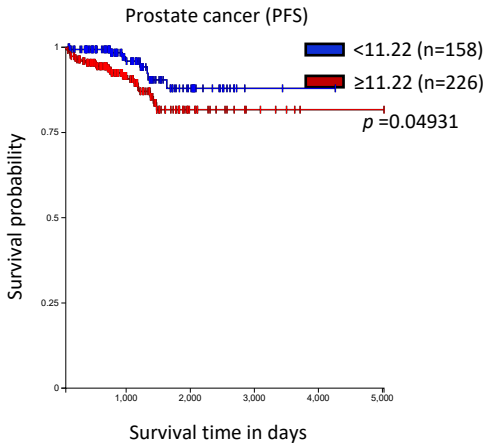

Pancreatic cancer (OS)
<10.76 (n=64)
≥10.76 (n=119)
p =0.0352
Survival probability
1
0.75
0.5
0.25
0
0
500
1,000
1,500
2,000
2,500
Survival time in days


Bladder cancer (PFS)
<11.05 (n=206)
≥11.05 (n=220)
p =0.005994
Survival probability
1
0.75
0.5
0.25
0
0
1,000
2,000
3,000
4,000
Survival time in days

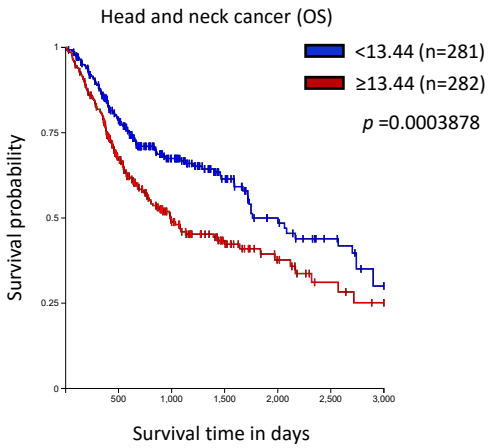

Cervical cancer (PFS)
<11.36 (n=88)
≥11.36 (n=88)
p =0.008712
Survival probability
Survival time in days

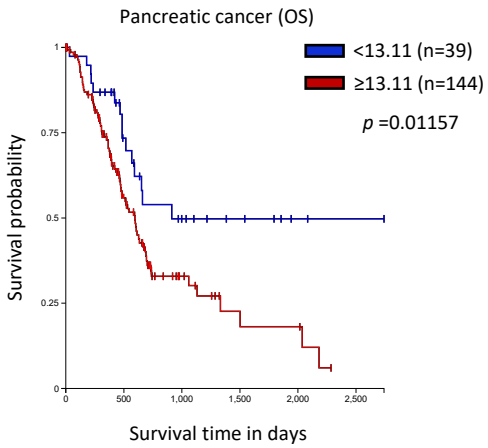

Lung cancer (PFS)
<11.02 (n=279)
≥11.02 (n=381)
p =0.007317
Survival probability
Survival time in days


Pancreatic cancer (PFS)
<10.76 (n=64)
≥10.76 (n=119)
p =0.01699
Survival probability
Survival time in days


Prostate cancer (PFS)
<11.22 (n=158)
≥11.22 (n=226)
p =0.04931
Survival probability
Survival time in days

E


Head and neck cancer (OS)
<13.44 (n=281)
≥13.44 (n=282)
p =0.0003878
Survival probability
Survival time in days


Pancreatic cancer (OS)
<13.11 (n=39)
≥13.11 (n=144)
p =0.01157
Survival probability
Survival time in days

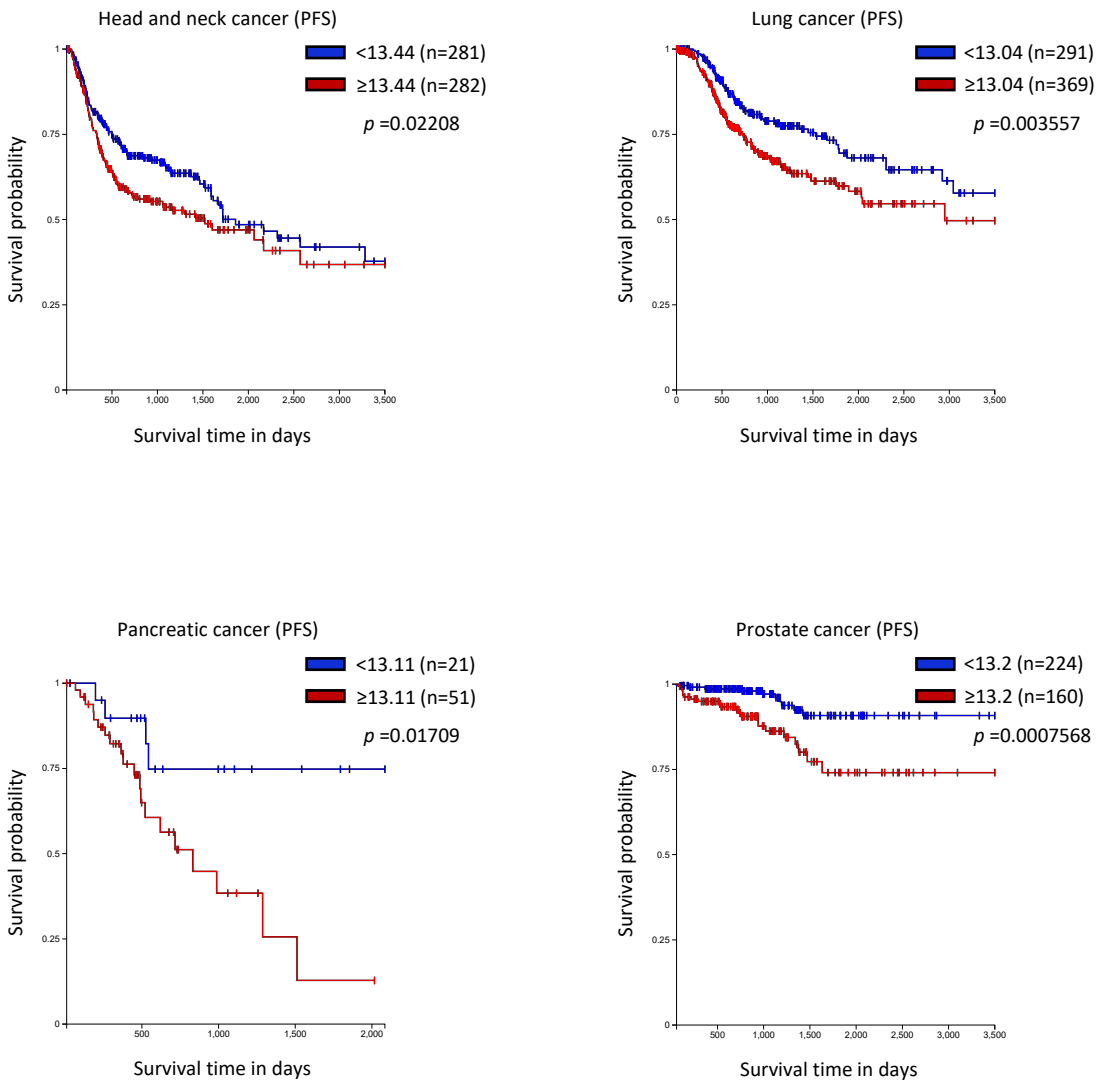


Figure 6.3 Gene expression profiling and survival analysis using expression data for *PRMT5*, *E2F1* and *CTTN* from the TCGA database. (A) Expression levels for *PRMT5* and *E2F1* genes in several human cancers (bladder, breast, cervical, colon, oesophagus, head and neck, liver, lung, ovarian, pancreatic, prostate, and gastric cancer) compared with normal tissues, that was generated using the Xena Browser (https://xenabrowser.net/). Data from TCGA and GTEx projects were used to display the expression levels from cancer tissues or healthy tissues, respectively. (B) The expression level for the *CTTN* gene in head and neck cancer and pancreatic cancer compared with normal tissues, that was generated using the Xena Browser. (C) the expression levels for the *CTTN* gene among the subtypes of lung cancer and in the various clinical stages. Kaplan–Meier analysis curves for OS and PFS associated with *PRMT5* (D) and *CTTN* (E) risk stratification in the TCGA cohort. For each analysis, patients were classified into two groups based on high expression (above or equal to the average gene expression in all patients; red line) or low expression (below the average gene expression in all patients; blue line).

6.5 Chapter summary

We verified that *CTTN* is an E2F1 target gene by examining the results for E2F1 ChIP in cells. The TF-DNA binding site for E2F1 was ~200 bp upstream of the first exon of *CTTN*. Next, we assessed the effects of *CTTN* silencing with and without PRMT5 inhibition on cell adhesion, migration, and invasion by using siRNA targeting of *CTTN*, and compared the effects due to PRMT5 inhibition or *CTTN* silencing. We observed that both siRNA knockdown of *CTTN* or treatment with the PRMT5 inhibitor lead to a decrease in cellular migratory and invasive ability. Interestingly, the combined treatment of PRMT5 inhibition and *CTTN* siRNA silencing did not cause a further decrease in the effects on cell migration and invasion, highlighting a cell migratory and invasion related mechanism shared between PRMT5 and *CTTN*. Similarly, we observed an increase of cell index assessing cell adhesive ability due to PRMT5 inhibition or the siRNA silencing treatment of *CTTN*, and the combined treatment did not cause the accumulation of pharmacological effects. Thus, E2F1 plays a pivotal role in PRMT5 modulated cell adhesion and migration by altering a cluster of adjacent-related genes, such as *CTTN*.

Further, we mined the TCGA database to generate the gene expression profiles for *PRMT5*, *E2F1*, and *CTTN* across all 31 tumour samples and paired normal tissues. The expression of *PRMT5*, *E2F1*, and *CTTN* was found to be significantly upregulated in several tumour types. Overexpression of *PRMT5* or *CTTN* was associated with poor clinical outcomes in several cancer types. Using the Kaplan-Meier analysis, the levels

of *PRMT5* and *CTTN* were linked to survival probability, with higher expression for *PRMT5* and *CTTN* linked to poor OS and PFS.

Overall, we found that the PRMT5-E2F1 axis regulates cell adhesion and migration by modulating the expression of *CTTN* and its co-expressed adhesion related genes. Besides, a coincidence is apparent between the expression of PRMT5 and E2F1 in human tumours, and elevated levels of *PRMT5*, *E2F1* and *CTTN* were observed in a range of cancers and were linked to poor OS or PFS, indicating poor outcomes in cancer patients. Thus, *PRMT5* may serve as a promising prognostic and therapeutic target for the treatment of certain cancers.

Chapter 7: Discussion

7.1 Summary of findings

The pRB-E2F1 complex plays an important role in tumorigenesis as it contributes to the essential steps. pRB interacts with E2F1 and blocks the transcriptional activity of E2F1 before the G1/S transition[133-135]. Arginine methylation by PRMT5 plays a key role in governing E2F1 activity. E2F1 is a direct target of PRMT5-dependent methylation at the arginine residues R111 and R113[196]. E2F1 is methylated in cancer cells, and is an important transcription factor that mediates multiple cellular processes, including cellular apoptosis, cell growth, the cell cycle, and it binds to thousands of downstream genes[190]. Therefore, a dysfunctional E2F1 leads to pathological oncogenesis[133-135].

This study has demonstrated that J579-44 is an effective small-molecule inhibitor of PRMT5, with a low IC50 in cell models. J579-44 may prove to be useful as a powerful chemical tool to explore the biological mechanism underlying PRMT5 activities, and may serve as a clinically relevant drug in anti-tumour therapy. Using genome editing technology via the CRISPR-Cas9 system, we generated *E2F1* CRISPR cells and expanded the biological function of the PRMT5-E2F1 axis. Our results expanded the biological functions of PRMT5-E2F1 axis, including cell apoptosis, migration, invasion, and adherence.

Using a genome-wide expression analysis, a distinct set of genes under the control of PRMT5 and E2F1 was identified, including highly regulated genes such as *CTTN* that is related to cell adhesion. Additionally, the co-expression cluster of genes for *CTTN* was also identified, including *FLII*, *ITGA3*, *AIF1L*, and *TLE2*, that influenced cell adhesion and migration, affecting tumour metastasis and invasion in a PRMT5-dependent mechanism. These data were mined using the TCGA database, and our results demonstrated that high expression of these regulated genes lead to poor OS or PFS in cancer patients, highlighting an important role for the PRMT5-E2F1 axis in therapeutic intervention.

Overall, the study demonstrates for the first time the mechanisms underlying the influence of the PRMT5-E2F1 axis on different aspects of cancer cell biology, including cell apoptosis, migration, invasion, and adherence. At the genome level, the PRMT5-E2F1 axis regulates the expression of genes involved in cell adhesion, which in turn enables PRMT5 activity via E2F1 to be integrated with cell migration and invasion. These findings strengthen the case for PRMT5 to be used as a viable therapeutic target, and highlight its potential clinical utility against metastatic disease.

7.2 J579-44 is an effective inhibitor of arginine methyltransferase 5 in cell-based and enzyme assays

PRMT5 is the major type II arginine methyltransferase and acts its multiple biological functions by its methylation of a myriad of substrates[147,163]. PRMT5 might be a clinically relevant target as its overexpression is associated with multiple cancer types[157-163]. Targeting PRMT5 could be a potential anticancer therapy.

Various experimental therapeutic strategies aimed at targeting PRMT5 activity have identified a variety of selective small-molecule inhibitors. Most of these have low potency or lack methyltransferase activity in cell-based experiments[207,208]. Inhibitors reported could be divided into two groups: SAM uncompetitive inhibitors and SAM competitive inhibitors[208]. After the optimisation of various physicochemical properties, the SAM uncompetitive inhibitor EPZ015666 was obtained and it showed a correlation between the inhibition of the PRMT5 enzyme and the reduction of the expression of SmD3me2s in a concentration-dependent manner, while retaining its potency with an IC50 value as low as 22 nM in MCL models[209]. EPZ015666 also showed significant tumour growth inhibition in mouse models. Accordingly, the symmetric methylation level in the xenograft tumours decreased in a dose-dependent manner. Additionally, the results from a study highlighted the role of EPZ015666 as an effective substrate-competitor. This result was confirmed by the co-crystal structure of the MEP50–SAM–EPZ015666 co-crystal complex[209]. LLY-283 is a SAM competitive inhibitor, with the methionine moiety replaced by a phenyl group. LLY-283 exhibits potent PRMT5

enzyme inhibitory activity with an IC50 value of 20 nM. In MCF-7 and A375 cells, LLY-283 inhibited the methylation of SmBB with an IC50 of 25 nM and 40 nM seperately. Although LLY-283 exhibits anti-proliferative activity in tumour cell lines and anti-tumour effects in A375 mouse xenografts, its regulation of histone arginine methylation was not so evident in cell-based experiments[210].

In this study, we have demonstrated that J579-44 is an effective PRMT5 inhibitor and we used the analogue J578-68 as a control. The cellular activity of the candidate PRMT5 inhibitors was evaluated by assessing the cytotoxic effects using an MTT assay in U2OS cells, measuring the anti-proliferative effects via colony formation assays in HCT116 cells, monitoring symmetric dimethylation in HCT116 cells by western blotting, activating the release of E2F1, and by studying the accumulation of cleaved-PARP that serves as a cellular apoptotic biomarker in U2OS cells using western blots. After 6 days of treatment with PRMT5 inhibitors, J579-44 (IC50 = 0.0161 ± 0.0029 μM) showed a strong cytotoxic effect relative to the less active analogue J578-68 (IC50 = 2.7700 ± 0.3422 μM). J579-44 also showed a significant anti-proliferative effect, as assessed by a colony formation assay in HCT116 cells. Although a serial incrementally increasing concentration was used, a significant decrease in the cellular reproductive and anti-proliferative effects was observed at concentrations as low as 16 nM. PRMT5 is an important enzyme that catalyses symmetric dimethylation of arginine residues on its substrate proteins, including histone and non-histone proteins[177]. In this study, western blotting experiments showed that J579-44 caused a notable decrease in SDMe

levels in cells and inhibited the PRMT5 methyltransferase enzymatic activity. Additionally, PRMT5 methylates arginine residues in target proteins, such as p53 and E2F1, and was found to regulate the expression of E2F1, proving its inhibition of the cellular catalytic ability of PRMT5. Further, J579-44 led to the accumulation of cleaved-PARP in cells. As cleaved-PARP is an early marker of the apoptotic stage, its accumulation provides strong evidence that J579-44 triggers apoptosis in cells.

We performed an enzyme assay to assess the inhibitory activity of the two compounds J579-44 and J578-68 *in vitro* by determining the EC50 values in the presence of the peptide substrate and SAM. PRMT5 catalyses the symmetric demethylation of H4R3. Therefore, we used a PRMT5 Chemiluminescent enzyme kit to monitor the transfer of a methyl group from the donor SAM to the H4 peptide substrate, and demonstrated that J579-44 inhibited PRMT5 activity in enzyme assay with an EC50 of 0.804 μM. In the same assay, the control J578-68 was ~50-fold less active (EC50 of 41.37 μM).

Thus, we have shown that J579-44 is an enzymatic inhibitor of PRMT5 that functions at low nanomolar concentrations in cell-based assays. Furthermore, J579-44 triggered cellular apoptosis, induced anti-proliferative activity, altered the expression level of SDMe, and induced the expression of PRMT5 target proteins. Both anti-proliferative activity in tumour cells and regulation of histone arginine methylation was evident *in vitro*. Additionally, we demonstrated that J579-44 inhibits PRMT5 enzymatic activity. Thus, we have identified an effective PRMT5 inhibitor that can be used

as an effective chemical tool to decode the mechanism underlying the cell-transforming capabilities of PRMT5 and to evaluate the pharmacology of PRMT5 inhibition.

7.3 The PRMT5 inhibitor induces cellular responses via E2F1

PRMT5 plays an important and complex role during oncogenesis. Deregulation of the catalytic activity of PRMT5 alters the arginine methylation levels of target proteins that play a role in regulating gene expression by histone and non-histone methylation, gene splicing, signal transduction, and other mechanisms[177].

PRMT5 acts its multiple biological functions by its methylation of multiple substrate proteins, including histone H3 and H4[163], p53[189], and E2F1[190], et al. The transcription factors p53 and E2F1 are important PRMT5 substrates and play a role in transcriptional regulation, cell cycle arrest, DNA damage response, and the gene-splicing processes[189,190,195,196]. P53 undergoes methylation by PRMT5 at R333, R335 and R337 leads to cancer cells unable to induce G1 phase arrest and trigger p53-dependent DNA damage response[189,195]. E2F1 is identified to undergo symmetric arginine methylation on R111 and R113 by PRMT5[190]. PRMT5 mediates the methylation status of transcription factor E2F1 and thus reduces its ability to suppress cell growth and to promote apoptosis[190,196]. A reader of the symmetric methyl marks has been identified. The tudor domain of the methyl binding protein TSN was identified to specifically bind symmetrically methylated R111 and R113[190,196]. Both p53 and E2F1 are integrated in the PRMT5 induced DNA damage response machinery[196].

The results from our study show that PRMT5 inhibition triggers cellular apoptosis and induces the accumulation of cells in the sub-G1 phase. PRMT5 inhibition also

impairs cell proliferation, viability, cell migration, and invasion. We edited *E2F1* in p53+/+ and p53-/- cells by using the CRISPR-Cas9 technology, and evaluated the cellular response of *E2F1* CRISPR knockout cells and the controls in cells showing PRMT5 inhibition. Interestingly, by comparing the sub-G1 cell populations between p53+/+ *E2F1* CRISPR knockout cells and the p53+/+ control cells upon PRMT5 inhibition, we observed that p53 masks the interplay between PRMT5 and E2F1. Additionally, in p53-/- cells, PRMT5 inhibition induced an increase in the sub-G1 cell population in *E2F1* control cells relative to *E2F1* CRISPR knockout cells. Our study showed that cellular apoptosis induced by PRMT5 inhibition is directly mediated by regulating E2F1 levels and activity. The inhibition of PRMT5 upregulates the expression level of p53, and triggers p53 related pathways based on the evidence that the absence of p53 augments the accumulation of cells in the sub-G1 phase. Further, PRMT5 inhibition upregulates the expression of cleaved-PARP, and E2F1 acts as a predominant regulator in PRMT5 regulated cell apoptosis, migration, and invasion.

In summary, our study showed that both p53 and E2F1 are integrated in the PRMT5 induced cell-cycle arrest, apoptosis, cell proliferation, cell adhesion, migration, and invasion processes. However, the PRMT5-dependent effects were marginally influenced by p53 status. In fact, the effects regulated by PRMT5 was in association mainly with E2F1. The PRMT5-E2F1 axis was found to regulate cellular apoptosis, cell adhesion and migratory phenotypes, and further affect cellular metastasis and invasion.

7.4 PRMT5 regulates cellular adhesion and migration by modulating the expression of E2F1 target *CTTN* and its co-expressed genes

Through RNA-Seq analysis, we generated a global expression map for PRMT5 and E2F1. Each group of DEGs identified in the specific conditions analysed represented different sets of differentially expressed E2F1 target genes. These genes were found to be regulated by E2F1 or PRMT5, and by both E2F1 and PRMT5. For example, specific up and down-regulated DEGs in the J579-44 treated WT *E2F1* cells represents genes regulated by both PRMT5 and E2F1. Based on DEG analysis, we performed a KEGG and GO analysis, and the results indicated a widespread biological role for PRMT5 and E2F1 in cancer, for example, in cell adhesion, migration, metabolism, cell signalling, and splicing. Interestingly, both KEGG and GO studies highlighted the cell adhesion and migration pathways related to DEGs regulated by PRMT5 and E2F1. The RNA-Seq data analysis results were consistent with those from previous studies for cell migration and invasion assays, reinforcing that the PRMT5-E2F1 axis controls cell adhesion and migratory patterns (Figure 4.9).

Combined with the analysis for DEGs, KEGG, and GO studies, we found the differential regulation of several genes related to cell adhesion and migration. One of the top changing DEGs was *CTTN*, an actin nucleation promoting factor that is significantly downregulated upon PRMT5 inhibition in WT *E2F1* cells. The knockout for *E2F1* masks the interplay between PRMT5 inhibition and its regulation of *CTTN*. As an actin nucleation promoting factor, cortactin (encoded by *CTTN*) directly

regulates the polymerisation of actin during cell motility through activating the Arp2/3 complex[66]. Cortactin is also essential for the formation and function of invadopodia, which are actin-driven protrusions and are related to modulate cell migratory pattern in invasive cancers[76]. In general, cortactin binds to actin networks in cells and has significant clinical value in cancer metastasis. Its overexpression is related to invasive cancers, including melanoma, colorectal cancer, and glioblastoma, metastatic breast carcinomas[72]. Gene expression clustering analysis suggested several actin-related genes highly related with *CTTN* in modulating cell adhesion and migration. Similar as *CTTN*, *FLII* was downregulated upon PRMT5 inhibition in WT *E2F1* cells. Previous studies described *FLII* as a focal adhesion-associated actin capping protein that modulates cell migratory pattern through activation of β1-integrins and vinculin, as well as the increase of filamentous actin content of adhesions[222,223]. Another down-regulated gene upon PRMT5 inhibition in WT *E2F1* cells is *ITGA3*. *ITGA3* interacts with a beta 1 subunit to form integrins, which act as cell surface adhesion proteins and facilitate cell-extracellular matrix adhesion. The aberrant overexpression of *ITGA3* is related to many malignant human tumours, including colorectal and prostate cancers. Besides, its overexpression is related to several malignant clinicopathological characteristics in intrahepatic cholangiocarcinoma patients, such as gross tumour size, lymph node metastasis, and the TNM stage[224]. The other two actin-related co-expressed genes were *AIF1L* and *TLE2*, which are specifically downregulated by PRMT5 inhibition in WT *E2F1* cells. *AIF1L* is a homolog of the allograft inflammatory factor 1 (AIF1 or IBA1), which performs actin bundling and cross-linking functions as well

as co-localization and sedimentation with F-actin[225]. *TLE2* is a member of the *TLE* gene family, and it is a promising biomarker for individualised bladder cancer therapy, including cancer subclassification, and is associated with cancer patient survival and progression[226].

Further, we evaluated the expression of the cluster of genes, including the central component *CTTN* and the co-expressed genes *FLII*, *ITGA3*, *AIF1L*, and *TLE2* in p53+/+ and *E2F1* CRISPR knockout cells upon PRMT5 inhibition. Interestingly, the reduced *CTTN* level upon PRMT5 inhibition compared to the DMSO control in WT *E2F1* cells was not statistically significant. The result was different from the reduced effect of *CTTN* on PRMT5 inhibition in p53-/- WT *E2F1* cells. The reduced level of *CTTN* was statistically significant, with *a p*-value less than 0.0001 compared to the DMSO-treated control group. The absence of p53 increased the effect of PRMT5 inhibition in reducing the level of *CTTN*, proving that p53 marginally influences the effect of PRMT5, and *E2F1* is the predominant factor. However, there was no significant difference in the reduced levels of *FLII*, *ITGA3*, *AIF1L*, and *TLE2* between p53+/+ and p53-/- cells. This result may be explained by the fact that *CTTN* is the main central dominant component in modulating PRMT5 related cellular adhesion and migratory pattern.

We examined the localisation of the TF-DNA binding site for E2F1 that is found ~200bp upstream of the first exon of *CTTN*. This provides direct evidence that E2F1

binds its downstream target *CTTN* to modulate cortactin-related cellular processes such as cell adhesion, migration, and invasive capacity.

Reducing the expression of *CTTN* via siRNA treatment and PRMT5 inhibition were shown to impact cellular adhesion, migration, and invasive capacity. Interestingly, the combination of siRNA treatment for *CTTN* and the inhibition of PRMT5 did not augment the impact on cell adhesion, migration, and invasive capacity. The results demonstrated the presence of a shared mechanism between *CTTN* and PRMT5, which regulate cell adhesion and migration that is related to cellular metastasis and invasion. Further, we observed that the impact of PRMT5 inhibition on cell migration and invasion was impaired in the absence of *E2F1* in cells. *E2F1* is the prerequisite that is dominant in PRMT5 regulated cell adhesion and migration pathways. In summary, the PRMT5-E2F1 axis controls cell adhesion and migration mainly by altering the expression of E2F1 target genes, like top changing DEG *CTTN* and its co-expressed actin-related genes. Figure 7.1 summarised the PRMT5-E2F1 model and its interplay between PRMT5, E2F1, and E2F1 target gene *CTTN* in regulating motility in migration, invasion, and adhesion.

Figure 7.1 The PRMT5-E2F1 model illustrates the interplay between PRMT5, E2F1, and E2F1 target gene *CTTN* in regulating cellular adhesion and migratory phenotypes

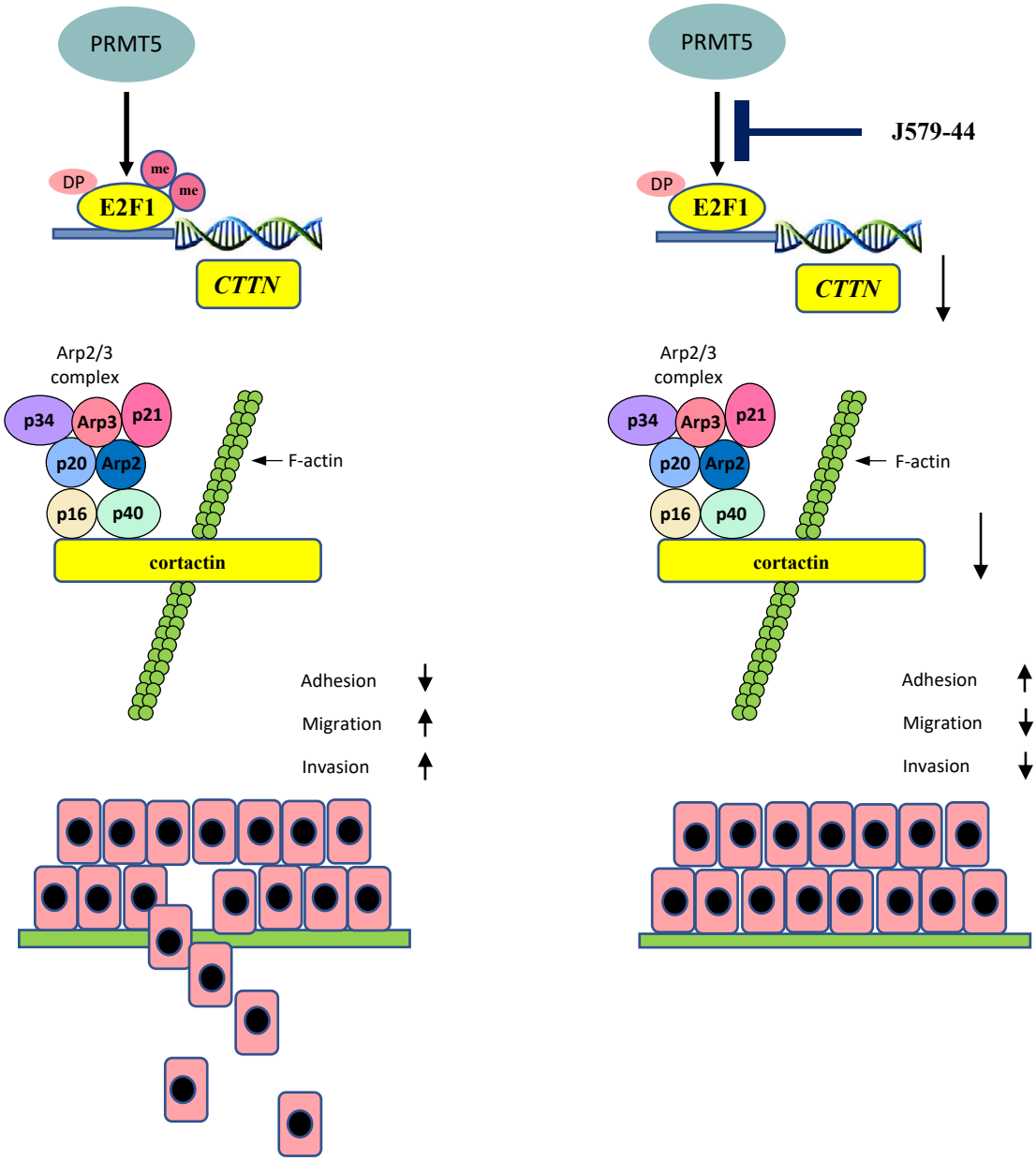


Figure 7.1 The PRMT5-E2F1 model illustrates the interplay between PRMT5, E2F1, and E2F1 target gene *CTTN* in regulating cellular adhesion and migratory phenotypes. PRMT5 influences the expression level of actin-related genes such as *CTTN* by regulating the methylation of E2F1. In the absence of E2F1 methylation (in conditions of PRMT5 inhibition), the expression of *CTTN* is decreased, which regulates the branched actin networks, affects the formation of dynamic cortical actin-associated structures, affects the actin cytoskeleton assembly and ECM degradation, thereby promoting adhesion and reducing migratory ability, further decreasing tumour metastasis and invasion.

7.5 Clinical use for *PRMT5*, *E2F1*, and *CTTN*

Studies have shown that PRMT5 acts as an oncogene during tumorigenesis, and PRMT5 regulates cell proliferation and its direct interaction with proteins commonly misregulated or mutated in multiple cancers[177]. In our study, we evaluated the prognostic and clinical impact of the expression of *PRMT5*, *E2F1*, and *CTTN*, and validated these results using the TCGA database. To evaluate the translational benefit, gene expression was compared between normal and tumour tissues from 31 different primary sites. PRMT5 was found to be overexpressed in cancer of the bladder, breast, cervix, colon, oesophagus, head and neck cancer, liver, lung, ovarian, pancreatic, prostate, and gastric cancer. Overexpression of *PRMT5* in several cancer types leads to reduced OS (in breast, head and neck, and pancreatic cancer) or PFS (bladder, cervical, lung, pancreatic, and prostate cancer). Collectively, PRMT5 may be useful as a prognostic and therapeutic target for the treatment of certain cancers.

Progress has been made in decoding biological functions of cortactin (encoded by *CTTN*) in modulating cell migration, invadopodia formation, and cancer cell invasion and metastasis[72]. The abnormal expression of cortactin is associated with increased aggressiveness of head and neck squamous cell carcinoma cells, even in severe growth conditions[77]. Additionally, phosphorylated cortactin improves the aggressiveness of cancer cells and is required for metastasis in a mouse model. On the contrary, the inhibition of phosphorylation decreases metastasis[72]. Collectively, cortactin is highly related with cell motility, thus affects invasion and metastasis. Invasive cancers and

cancer metastasis usually lead to the failure of cancer therapy[52]. Analysis of data from the TCGA project database indicated that the increased expression of *CTTN* is found in several cancers, including head and neck, and pancreatic cancer. In lung and prostate cancer, the overexpression of *CTTN* correlates with poor PFS. Elevated *CTTN* expression in pancreatic, head and neck cancer, and cervical cancer is highly correlated with poor survival, including OS and PFS, in a large number of patients.

In our study, we have demonstrated the mechanism by which the PRMT5-E2F1 axis plays a crucial role in regulating cancer cell adhesion and migration. Our results suggest that PRMT5, E2F1, and *CTTN* are linked through a shared pathway of control that impacts cell adhesion and migration, affecting tumour metastasis and invasion. This study is the first time to show that the PRMT5-E2F1 axis influences cancer cell growth and division, and also augments the migration and invasive properties of tumour cells. As a positive regulator of the E2F1 axis, this strengthens the case for the use of inhibitors for PRMT5 as a viable therapeutic target, and further suggests the clinical utility of drugs targeting PRMT5. This study helps resolve the biological mechanisms underlying the action of the PRMT5 inhibitor in cancer cells. These new findings may pave the way for the development of novel epigenetic therapy and benefit society.

7.6 Conclusions

In conclusion, we have explored the functional role of the PRMT5-E2F1 axis and highlighted its influence on different aspects of cancer cell biology, including cell apoptosis, migration, invasion, and adhesion. In a genome-wide expression analysis, a distinct set of genes under the control of PRMT5 and E2F1 was identified, including several highly regulated genes that influence cell adhesion and migration thus resulting in metastasis and invasion, via a PRMT5-dependent mechanism. Significantly, the expression of PRMT5 and E2F1 in human tumours was related, and elevated levels of *PRMT5* and *CTTN* correlated with a poor prognosis. Our results suggest a causal relationship between PRMT5 and E2F1 in driving the malignant phenotype, highlighting an important pathway for therapeutic intervention.

References

1. WHO Cancer. *WHO* (2018).
2. Freddie B. et al. Global Cancer Statistics 2018: GLOBOCAN Estimates of incidence and Mortality Worldwide for 36 Cancers in 185 Countries. *CA CANCER J CLIN* **68**:394-424.
3. Hanahan, D. & Weinberg, R.A. The hallmarks of cancer. *Cell* **100**, 57-70 (2000).
4. Hanahan, D. & Weinberg, R.A. Hallmarks of cancer: the next generation. *Cell* **144**, 646-674 (2011).
5. Hnisz, D., Weintraub, A. S., Day, D. S., Valton, A. L., Bak, R. O., Li, C. H., et al. Activation of proto-oncogenes by disruption of chromosome neighborhoods. *Science* **351**, 1454-1458 (2016).
6. Weinberg, R. A. *The biology of cancer* 2nd edition. Garland Science: New York (2013).
7. Frankel, T. L., Vakiani, E., Nathan, H. et al. Mutation Location on the RAS Oncogene Affects Pathologic Features and Survival After Resection of Colorectal Liver Metastases. *Cancer* **123**, 568-575 (2017).
8. Dang CV. MYC on the path to cancer. *Cell* **149**, 22-35 (2012).
9. Herrero, A., Pinto, A., Colón-Bolea, P. et al. Small Molecule Inhibition of ERK Dimerization Prevents Tumorigenesis by RAS-ERK Pathway Oncogenes. *Cancer Cell* **28**, 170-182 (2015).
10. Croce C.M. Oncogenes and cancer. *The New England Journal of Medicine*. **358**, 502-511 (2008).
11. Thomas, R. K., Baker, A. C., Debiasi, R. M., et al. High-throughput oncogene mutation profiling in human cancer. *Nat Genet*. **39**, 347-351 (2007).
12. Aubrey, B. J., Kelly, G. L., Janic, A., Herold, M. J., & Strasser, A. How does p53 induce apoptosis and how does this relate to p53-mediated tumour suppression? *Cell Death Differ*. **25**, 104-113 (2018).
13. Vicente-Dueñas, C., Romero-Camarero, I., Cobaleda, C., & Sánchez-García, I. Function of oncogenes in cancer development: a changing paradigm. *EMBO J.* **32**, 1502-1513 (2013).
14. Rossari, F., Minutolo, F., & Orciuolo, E. Past, present, and future of Bcr-Abl inhibitors: from chemical development to clinical efficacy. *Journal of hematology & oncology* **11**, 84 (2018).
15. Sharma, S. V., Bell, D. W., Settleman, J., & Haber, D. A. Epidermal growth factor receptor mutations in lung cancer. *Nat Rev Cancer*. **7**, 169-181 (2007).
16. Guo, X. E., Ngo, B., Modrek, A. S., & Lee, W. H. Targeting tumor suppressor networks for cancer therapeutics. *Curr Drug Targets*. **15**, 2-16 (2014).
17. Luo, J., Solimini, N. L., & Elledge, S. J. Principles of Cancer Therapy: Oncogene and Non-oncogene Addiction. *Cell* **136**, 823-837 (2009).
18. Swaffer, M. P., Jones, A. W., Flynn, H. R., Snijders, A. P., & Nurse, P. CDK Substrate Phosphorylation and Ordering the Cell Cycle. *Cell* **167**, 1750-1761 (2016).

19. Alberts B., Johnson A., Lewis J. et al. An overview of the cell cycle. 4th edition. New York: Garland Science (2002).
20. Barnum KJ, O'Connell MJ. Cell cycle regulation by checkpoints. *Methods Mol Biol.* **1170**, 29-40 (2014).
21. Otto, T., & Sicinski, P. Cell cycle proteins as promising targets in cancer therapy. *Nat Rev Cancer*. **17**, 93-115 (2017).
22. Hochegger, H., Takeda, S. & Hunt, T. Cyclin-dependent kinases and cell-cycle transitions: does one fit all? *Nature Rev. Mol. Cell Biol*. **9**, 910-916 (2008).
23. Wood, D. J., & Endicott, J. A. Structural insights into the functional diversity of the CDK-cyclin family. *Open biology* **8**, 180-112 (2018).
24. M. Malumbres, M. & Barbacid. Cell cycle, CDKs and cancer: a changing paradigm. *Nat. Rev Cancer* **9**, 153-166 (2009).
25. Asghar, U., Witkiewicz, A. K., Turner, N. C., & Knudsen, E. S. The history and future of targeting cyclin-dependent kinases in cancer therapy. *Nat Rev Drug Discov*.**14**, 130-146 (2015).
26. Palmer, N., & Kaldis, P. Less-well known functions of cyclin/CDK complexes. *Semin Cell Dev Biol*. **107**, 54-62 (2020).
27. Gao X, Leone GW, Wang H. Cyclin D-CDK4/6 functions in cancer. *Adv Cancer Res* **148**, 147-169 (2020).
28. Schmidt M, Rohe A, Platzer C, Najjar A, Erdmann F, Sippl W. Regulation of G2/M Transition by Inhibition of WEE1 and PKMYT1 Kinases. *Molecule*s **22**, 2045 (2017).
29. Heptinstall, A. B., Adiyasa, I., Cano, C., & Hardcastle, I. R. Recent advances in CDK inhibitors for cancer therapy. *Future Med Chem*. **10**, 1369-1388 (2018).
30. Liu, K., Zheng, M., Lu, R. et al. The role of CDC25C in cell cycle regulation and clinical cancer therapy: a systematic review. *Cancer Cell Int*. **20**, 213 (2020).
31. Cheng, W., Yang, Z., Wang, S. et al. Recent development of CDK inhibitors: An overview of CDK/inhibitor co-crystal structures. *Eur J Med Chem*. **164**, 615-639 (2019).
32. Bertoli, C., Skotheim, J. M., & de Bruin, R. A. Control of cell cycle transcription during G1 and S phases. *Nat Rev Mol Cell Biol*. **14**, 518-528 (2013).
33. Razavipour SF, Harikumar KB, Slingerland JM. p27 as a Transcriptional Regulator: New Roles in Development and Cancer. *Cancer Res*. **80**, 3451-3458 (2020).
34. D'Arcangelo, D., Tinaburri, L., & Dellambra, E. The Role of p16INK4a Pathway in Human Epidermal Stem Cell Self-Renewal, Aging and Cancer. *Int J Mol Sci*. **18**, 1591 (2017).
35. Roskoski R Jr. Cyclin-dependent protein serine/threonine kinase inhibitors as anticancer drugs. *Pharmacol Res*. **139**, 471-488 (2019).
36. Janzen, V., Forkert, R., Fleming, H. E., et al. Stem-cell ageing modified by the cyclin-dependent kinase inhibitor p16INK4a. *Nature* **443**, 421-426 (2006).
37. Krishnamurthy, J., Ramsey, M. R., Ligon, K. L., et al. p16INK4a induces an age-dependent decline in islet regenerative potential. *Nature* **443**, 453-457 (2006).

38. Molofsky, A. V., Slutsky, S. G., Joseph, N. M., et al. Increasing p16INK4a expression decreases forebrain progenitors and neurogenesis during ageing. *Nature* **443**, 448-452 (2006).
39. Rosu-Myles, M., Taylor, B. J., & Wolff, L. Loss of the tumor suppressor p15Ink4b enhances myeloid progenitor formation from common myeloid progenitors. *Exp. Hematol* **35**, 394-406 (2007).
40. Yu, H., Yuan, Y., Shen, H., & Cheng, T. Hematopoietic stem cell exhaustion impacted by p18INK4C and p21Cip1/Waf1 in opposite manners. *Blood* **107**, 1200-1206 (2006).
41. Besson, A., Dowdy, S. F., & Roberts, J. M. CDK inhibitors: cell cycle regulators and beyond. *Dev Cell*. 14, 159-169 (2008).
42. Blais, A., & Dynlacht, B. D. E2F-associated chromatin modifiers and cell cycle control. *Curr Opin Cell Biol*. **19**, 658-662 (2007).
43. Anders, L., Ke, N., Hydbring, P., et al. A Systematic Screen for CDK4/6 Substrates Links FOXM1 Phosphorylation to Senescence Suppression in Cancer Cells. *Cancer Cell* **20**, 620-634 (2011).
44. Gopinathan, L., Tan, S. L. W., Padmakumar, V. C. et al. Loss of Cdk2 and Cyclin A2 Impairs Cell Proliferation and Tumorigenesis. *Cancer Res*. **74**, 3870-3879 (2014).
45. Malumbres, M., Pevarello, P., Barbacid, M., & Bischoff, J. R. CDK inhibitors in cancer therapy: what is next? *Trends Pharmacol. Sci.* **29**, 16-21 (2008).
46. Jeong, E. H., Lee, T. G., Ko, Y. J., et al. Anti-tumor effect of CDK inhibitors on CDKN2A-defective squamous cell lung cancer cells. *Cell Oncol (Dordr)*. **41**, 663-675 (2018).
47. Chen, Z., Wang, Z., Pang, J. C., et al. Multiple CDK inhibitor dinaciclib suppresses neuroblastoma growth via inhibiting CDK2 and CDK9 activity. *Sci Rep*. **6** (2016).
48. Whittaker, S. R., Te Poele, R. H., Chan, F., et al. The cyclin-dependent kinase inhibitor seliciclib (Rroscovitine; CYC202) decreases the expression of mitotic control genes and prevents entry into mitosis. *CELL CYCLE* **6**, 3114-3131 (2007).
49. Kettner, N. M., Vijayaraghavan, S., Durak, M. G., et al. Combined Inhibition of STAT3 and DNA Repair in Palbociclib-Resistant ER-Positive Breast Cancer. *Clin Cancer Res*. **25**, 3996-4013 (2019).
50. Rugo, H. S., Finn, R. S., Diéras, V., et al. Palbociclib plus letrozole as first-line therapy in estrogen receptor-positive/human epidermal growth factor receptor 2-negative advanced breast cancer with extended follow-up. *Breast Cancer Res Treat*. **174**, 719-729 (2019).
51. Dorland, W. A. Dorland's Illustrated Medical Dictionary, Ed. 24. Philadelphia: W. B. Saunders Co. (1965).
52. I.J. Fidler. The pathogenesis of cancer metastasis: the 'seed and soil' hypothesis revisited. *Nat. Rev. Cancer* **3**, 453-458 (2013).
53. Kalluri R and Weinberg RA: The basics of epithelial-mesenchymal transition. *J Clin Invest*. **119**, 1420-1428 (2009).
54. Lamouille, S., Xu, J., & Derynck, R. Molecular mechanisms of epithelial-mesenc-

hymal transition. *Nat Rev Mol Cell Biol*. **15**, 178-196 (2014).
55. Tran, H. D., Luitel, K., Kim, M., Zhang, K., Longmore, G. D., & Tran, D. D. Transient SNAIL1 expression is necessary for metastatic competence in breast cancer. *Cancer Res*. **74**, 6330-6340 (2014).
56. Yang, J., Mani, S. A., Donaher, J. L., et al. Twist, a master regulator of morphogenesis, plays an essential role in tumor metastasis. *Cell* **117**, 927-939 (2004).
57. Chaffer, C. L., Marjanovic, N. D., Lee, T., et al. Poised chromatin at the ZEB1 promoter enables breast cancer cell plasticity and enhances tumorigenicity. *Cell* **154**, 61-74 (2013).
58. Nieto, M. A., Huang, R. Y., Jackson, R. A. & Thiery, J. P. EMT: 2016. *Cell* **166**, 21-45 (2016).
59. Kahlert, U. D., Joseph, J. V., & Kruyt, F. EMT and MET-related processes in nonepithelial tumors: importance for disease progression, prognosis, and therapeutic opportunities. *Mol. Oncol* **11**, 860-877 (2017).
60. Brabletz, T. To differentiate or not- routes towards metastasis. *Nat. Rev. Cancer* **12**, 425-436 (2012).
61. J. Condeelis, R. Singer, J.E. Segall. The great escape: when cancer cells hijack the genes for chemotaxis and motility. *Annu. Rev Cell Dev Biol*. **21**, 695-718 (2005).
62. E. Sahai. Mechanisms of cancer cell invasion. *Curr Opin Genet Dev*. **15**, 87-96 (2005),
63. M. Bailly, J. Condeelis. Cell motility: insights from the backstage. *Nat Cell Biol.* **4**, 292-294 (2002).
64. Sahai, E. & Marshall, C.J. Rho-GTPases and cancer. *Nat Rev Cancer.* **2**, 133-142 (2002).
65. Lin, M. & Golen, K. L. Rho-Regulatory Proteins in Breast Cancer Cell Motility and Invasion. *Breast Cancer Res Treat*. **84**, 49-60 (2004).
66. Uruno, T., Liu, J., Zhang, P., et al. Activation of Arp2/3 complex-mediated actin polymerization by cortactin. *Nat Cell Biol.* **3**, 259-266 (2001).
67. Yin, M., Ma, W., & An, L. Cortactin in cancer cell migration and invasion. *Oncotarget.* **8**, 88232-88243 (2017).
68. Goode, B. L., Rodal, A. A., Barnes, G., & Drubin, D. G. Activation of the Arp2/3 complex by the actin filament binding protein Abp1p. *J Cell Biol*. **153**, 627-634 (2001).
69. Shvetsov, A., Berkane, E., Chereau, D., Dominguez, R., & Reisler, E. The actin-binding domain of cortactin is dynamic and unstructured and affects lateral and longitudinal contacts in F-actin. *Cell Motil Cytoskeleton*. **66**, 90-98 (2009).
70. Kowalski, J. R., Egile, C., Gil, S., Snapper, S. B., Li, R., & Thomas, S. M. Cortactin regulates cell migration through activation of N-WASP. *J Cell Sci*. **118**, 79-87 (2005).
71. Ammer, A. G., & Weed, S. A. Cortactin branches out: roles in regulating protrusive actin dynamics. *Cell Motil Cytoskeleton*. **65**, 687-707 (2008).
72. MacGrath, S. M., & Koleske, A. J. Cortactin in cell migration and cancer at a glance. *J Cell Sci.* **125**, 1621-1626 (2012).

73. Martinez-Quiles, N., Ho, H. Y., Kirschner, M. W., Ramesh, N., & Geha, R. S. Erk/Src phosphorylation of cortactin acts as a switch on-switch off mechanism that controls its ability to activate N-WASP. *Mol Cell Biol*. **24**, 5269-5280 (2004).
74. Tehrani, S., Tomasevic, N., Weed, S., Sakowicz, R., & Cooper, J. A. Src phosphorylation of cortactin enhances actin assembly. *Proc Natl Acad Sci U S A*. 104, 11933-11938 (2007).
75. Zhang, Y., Zhang, M., Dong, H., Yong, S., Li, X., Olashaw, N., et al. Deacetylation of cortactin by SIRT1 promotes cell migration. *Oncogene* **28**, 445-460 (2009).
76. Bryce, N. S., Clark, E. S., Leysath, J. L., Currie, J. D., Webb, D. J., & Weaver, A. M. Cortactin promotes cell motility by enhancing lamellipodial persistence. *Curr Biol*. **15**, 1276-1285 (2005).
77. Hofman, P., Butori, C., Havet, K., Hofman, V., Selva, E., Guevara, N., et al. Prognostic significance of cortactin levels in head and neck squamous cell carcinoma: comparison with epidermal growth factor receptor status. *Br J Cancer*. **98**, 956-964 (2008).
78.Yamada, S., Yanamoto, S., Kawasaki, G., Mizuno, A., & Nemoto, T.K. Overexpression of cortactin increases invasion potential in oral squamous cell carcinoma. *Pathol Oncol Res*. **16**, 523-531 (2010).
79. Noh, S. J., Baek, H. A., Park, H. S., Jang, K. Y., Moon, W. S., Kang, M. J., et al. Expression of SIRT1 and cortactin is associated with progression of non-small cell lung cancer. *Pathol Res Pract*. **209**, 365-370 (2013).
80. Chen, J. H., Chen, K. Y., Ma, H. I., Yu, C. P., Nieh, S., Lee, H. S., et al. Cortactin, fascin and survivin expression associated with clinicopathological parameters in brain gliosarcoma. *Chin J Physiol*. **53**, 234-244 (2010).
81.Mader, C. C., Oser, M., Magalhaes, M. A., Bravo-Cordero, J. J., Condeelis, J., Koleske, A. J., et al. An EGFR-Src-Arg-cortactin pathway mediates functional maturation of invadopodia and breast cancer cell invasion. *Cancer Res*. **71**, 1730-1741 (2011).
82.Radhakrishnan, V. M., Kojs, P., Young, G., Ramalingam, R., Jagadish, B., Mash, E. A., et al. pTyr421 cortactin is overexpressed in colon cancer and is dephosphorylated by curcumin: involvement of non-receptor type 1 protein tyrosine phosphatase (PTPN1). *PLoS One*. **9**, e85796 (2014).
83. Xu, X. Z., Garcia, M. V., Li, T. Y., Khor, L. Y., Gajapathy, R. S., Spittle, C., et al. Cytoskeleton alterations in melanoma: aberrant expression of cortactin, an actin-binding adapter protein, correlates with melanocytic tumor progression. *Mod Pathol*. **23**, 187-196 (2010).
84. Buday, L., & Downward, J. Roles of cortactin in tumor pathogenesis. *Biochim Biophys Acta*. **1775**, 263-273 (2007).
85. Nevins, J. R. E2F: a link between the Rb tumor suppressor protein and viral oncoproteins. *Science* **258**, 424-429 (1992).
86. Wu, Z., Zheng, S., & Yu, Q. The E2F family and the role of E2F1 in apoptosis. *Int J Biochem Cell Biol*. **41**, 238-2397 (2009).

87. DeGregori, J., & Johnson, D. Distinct and Overlapping Roles for E2F Family Members in Transcription, Proliferation and Apoptosis. *Curr Mol Med*. **6**, 739-748 (2006).
88. Stevens, C., & La Thangue, N. B. E2F and cell cycle control: a double-edged sword. *Arch Biochem Biophys*. **412**, 157-169 (2003).
89. Trimarchi, J. M., & Lees, J. A. Sibling rivalry in the E2F family. *Nat. Rev. Mol. Cell. Biol.* **3**: 11-20 (2002).
90. Crosby, M. E., Jacobberger, J., Gupta, D., et al. E2F4 regulates a stable G2 arrest response to genotoxic stress in prostate carcinoma. *Oncogene* **26**, 1897-1909 (2006).
91. Maiti, B., Li, J., de Bruin, A., et al. Cloning and characterization of mouse E2F8, a novel mammalian E2F family member capable of blocking cellular proliferation. *J Biol Chem*. **280**, 18211-18220 (2005).
92. Weijts, B. G., Bakker, W. J., Cornelissen, P. W., et al. E2F7 and E2F8 Promote Angiogenesis Through Transcriptional Activation of VEGFA in Cooperation with HIF-1. *EMBO* **31**, 3871-3884 (2012).
93. Ouseph, M. M., Li, J., Chen, H. Z., et al. Atypical E2F Repressors and Activators Coordinate Placental Development. *Dev Cell*. **22**, 849-862 (2012).
94. Morgunova, E., Yin, Y., Jolma, A.et al. Structural insights into the DNA-binding specificity of E2F family transcription factors. *Nat Commun*. **6** (2015).
95. de, Bruin, A, Maiti, B. Jakoi, L. Timmers, C. Buerki, R. Leone, G. Identification and characterization of E2F7, a novel mammalian E2F family member capable of blocking cellular proliferation. *J Biol Chem.* **278**, 42041-42049 (2003).
96. Emanuele, M. J., Enrico, T. P., Mouery, R. D., Wasserman, D., Nachum, S., & Tzur, A. Complex Cartography: Regulation of E2F Transcription Factors by Cyclin F and Ubiquitin. *Trends Cell Biol*. **30**, 640-652 (2020).
97. Okuda, M., Araki, K., Ohtani, K., & Nishimura, Y. The Interaction Mode of the Acidic Region of the Cell Cycle Transcription Factor DP1 with TFIIH. *J Mol Biol*. **428**, 4993-5006 (2016).
98. Blais A. A new mode of cell cycle stimulation: cyclin E and CDK2-mediated cytoplasmic retention of repressive E2F complexes. *Cell cycle* **11**, 2978 (2012).
99. Pennycook, B. R., Vesela, E., Peripolli, S. et al. E2F-dependent transcription determines replication capacity and S phase length. *Nat Commun*. **11**, 3503 (2020).
100. Kent, L. N., & Leone, G. The broken cycle: E2F dysfunction in cancer. *Nat Rev Cancer.* **19**, 326-338 (2019).
101. Iglesias-Ara, A., & Zubiaga, A. M. The stress of coping with E2F loss. *Mol Cell Oncol*. **3**, e1038423 (2015).
102. Johnson, J., Thijssen, B., McDermott, U., Garnett, M., Wessels, L. F., & Bernards, R. Targeting the RB-E2F pathway in breast cancer. *Oncogene* **35**, 4829-4835 (2016).
103. Grant, G. D., & Cook, J. G. The Temporal Regulation of S Phase Proteins During G1. *Adv Exp Med Biol*. **1042**, 335-369 (2017).
104. Cuitiño, M. C., Pécot, T., Sun, D., et al. Two Distinct E2F Transcriptional Modules Drive Cell Cycles and Differentiation. *Cell Rep*. **27**, 3547-3560.e5 (2019).

105. Ouseph, M. M., Li, J., Chen, H. Z., et al. Atypical E2F repressors and activators coordinate placental development. *Dev Cell*. **22**, 849-862 (2012).
106. Ruijtenberg, S., & van den Heuvel, S. Coordinating cell proliferation and differentiation: Antagonism between cell cycle regulators and cell type-specific gene expression. *Cell Cycle* **15**, 196-212 (2016).
107. Hsu, J., Arand, J., Chaikovsky, A., et al. E2F4 regulates transcriptional activation in mouse embryonic stem cells independently of the RB family. *Nat Commun*. **10**, 2939 (2019).
108. Danielian, P. S., Hess, R. A., & Lees, J. A. E2f4 and E2f5 are essential for the development of the male reproductive system. *Cell Cycle* **15**, 250-260 (2016).
109. Komori, H., Goto, Y., Kurayoshi, K., et al. Differential requirement for dimerization partner DP between E2F-dependent activation of tumor suppressor and growth-related genes. *Sci Rep*. **8**, 8438 (2018).
110. Kohn, M. J., Leung, S. W., Criniti, V., Agromayor, M., & Yamasaki, L. Dp1 is largely dispensable for embryonic development. *Mol Cell Biol*. **24**, 7197-7205 (2004).
111. Lazzerini Denchi, E., & Helin, K. E2F1 is crucial for E2F-dependent apoptosis. *EMBO Rep*. **6**, 661-668 (2005).
112. Ginsberg D. E2F1 pathways to apoptosis. *FEBS letters*. **529**, 122-125 (2002).
113. Chen, D., Chen, Y., Forrest, D., & Bremner, R. E2f2 induces cone photoreceptor apoptosis independent of E2f1 and E2f3. *Cell Death Differ*. **20**, 931-940 (2013).
114. Chen, H. Z., Tsai, S. Y., & Leone, G. Emerging roles of E2Fs in cancer: an exit from cell cycle control. *Nat Rev Cancer*. **9**, 785-797 (2009).
115. Aslanian,A., Iaquinta, P. J., Verona, R., et al. Repression of the Arf tumor suppress-
or by E2F3 is required for normal cell cycle kinetics. *Genes Dev*. **18**, 1413-1422 (2004).
116. Hershko, T., Chaussepied, M., Oren, M., & Ginsberg, D. Novel link between E2F and p53: proapoptotic cofactors of p53 are transcriptionally upregulated by E2F. *Cell Death Differ*. **12**, 377-383 (2005).
117. Bell, L. A., & Ryan, K. M. Life and death decisions by E2F-1. *Cell Death Differ*. **11**: 137-142 (2004).
118. Zheng, C., Ren, Z., Wang, H., et al. E2F1 Induces tumor cell survival via nuclear factor-kappaB-dependent induction of EGR1 transcription in prostate cancer cells. *Cancer Res*. **69**, 2324-2331 (2009).
119. Moroni, M. C., Hickman, E. S., Lazzerini Denchi, E., et al. Apaf-1 is a transcriptional target for E2F and p53. *Nat Cell Biol*. **3**, 552-558 (2001).
120. Bracken, A. P., Ciro, M., Cocito, A., & Helin, K. E2F target genes: unraveling the biology. *Trends Biochem Sci*. **29**, 409-417 (2004).
121. Pützer, B. M. E2F1 death pathways as targets for cancer therapy. *J Cell Mol Med*. **11**, 239-251 (2007).
122. Stanelle, J., Stiewe, T., Theseling, C. C., Peter, M., & Pützer, B. M. Gene expression changes in response to E2F1 activation. *Nucleic Acids Res*. **30**, 1859-1867 (2002).

123. Tanaka, H., Matsumura, I., Ezoe, S., et al. E2F1 and c-Myc potentiate apoptosis through inhibition of NF-kappaB activity that facilitates MnSOD-mediated ROS elimination. *Mol Cell*. **9**, 1017-1029 (2002).
124. Mordes, D. A., Glick, G. G., Zhao, R., & Cortez, D. TopBP1 activates ATR through ATRIP and a PIKK regulatory domain. *Genes Dev*. **22**, 1478–1489 (2008).
125. Ianari, A., Natale, T., Calo, E., et al. Proapoptotic function of the retinoblastoma tumor suppressor protein. *Cancer cell* **15**, 184-194 (2009).
126. Lin, W. C., Lin, F. T., & Nevins, J. R. Selective induction of E2F1 in response to DNA damage, mediated by ATM-dependent phosphorylation. *Genes Dev* **15**, 1833-1844 (2001).
127. Bartek J., Lukas J. Chk1 and Chk2 kinases in checkpoint control and cancer. *Cancer Cell*. **3**, 421-429 (2003).
128. Wang, C., Rauscher, F. J., 3rd, Cress, W. D., & Chen, J. Regulation of E2F1 function by the nuclear corepressor KAP1. *J Biol Chem*. **282**, 29902-29909 (2007).
129. Pillai, S., Kovacs, M., & Chellappan, S. Regulation of vascular endothelial growth factor receptors by Rb and E2F1: role of acetylation. *Cancer Res*. **70**, 4931-4940 (2010).
130. Merdzhanova, G., Gout, S., Keramidas, M., et al. The transcription factor E2F1 and the SR protein SC35 control the ratio of pro-angiogenic versus antiangiogenic isoforms of vascular endothelial growth factor-A to inhibit neovascularization in vivo. *Oncogene* **29**, 5392-5403 (2010).
131. Goodrich D. W. The retinoblastoma tumor-suppressor gene, the exception that proves the rule. *Oncogene* **25**, 5233-5243 (2006).
132. Manickavinayaham, S., Velez-Cruz, R., Biswas, A. K., Chen, J., Guo, R., & Johnson, D. G. The E2F1 transcription factor and RB tumor suppressor moonlight as DNA repair factors. *Cell Cycle* **19**, 2260-2269 (2020).
133. Sheldon L. A. Inhibition of E2F1 activity and cell cycle progression by arsenic via retinoblastoma protein. *Cell Cycle* **16**, 2058-2072 (2017).
134. Burke, J. R., Deshong, A. J., Pelton, J. G., & Rubin, S. M. Phosphorylation-induced conformational changes in the retinoblastoma protein inhibit E2F transactivation domain binding. *J Biol Chem*. **285**, 16286-16293 (2010).
135. Burke, J. R., Liban, T. J., Restrepo, T., Lee, H. W., & Rubin, S. M. Multiple mechanisms for E2F binding inhibition by phosphorylation of the retinoblastoma protein C-terminal domain. *J Mol Biol*. **426**, 245-255 (2014).
136. Zhao, Y., Tan, J., Zhuang, L., et al. Inhibitors of histone deacetylases target the Rb-E2F1 pathway for apoptosis induction through activation of proapoptotic protein Bim. *Proc Natl Acad Sci U S A*. **102**, 16090-16095 (2005).
137. Rubin, S. M., Gall, A. L., Zheng, N., & Pavletich, N. P. Structure of the Rb C-terminal domain bound to E2F1-DP1: a mechanism for phosphorylation-induced E2F release. *Cell* **123**, 1093-1106 (2005).
138. Finzer, P., Krueger, A., Stöhr, M., et al. HDAC inhibitors trigger apoptosis in HPV-positive cells by inducing the E2F-p73 pathway. *Oncogene* **23**, 4807-4817 (2004).

139. Firestein, R., Bass, A. J., Kim, S. Y., et al. CDK8 is a colorectal cancer oncogene that regulates beta-catenin activity. *Nature* **455**, 547-551 (2008).
140. Morris, E. J., Ji, J. Y., Yang, F. et al. E2F1 represses beta-catenin transcription and is antagonized by both pRB and CDK8. *Nature* **455**, 552-556 (2008).
141. Dhar, S., Vemulapalli, V., Patananan, A. N., Huang, G. L., Di Lorenzo, A., Richard, S., et al. Loss of the major Type I arginine methyltransferase PRMT1 causes substrate scavenging by other PRMTs. *Sci. Rep*. **3**, 1311 (2013).
142. Trojer, P., Dangl, M., Bauer, I., Graessle, S., Loidl, P., & Brosch, G. Histone methyltransferases in Aspergillus nidulans: evidence for a novel enzyme with a unique substrate specificity. *Biochemisty* **43**, 10834-10843 (2004).
143. Pahlich, S., Zakaryan, R. P., & Gehring, H. Protein arginine methylation: Cellular functions and methods of analysis. *Biochim Biophys Acta*. **1764**, 1890-1903 (2006).
144. Aletta, J. M & Hu, J. C. Protein arginine methylation in health and disease. *Biotechnol Annu Rev* **14**, 203-224 (2008).
145. Wolf, S. S. The protein arginine methyltransferase family: an update about function, new perspectives and the physiological role in humans. *Cell. Mol. Life Sci.* **66**, 2109-2121 (2009).
146. Tang, J., Frankel, A., Cook, R. J., et al. PRMT1 is the predominant type I protein arginine methyltransferase in mammalian cells. *J Biol Chem* **275**, 7723-7730 (2000).
147. Yang, Y., Bedford, M. Protein arginine methyltransferases and cancer. *Nat Rev Cancer* **13,** 37–50 (2013).
148. Choucair, A., Pham, T. H., Omarjee, S., et al. The arginine methyltransferase PRMT1 regulates IGF-1 signaling in breast cancer. *Oncogene* **38**, 4015-4027 (2019).
149. Avasarala, S., Van Scoyk, M., Karuppusamy Rathinam, M. K., et al. PRMT1 is a Novel Regulator of Epithelial-Mesenchymal-Transition in Non-small Cell Lung Cancer. *J Biol Chem.* **290**, 13479-13489 (2015).
150. Mathioudaki, K., Papadokostopoulou, A., Scorilas, A., Xynopoulos, D., Agnanti, N., & Talieri, M. The PRMT1 gene expression pattern in colon cancer. *Br J Cancer*. **99**, 2094-2099 (2008).
151. Yoshimatsu, M., Toyokawa, G., Hayami, S., et al. Dysregulation of PRMT1 and PRMT6, Type I arginine methyltransferases, is involved in various types of human cancers. *Int J Cancer* **128**, 562-573 (2011).
152. Zhong, J., Cao, R. X., Zu, X. Y., et al. Identification and characterization of novel spliced variants of PRMT2 in breast carcinoma. *FEBS J.* **279**, 316-335 (2012).
153. Zhong, J., Cao, R. X., Hong, T., et al. Identification and expression analysis of a novel transcript of the human PRMT2 gene resulted from alternative polyadenylation in breast cancer. *Gene* **487**, 1-9 (2011).
154. Jiang, W., & Newsham, I. F. The tumor suppressor DAL-1/4.1B and protein methylation cooperate in inducing apoptosis in MCF-7 breast cancer cells. *Mol Cancer* **5** (2006).
155. Liu, J., Feng, J., Li, L., et al. Arginine methylation-dependent LSD1 stability promotes invasion and metastasis of breast cancer. *EMBO Rep*. **21**, e48597 (2020).

156. O'Brien, K. B., Alberich-Jordà, M., Yadav, N., et al. CARM1 is required for proper control of proliferation and differentiation of pulmonary epithelial cells. *Development* **137**, 2147-2156 (2010).
157. Chen, H., Lorton, B., Gupta, V., & Shechter, D. A TGFβ-PRMT5-MEP50 axis regulates cancer cell invasion through histone H3 and H4 arginine methylation coupled transcriptional activation and repression. *Oncogene* **36**, 373-386 (2017).
158. Radzisheuskaya, A., Shliaha, P. V., Grinev, V., et al. PRMT5 methylome profiling uncovers a direct link to splicing regulation in acute myeloid leukemia. *Nat Struct Mol Biol*. **26**, 999-1012 (2019).
159. Chung, J., Karkhanis, V., Baiocchi, R. A., & Sif, S. Protein arginine methyltransferase 5 (PRMT5) promotes survival of lymphoma cells via activation of WNT/β-catenin and AKT/GSK3β proliferative signaling. *J Biol Chem*. **294**, 7692-7710 (2019).
160. Chiang, K., Zielinska, A. E., Shaaban, A. M., et al. PRMT5 Is a Critical Regulator of Breast Cancer Stem Cell Function via Histone Methylation and FOXP1 Expression. *Cell Rep*. **21**, 3498-3513 (2017).
161. Nicholas, C., Yang, J., Peters, S. B., et al. PRMT5 is upregulated in malignant and metastatic melanoma and regulates expression of MITF and p27(Kip1.). *PLoS One* **8**, e74710 (2013).
162. Liu, M., Yao, B., Gui, T., et al. PRMT5-dependent transcriptional repression of c-Myc target genes promotes gastric cancer progression. *Theranostics* **10**, 4437-4452 (2020).
163. Hartley, A. V., Wang, B., Mundade, R., et al. PRMT5-mediated methylation of YBX1 regulates NF-κB activity in colorectal cancer. *Sci Rep*. **10**, 15934 (2020).
164. Avasarala, S., Wu, P. Y., Khan, S. Q., et al. PRMT6 Promotes Lung Tumor Progression via the Alternate Activation of Tumor-Associated Macrophages. *Mol Cancer Res.* **18**, 166-178 (2020).
165. Yao, R., Jiang, H., Ma, Y., et al. PRMT7 induces epithelial-to-mesenchymal transition and promotes metastasis in breast cancer. *Cancer Res.* **74**, 5656-5667 (2014).
166. Hernandez, S. J., Dolivo, D. M., & Dominko, T. PRMT8 demonstrates variant-specific expression in cancer cells and correlates with patient survival in breast, ovarian and gastric cancer. *Oncol Lett*. **13**, 1983-1989 (2017).
167. Jiang, H., Zhou, Z., Jin, S., et al. PRMT9 promotes hepatocellular carcinoma invasion and metastasis via activating PI3K/Akt/GSK-3β/Snail signaling. *Cancer Sci.* **109**, 1414-1427 (2018).
168. Mathioudaki, K., Scorilas, A., Ardavanis, A., et al. Clinical evaluation of PRMT1 gene expression in breast cancer. *Tumour Biol*. **32**, 575-582 (2011).
169. Elakoum, R., Gauchotte, G., Oussalah, A., et al. CARM1 and PRMT1 are dysregulated in lung cancer without hierarchical features. *Biochimie.* **97**, 210-218 (2014).
170. Le Romancer, M., Treilleux, I., Leconte, N., et al. Regulation of estrogen rapid signaling through arginine methylation by PRMT1. *Mol Cell*. **31**, 212-221 (2008).

171. Poulard, C., Treilleux, I., Lavergne, E., et al. Activation of rapid oestrogen signalling in aggressive human breast cancers. *EMBO Mol Med.* **4**, 1200-1213 (2012).
172. Boisvert, F. M., Déry, U., Masson, J. Y., & Richard, S. Arginine methylation of MRE11 by PRMT1 is required for DNA damage checkpoint control. *Genes Dev*. **19**, 671-676 (2005).
173. Schmalhofer O, Brabletz S, Brabletz T. E-cadherin, beta-catenin, and ZEB1 in malignant progression of cancer. *Cancer Metastasis Rev*. **28**, 151-166 (2009).
174. Guendel, I., Carpio, L., Pedati, C., et al. Methylation of the tumor suppressor protein, BRCA1, influences its transcriptional cofactor function. *PLoS One* **5**, e11379 (2010).
175. Gao, Y., Zhao, Y., Zhang, J., et al. The dual function of PRMT1 in modulating epithelial-mesenchymal transition and cellular senescence in breast cancer cells through regulation of ZEB1. *Sci Rep*. **6**, 19874 (2016).
176. Antonysamy, S., Bonday, Z., Campbell, R. M., et al. Crystal structure of the human PRMT5:MEP50 complex. *Proc Natl Acad Sci U S A.* **109**, 17960-17965 (2012).
177. Stopa, N., Krebs, J. E., & Shechter, D. The PRMT5 arginine methyltransferase: many roles in development, cancer and beyond. *Cell Mol Life Sci*. **72**, 2041-2059 (2015).
178. Ho, M. C., Wilczek, C., Bonanno, J. B., et al. Structure of the arginine methyl-transferase PRMT5-MEP50 reveals a mechanism for substrate specificity. *PLoS One* **8**, (2013).
179. Furuno, K., Masatsugu, T., Sonoda, M., Sasazuki, T., & Yamamoto, K. Association of Polycomb group SUZ12 with WD-repeat protein MEP50 that binds to histone H2A selectively in vitro. *Biochem Biophys Res Commun*. **345**, 1051-1058 (2006).
180. Pesiridis, G. S., Diamond, E., & Van Duyne, G. D. Role of pICLn in methylation of Sm proteins by PRMT5. J Biol Chem. **284**, 21347-21359 (2009).
181. Guderian, G., Peter, C., Wiesner, J., et al. RioK1, a new interactor of protein arginine methyltransferase 5 (PRMT5), competes with pICln for binding and modulates PRMT5 complex composition and substrate specificity. *J Biol Chem*. **286**, 1976-1986 (2011).
182. Andreu-Pérez, P., Esteve-Puig, R., de Torre-Minguela, C., et al. Protein arginine methyltransferase 5 regulates ERK1/2 signal transduction amplitude and cell fate through CRAF. *Sci Signal*. **4**, ra58 (2011).
183. Branscombe, T. L., Frankel, A., Lee, J. H., et al. PRMT5 (Janus kinase-binding protein 1) catalyzes the formation of symmetric dimethylarginine residues in proteins. *J Biol Chem*. **276**, 32971-32976 (2001).
184. Fabbrizio, E., El Messaoudi, S., Polanowska, J., et al. Negative regulation of transcription by the type II arginine methyltransferase PRMT5. *EMBO Rep*. **3**, 641-645 (2002).
185. Pal, S.,Vishwanath, S. N.,Erdjument-Bromage, H., Tempst, P. & Sif, S. Human SWI/SNF-associated PRMT5 methylates histone H3 arginine 8 and negatively

regulates expression of ST7 and NM23 tumor suppressor genes. *Mol Cell Biol*. **24**, 9630-9645 (2004).
186. Pal, S., Baiocchi, R. A., Byrd, J. C., Grever, M. R., Jacob, S. T., & Sif, S. Low levels of miR-92b/96 induce PRMT5 translation and H3R8/H4R3 methylation in mantle cell lymphoma. *EMBO J*. **26**, 3558-3569 (2007).
187. Wang, Y., Hu, W., & Yuan, Y. Protein Arginine Methyltransferase 5 (PRMT5) as an Anticancer Target and Its Inhibitor Discovery. *J Med Chem*. **61**, 9429-9441 (2018).
188. Harris, D. P., Bandyopadhyay, S., Maxwell, T. J., et al. Tumor necrosis factor (TNF)-α induction of CXCL10 in endothelial cells requires protein arginine methyltransferase 5 (PRMT5)-mediated nuclear factor (NF)-κB p65 methylation. *J Biol Chem*. **289**, 15328-15339 (2014).
189. Jansson, M., Durant, S. T., Cho, E. C., et al. Arginine methylation regulates the p53 response. *Nature Cell Biol*. **10**, 1431-1439 (2008).
190. Zheng, S., Moehlenbrink, J., Lu, Y. C., et al. Arginine methylation-dependent reader-writer interplay governs growth control by E2F-1. *Mol Cell*. **52**, 37-51(2013).
191. Bandyopadhyay, S. et al. HOXA9 methylation by PRMT5 is essential for endothelial cell expression of leukocyte adhesion molecules. *Mol Cell Biol*. **32**, 1202-1213 (2012).
192. He, W., Ma, X., Yang, X., Zhao, Y., Qiu, J., & Hang, H. A role for the arginine methylation of Rad9 in checkpoint control and cellular sensitivity to DNA damage. *Nucleic Acids Res*. **39**, 4719-4727 (2011).
193. Guccione, E., Richard, S. The regulation, functions and clinical relevance of arginine methylation. *Nat Rev Mol Cell Biol* **20**, 642-657 (2019).
194. Wei, H., Wang, B., Miyagi, M., et al. PRMT5 dimethylates R30 of the p65 subunit to activate NF-κB. *Proc Natl Acad Sci U S A*. **110**, 13516-13521 (2013).
195. Durant, S. T., Cho, E. C. & La Thangue, N. B. p53 methylation-the Arg-ument is clear. *Cell Cycle* **8**, 801-802 (2009).
196. Cho, E. C., Zheng, S., Munro, S., et al. Arginine methylation controls growth regulation by E2F-1. *EMBO J.* **31**, 1785-1797 (2012).
197. Hsu, J. M., Chen, C. T., Chou, C. K., et al. Crosstalk between Arg 1175 methylation and Tyr 1173 phosphorylation negatively modulates EGFR-mediated ERK activation. *Nat Cell Biol.* **13**, 174-181 (2011).
198. Dorrello, N. V., Peschiaroli, A., Guardavaccaro, D., Colburn, N. H., Sherman, N. E., & Pagano, M. S6K1- and betaTRCP-mediated degradation of PDCD4 promotes protein translation and cell growth. *Science* **314**, 467-471 (2006).
199. Wei, T. Y., Juan, C. C., Hisa, J. Y., et al. PRMT5 is a potential oncoprotein that upregulates G1 cyclins/CDKs and the PI3K/AKT signaling cascade. *Cancer Sci*. **103**, 1640-1645 (2012).
200. Scoumanne, A., Zhang, J., & Chen, X. PRMT5 is required for cell-cycle progression and p53 tumor suppressor function. *Nucleic Acids Res*. **37**, 4965-4976 (2009).

201. Wang, L., Pal, S., & Sif, S. Protein arginine methyltransferase 5 suppresses the transcription of the RB family of tumor suppressors in leukemia and lymphoma cells. *Mol Cell Biol*. **28**, 6262-6277 (2008).
202. Hou, Z., Peng, H., Ayyanathan, K., et al. The LIM protein AJUBA recruits protein arginine methyltransferase 5 to mediate SNAIL-dependent transcriptional repression. *Mol Cell Biol*. **28**, 3198-3207 (2008).
203. Ge, L., Wang, H., Xu, X., et al. PRMT5 promotes epithelial-mesenchymal transition via EGFR-β-catenin axis in pancreatic cancer cells. *J Cell Mol Med.* **24**, 1969-1979 (2020).
204. Xu, X., Shi, R., Zheng, L., et al. SUMO-1 modification of FEN1 facilitates its interaction with Rad9-Rad1-Hus1 to counteract DNA replication stress. *J Mol Cell Biol*. **10**, 460-474 (2018).
205. Ren, J., Wang, Y., Liang, Y., Zhang, Y., Bao, S., & Xu, Z. Methylation of ribosomal protein S10 by protein-arginine methyltransferase 5 regulates ribosome biogenesis. *J Biol Chem*. **285**, 12695-12705 (2010).
206. Zhang, X., Wu, J., Wu, C., et al. The LINC01138 interacts with PRMT5 to promote SREBP1-mediated lipid desaturation and cell growth in clear cell renal cell carcinoma. *Biochem Biophys Res Commun.* **507**, 337-342 (2018).
207. Smil, D., Eram, M. S., Li, F., et al. Discovery of a Dual PRMT5-PRMT7 Inhibitor. *ACS Med Chem Lett*. **6**, 408-412 (2015).
208. Kaniskan, H. Ü., Konze, K. D., & Jin, J. Selective inhibitors of protein methyltransferases. *J Med Chem*. **58**, 1596-1629 (2015).
209. Chan-Penebre, E., Kuplast, K. G., Majer, C. R., et al. A selective inhibitor of PRMT5 with in vivo and in vitro potency in MCL models. *Nat Chem Biol*. **11**, 432-437 (2015).
210. Bonday, Z. Q., Cortez, G. S., Grogan, M. J., et al. LLY-283, a Potent and Selective Inhibitor of Arginine Methyltransferase 5, PRMT5, with Antitumor Activity. *ACS Med Chem Lett.* **9**, 612-617 (2018).
211. ClinicalTrials.gov https://clinicaltrials.gov/
212. Mavrakis, K. J., McDonald, E. R., 3rd, Schlabach, M. R. et al. Disordered methionine metabolism in MTAP/CDKN2A-deleted cancers leads to dependence on PRMT5. *Science* **351**, 1208-1213 (2016).
213. Barbarino, M., Cesari, D., Bottaro, M., et al. PRMT5 silencing selectively affects MTAP-deleted mesothelioma: In vitro evidence of a novel promising approach. *J Cell Mol Med*. **24**, 5565-5577 (2020).
214. Kryukov, G. V., Wilson, F. H., Ruth, J. R., et al. MTAP deletion confers enhanced dependency on the PRMT5 arginine methyltransferase in cancer cells. *Science* **351**, 1214-1218 (2016).
215. Wang, Y., Hu, W., & Yuan, Y. Protein Arginine Methyltransferase 5 (PRMT5) as an Anticancer Target and Its Inhibitor Discovery. *J Med Chem*. **61**, 9429-9441 (2018).
216. Ran, F. A., Hsu, P. D., Wright, J., Agarwala, V., Scott, D. A., & Zhang, F. Genome engineering using the CRISPR-Cas9 system. *Nat Protoc*. **8**: 2281-2308 (2013).

217. Morales, J., Li, L., Fattah, F. J., et al. Review of poly (ADP-ribose) polymerase (PARP) mechanisms of action and rationale for targeting in cancer and other diseases. *Crit Rev Eukaryot Gene Expr*. **24**, 15-28 (2014).
218. Marioni, J. C., Mason, C. E., Mane, S. M., Stephens, M., & Gilad, Y. RNA-seq: an assessment of technical reproducibility and comparison with gene expression arrays. *Genome Res*. **18**, 1509-1517 (2008).
219. Mäder, U., Nicolas, P., Richard, H., Bessières, P., & Aymerich, S. Comprehens -ive identification and quantification of microbial transcriptomes by genome-wide unbiased methods. *Curr Opin Biotechnol*. **22**, 32-41 (2011).
220. Wang, L., Feng, Z., Wang, X., Wang, X., & Zhang, X. DEGseq: an R package for identifying differentially expressed genes from RNA-seq data. *Bioinformatics* **26**, 136-138 (2010).
221. Costa, V., Angelini, C., De Feis, I., & Ciccodicola, A. Uncovering the complexity of transcriptomes with RNA-Seq. *J Biomed Biotechnol.* **2010**, 853916 (2010).
222. Kopecki, Z., Yang, G. N., Jackson, J. E., et al. Cytoskeletal protein Flightless I inhibits apoptosis, enhances tumor cell invasion and promotes cutaneous squamous cell carcinoma progression. *Oncotarget* **6**, 36426-36440 (2015).
223. Mohammad, I., Arora, P. D., Naghibzadeh, Y., et al. Flightless I is a focal adhesion-associated actin-capping protein that regulates cell migration. *FASEB J*. **26**, 3260-3272 (2012).
224. Nagata, M., Noman, A. A., Suzuki, K., et al. ITGA3 and ITGB4 expression biomarkers estimate the risks of locoregional and hematogenous dissemination of oral squamous cell carcinoma. *BMC Cancer*. **13**, 410 (2013).
225. Liu, P., Li, W., Hu, Y., & Jiang, Y. Absence of AIF1L contributes to cell migration and a poor prognosis of breast cancer. *OncoTargets and therapy* **11**, 5485-5498 (2018).
226. Wu, S., Nitschke, K., Heinkele, J., et al. ANLN and TLE2 in Muscle Invasive Bladder Cancer: A Functional and Clinical Evaluation Based on In Silico and In Vitro Data. *Cancers (Basel)* **11**, 1840 (2019).
227. Janiszewska, M., Primi, M. C., & Izard, T. Cell adhesion in cancer: Beyond the migration of single cells. *J Biol Chem*. **295**, 2495-2505 (2020).
228. Bendas, G., & Borsig, L. Cancer cell adhesion and metastasis: selectins, integrins, and the inhibitory potential of heparins. *Int J Cell Biol*. **2012**, 676731 (2012).